Advanced Signal Processing Techniques for Multi-Target Tracking

by

Abdullahi Daniyan

A Doctoral Thesis submitted in partial fulfilment
of the requirements for the award of the degree of
Doctor of Philosophy
of Loughborough University

May 2018

Signal Processing and Networks Research Group
Wolfson School of Mechanical, Electrical and Manufacturing Engineering
Loughborough University

To my mother and my father

Declaration

I hereby declare that I am responsible for the work submitted in this thesis, that the original work is my own except as specified in acknowledgements or in footnotes, and that neither the thesis nor the original work therein has been submitted to this or any other institution for a degree.

Abdullahi Daniyan

May 2018

Acknowledgements

I am very grateful to my supervisors; Prof. Sangarapillai Lambotharan, and Dr. Alex Gong for their professional guidance, unwavering supports, stimulating suggestions, comments, for supporting me to go the extra mile and take on new challenges and for your patience in reading through numerous papers and multiple drafts of this thesis. Particularly, I want to thank Prof. Jonathon Chambers for inspiring me to do a PhD in the first place.

I would like to express my profound gratitude to those who have offered generous support in whatever form during my years of academic pursuit. A big thank you to my colleagues Ramadan, Tasos, Gaia, Abdulrazaq, Raed, Shadi and Ashraf. I am sure there are many more others and it would be impractical to mention all names, but your support is highly valued and acknowledged. Thank you all.

In addition, I wish to acknowledge the financial support provided by the UK Engineering and Physical Sciences Research Council (ESPRC), the MOD University Defence Research Collaboration (UDRC) in Signal Processing, UK and the Petroleum Technology Development Fund (PTDF), Nigeria and my employer, FUT Minna.

Lastly, I wish to express my deep and most sincere appreciation and thanks to my Mom, Dr. (Mrs.) S.Y. Daniyan and Dad, Prof. M.A. Daniyan for their continual and unrelenting support and for always being there for me. A special thanks to my darling wife Aisha for her support, patience and love, my lovely kids, Abdurrahman and Fatimah for their patience and love. A special thanks to Aisha (Tutu), Ummi, Abba and the rest of my siblings, thank you all. To my uncle, Prof. M.K. Yahaya, thank you for your support. A big thank you to my friends and family for your support and prayers.

All praise is due to Allah with Whose favour good things are completed!

Abstract

The multi-target tracking problem essentially involves the recursive *joint estimation* of the *state* of unknown and time-varying *number* of targets present in a tracking scene, given a series of observations. This problem becomes more challenging because the sequence of observations is noisy and can become corrupted due to miss-detections and false alarms/clutter. Additionally, the detected observations are indistinguishable from clutter. Furthermore, whether the target(s) of interest are *point* or *extended* (in terms of spatial extent) poses even more technical challenges.

An approach known as random finite sets provides an elegant and rigorous framework for the handling of the multi-target tracking problem. With a random finite sets formulation, both the multi-target states and multi-target observations are modelled as finite set valued random variables, that is, random variables which are random in both the number of elements and the values of the elements themselves. Furthermore, compared to other approaches, the random finite sets approach possesses a desirable characteristic of being free of explicit data association prior to tracking. In addition, a framework is available for dealing with random finite sets and is known as finite sets statistics. In this thesis, advanced signal processing techniques are employed to provide enhancements to and develop new random finite sets based multi-target tracking algorithms for the tracking of both *point* and *extended targets* with the aim to improve tracking performance in cluttered environments.

To this end, firstly, a new and efficient Kalman-gain aided sequential Monte Carlo probability hypothesis density (KG-SMC-PHD) filter and a cardinalised particle probability hypothesis density (KG-SMC-CPHD) filter are proposed. These filters employ the Kalman-gain approach during weight update to correct predicted particle states by minimising

the mean square error between the estimated measurement and the actual measurement received at a given time in order to arrive at a more accurate posterior. This technique identifies and selects those particles belonging to a particular target from a given PHD for state correction during weight computation. The proposed SMC-CPHD filter provides a better estimate of the number of targets. Besides the improved tracking accuracy, fewer particles are required in the proposed approach. Simulation results confirm the improved tracking performance when evaluated with different measures.

Secondly, the KG-SMC-(C)PHD filters are particle filter (PF) based and as with PFs, they require a process known as resampling to avoid the problem of degeneracy. This thesis proposes a new resampling scheme to address a problem with the *systematic resampling* method which causes a high tendency of resampling very low weight particles especially when a large number of resampled particles are required; which in turn affect state estimation.

Thirdly, the KG-SMC-(C)PHD filters proposed in this thesis perform "filtering" and not "tracking", that is, they provide only "point" estimates of target states but do not provide "connected" estimates of target trajectories from one time step to the next. A new post processing step using game theory as a solution to this "filtering" - "tracking" problem is proposed. This approach was named the GTDA method. This method was employed in the KG-SMC-(C)PHD filter as a post processing technique and was evaluated using both simulated and real data obtained using the NI-USRP software defined radio platform in a passive bi-static radar system.

Lastly, a new technique for the joint tracking and labelling of multiple extended targets is proposed. To achieve multiple extended target tracking using this technique, models for the target measurement rate, kinematic component and target extension are defined and jointly propagated in time under the generalised labelled multi-Bernoulli (GLMB) filter framework. The GLMB filter is a random finite sets-based filter. In particular, a Poisson mixture variational Bayesian (PMVB) model is developed to simultaneously estimate the measurement rate of multiple extended targets and extended target extension was

modelled using B-splines. The proposed method was evaluated with various performance metrics in order to demonstrate its effectiveness in tracking multiple extended targets.

Contents

List of Acronyms

2D-CCF	Two-Dimensional Cross-Correlation Function
AP-PHD	Auxiliary Particle PHD
A-SMC-PHD	Auxiliary SMC-PHD
CE	Correlated Equilibrium
CFAR	Constant False Alarm Rate
CMeMBer	Cardinality-Balanced Multi-Target Multi-Bernoulli
CPHD	Cardinalised Probability Hypothesis Density
CT	Computation Time
CUT	Cell Under Test
EKF	Extended Kalman Filter
EPF	Extended Particle Filter
ET	Extended Target
FISST	Finite Sets Statistics
GLMB	Generalised Labelled Multi-Bernoulli
GLMB-S	Generalised Labelled Multi-Bernoulli Spline
GM	Gaussian Mixture
GM-P-PHD	GM Particle PHD
GTDA	Game Theoretic Data Association
i.i.d.	Independent and Identically Distributed
I-Q	In-Phase and Quadrature
ISR	Improved Systematic Resampling

JPDA	Joint Probabilistic Data Data Association
KF	Kalman Filter
KG-SMC-PHD	Kalman-Gain Aided Sequential Monte Carlo PHD
LMB	Labelled Multi-Bernoulli
LMS	Least Mean Square
MCMC	Markov Chain Monte Carlo
MC	Monte Carlo
MeMBer	Multi-Target Multi-Bernoulli
MHT	Multiple Hypothesis Tracker
MMSE	Minimum Mean Square Error
mOSPA	Modified OSPA
MSE	Mean Squared Error
MTT	Multi-Target Tracking
NE	Nash Equilibrium
NI	National Instruments
NN	Nearest Neighbour
OS-CFAR	Order Statistic CFAR
OSPA	Optimal Subpattern Assignment
PBR	Passive Bi-Static Radar
PDA	Probabilistic Data Association
pdf	Probability Density Function
PF	Particle Filter
$\mathbf{P}_{FA}$	Probability of False Alarm
PHD	Probability Hypothesis Density
PMVB	Poisson Mixture Variational Bayesian
RFS	Random Finite Set
RHM	Random Hypersurface Model
RM	Regret Matching

RMFF	Regret Matching with Forgetting Factor
SMC	Sequential Monte Carlo
SR	Systematic Resampling
STT	Single Target Tracking
TP	Transitional Prior
UIF	Unscented Information Filter
UKF	Unscented Kalman Filter
UK-P-PHD	Unscented Kalman Particle PHD
UPF	Unscented Particle Filter
USMC	Unscented Sequential Monte Carlo
USRP	Universal Software Radio Peripheral
VB	Variational Bayesian

List of Figures

List of Tables

Chapter 1

Introduction

1.1 Target Tracking

Target tracking can be defined as the problem of estimating over time the location and trajectory of an object/target as it moves within a tracking scene using sensor measurements/observations. Target tracking is of key importance in systems that perform functions such as surveillance, monitoring, guidance or obstacle avoidance. Typically, a tracking algorithm takes as input measurements obtained at intervals from sensors which provide the signals such as sonar, radar, image or video to output target state estimates at each point in time. The target state estimates can be such information as the target's position, velocity, acceleration or other attributes. The successive estimates obtained from the target tracker yields the target tracks which describe the path/trajectory of the target.

Target tracking has found its place in a variety of applications including motion-based recognition, automated security, autonomous vehicles and robotics, oceanography, navigation and surveillance, medical imaging and biomedical research, traffic control, air traffic control, defence, space applications, remote sensing, computer vision and human–computer interaction [5, 9, 11, 26, 33, 85, 105–107, 132, 136].

The focus of current research and directions for future research in the field of engineering include targeted drug release and medicine absorption monitoring in the medical field, autonomous vehicles (land, aerial and underwater) for military,

surveillance and product delivery/shipping, space debris tracking for satellite asset launch and protection among others. In all these areas, target tracking capability is vital and having robust and efficient tracking algorithms would be of benefit.

1.2 Multi-Target Tracking

In the 1960's, prompted by aerospace applications, multi-target tracking (MTT) was originally employed for target tracking using radar measurements [5]. MTT concerns the problem of recursively and jointly estimating the state or trajectories of unknown and time-varying number of targets present in a tracking scene using sensor measurements. Single-target tracking (STT) is a special case of MTT [143] where there is only one target, that may or may not be detected by a sensor which additionally receives a random number of false measurements.

In an MTT setting, the target states or trajectories and the number of targets vary owing to appearance of new targets and disappearance of exiting targets. The multi-target tracker receives a random number of noisy measurements which could be miss-detections and/or false alarms. False alarms are detections whose origin is not one of the observed targets. Additionally, the multi-target tracker has to deal with target births and deaths and process measurements from multiple sensors.

To achieve MTT, a number of algorithms have been proposed and used. The most widely applied of these algorithms are the global nearest neighbour (GNN) [9, 26], the joint probabilistic data association (JPDA) filter [8, 9, 59], multiple hypothesis tracking (MHT) [25, 26] and random finite set (RFS) based multi-target filters [105, 106].

The GNN, JPDA and MHT techniques essentially rely on the same principle in that they basically keep multiple instances of single target filters for all possible objects. In other words, they require data association followed by single target filtering. The data association partitions the measurements into potential tracks and false alarms while filtering estimates the state of the target given its measurement history [5]. In MTT, this data association problem usually involves ensuring that the correct measurement is given to each stochastic filter so that the trajectories of

each target can be accurately estimated, this is referred to as measurement-to-track association. Once measurement-to-track association is achieved, single target trackers such as the Kalman filter or the particle filter are employed to achieve filtering. The RFS based methods however possess a desirable characteristic of avoiding data association and focuses on filtering by seeking optimal and suboptimal estimates of the multi-target state [5].

For completeness, the popular algorithms listed above are briefly described. The GNN is a refinement of a method called the nearest neighbour (NN) method. The GNN searches for the best global association, considering all targets and measurements simultaneously [9]. The JPDA filter [8, 59] is an extension of the probabilistic data association (PDA) filter [8, 59] (JPDA is for MTT while PDA is for STT). The JPDA filter uses the same recursion as in the PDA filter for propagating individual states, except for the calculation of the association probabilities. Joint association events and joint association probabilities are used in the JPDA filter in order to avoid conflicting measurement to track assignments in the presence of multiple targets. The MHT filter [9] adopts what can be called a deferred data association decision to achieve MTT. In MHT, the strategy is to mitigate association uncertainty at the current time step by searching over all previous time steps for all possible combinations of measurement to target associations that are likely to constitute target tracks or trajectories. This involves the creation of multiple hypotheses. A hypothesis is the exhaustive association or assignment of all measurements received, both past and present, to either a single track or as clutter. In each time step, the MHT filter attempts to maintain a small set of hypotheses with high posterior probability. When a new set of measurements arrives, a new set of hypotheses is created from the existing hypotheses and their posterior probabilities are updated according to Bayes rule.

The RFS approached proposed by Mahler is an emerging technique and provides a Bayesian framework for the recursive update of the multi-target posterior density. Under the RFS approach, the targets and the measurements at each time step are modelled as finite set-valued random variables. A framework is available for dealing with as well as characterising the relative uncertainties in an RFS

formulation by using the probabilistic tools of finite sets statistics (FISST) [105]. FISST facilitates an intuitive application of the random finite set theory to MTT applications by casting the problem into the familiar framework of Bayesian statistics [104].

1.3 Thesis Outline

The organisation and outline the outline of this thesis is as follows:

In Chapter 2, some of the key challenges of multiple target tracking are introduced. In addition, this chapter features a literature review of the different state-of-the-art techniques and approaches that have been used to address these challenges. This chapter further highlights some key drawbacks of these techniques.

In order to aid the reader with the background required for the understanding of multiple target tracking techniques, Chapter 3 presents key concepts and preliminaries on the concept of Bayesian target filtering, Kalman and particle filter, importance sampling and random finite sets.

In Chapter 4, a new and efficient sequential Monte Carlo probability hypothesis density filter is proposed. This new technique employs the Kalman-gain approach during weight update to correct predicted particle states by minimising the mean square error between the estimated measurement and the actual measurement received at a given time in order to arrive at a more accurate posterior. The technique identifies and selects those particles belonging to a particular target from a given PHD for state correction during weight computation. Besides the improved tracking accuracy, fewer particles are required in the proposed approach. Additionally, an improved resampling technique is developed. The new resampling method attempts to address a problem associated with systematic resampling. Simulation results confirm improved tracking performance offered by the newly developed tracking filter when evaluated with different measures.

Chapter 5 features the introduction of the cardinalised version of the Kalman-gain aided tracking filter of Chapter 4. The new approach not only propagates

the PHD but also the probability distribution of target number hence having a better estimate of the number of targets. Simulated data is used to demonstrate the performance improvement of this approach.

In Chapter 6, a game theoretic data association technique for multi-target tracking (MTT) with varying number of targets is investigated. The problem of target state-estimate-to-track data association has been considered. The KG-SMC-(C)PHD filter of Chapters 4 and 5 is used to handle the multiple target tracking aspect to obtain target state estimates. The interaction between target tracks is modelled as a game by considering the tracks as players and the set of target state estimates as strategies. Utility functions for the players are defined and a regret-based learning algorithm with a forgetting factor is used to find the equilibrium of the game. This technique is applied to both simulated and real radar measurements from a passive bi-static radar set up. Results from both the simulated data and the passive radar data demonstrates the effectiveness of the proposed method.

In Chapter 7, a technique for the joint tracking and labelling of multiple extended targets is investigated. To achieve multiple extended target tracking using this technique, models for the target measurement rate, kinematic component and target extension are defined and jointly propagated in time under the generalised labelled multi-Bernoulli filter framework. In particular, a Poisson mixture variational Bayesian model to simultaneously estimate the measurement rate of multiple extended targets was developed. In addition, a model for representing the extension of extended targets using B-splines is proposed. The proposed extended target tracker is evaluated with various performance metrics in order to demonstrate the effectiveness of the approach.

Finally, concluding remarks are drawn and possible future research challenges are discussed in Chapter 8.

1.4 Original Contributions

The contributions of this thesis are mainly on the improvement of the RFS based multi-target trackers used for both point and extended target tracking. The specific

contributions of each chapter are supported either by international journal and conference papers and are outlined below.

Chapter 4

This chapter features a novel particle PHD filter which applies a Kalman-gain based approach to achieve efficient multi-target filtering with reduced computational complexity. In addition, an improved resampling technique is presented to aid in PF methods implementation [45, 46].

1. **A. Daniyan**, Y. Gong, S. Lambotharan, P. Feng and J. Chambers, "Kalman-Gain Aided Particle PHD Filter for Multi-target Tracking," in *IEEE Transactions on Aerospace and Electronic Systems*, vol. 53, no. 5, pp. 2251-2265, Oct. 2017.

2. **A. Daniyan**, Y. Gong and S. Lambotharan, "An improved resampling approach for particle filters in tracking," *2017 22nd International Conference on Digital Signal Processing (DSP)*, London, 2017, pp. 1-5.

Chapter 5

This chapter presents the cardinalised version of the new particle PHD filter developed in the previous chapter. This cardinalised version gives a better estimate of the target number (cardinality).

3. **A. Daniyan**, Y. Gong and S. Lambotharan, "Multi-target Tracking Using the Kalman-Gain Particle CPHD Filter," 2017 (Submitted).

Chapter 6

A new technique for achieving data association using regret matching and game theory in a multi-target tracking context is developed. Furthermore, the technique is demonstrated on both simulated data and real passive radar data [43, 44].

4. **A. Daniyan**, Y. Gong and S. Lambotharan, "Game Theoretic Data Association for Multi-target Tracking with Varying Number of Targets," *2016 IEEE Radar Conference (RadarConf)*, Philadelphia, PA, 2016, pp. 1-4.

5. **A. Daniyan**, A. Aldowesh, Y. Gong and S. Lambotharan, "Data Association using Game Theory for Multi-target Tracking in Passive Bistatic Radar," *2017 IEEE Radar Conference (RadarConf)*, Seattle, WA, 2017, pp. 0042-0046.

Chapter 7

This chapter investigates the use of B-splines and a Poisson mixture variational Bayesian within the labelled random finite sets context for the joint target state estimation and track association of multiple extended targets in clutter.

6. **A. Daniyan**, A. Deligiannis, Y. Gong, and S. Lambotharan, "Bayesian Multiple Extended Target Tracking Using Labelled Random Finite Sets and Splines," *IEEE Transactions on Signal Processing*, 2017 (Submitted).

Chapter 2

Literature Review

2.1 Introduction

In this chapter, firstly, the challenges associated with MTT are discussed. This is then followed by a discussion on the relevant attempts to the solution of the MTT problem. This chapter also reviews certain drawbacks and limitations associated with these proposed solutions.

2.2 Challenges to Multi-Target Tracking

MTT has been attracting significant interests in many engineering applications. As a testimony to this fact, RFS based MTT methods have been used in many applications including [143] radar tracking [135, 149], acoustic source tracking [7, 115], sonar image tracking [39, 79], terrain tracking [127], network based defence [1], distributed systems tracking [134], vehicle tracking for automatic cruise control/automatic emergency braking [98], simultaneous localisation and mapping [110, 111], tracking for robot vision [77], tracking with graph matching [99], tracking with millimetre-wave images [73], tracking with target amplitude feature information [38] and sinusoidal components tracking in audio [37]. However, some issues that are fundamental to the successful realisation of a fully robust and efficient multi-target tracker in clutter still need further attention. These include:

i. State and target number estimation (for both point and extended targets)

ii. Data association

iii. Targets giving rise to more than one measurement per time step, and

iv. High computational demand

The tracking of targets in challenging environments can be complex as targets' motion and environment clutter become non-linear and non-Gaussian. The RFS approach to Bayesian MTT offers a systematic and rigorous approach which does not require the association of objects with measurements. To achieve detection and tracking in such scenarios, RFS based algorithms including the probability hypothesis density (PHD) and the cardinalised PHD (CPHD) filter, the multi-target multi-Bernoulli (MeMBer) filter and CMeMBer and the GLMB and LMB recursions are used. In general, these recursions are computationally intractable. However, the use of SMC or particle filtering methods provides suboptimal solution to these recursions. These filters by design are able to simultaneously perform state and target number estimation for point targets at a very high computational demand. However, to achieve robust target model representation and data association, further processing is required with an added computational load. Hence, it is desirable to have MTT algorithms that give high performance and accuracy at a significantly reduced computational demand.

In what follows, a literature review of the state-of-the-art methods used to address some of the MTT challenges mentioned.

2.2.1 Estimation of State and Number of Targets

Multi-target tracking belongs to a class of dynamic state estimation problems [11, 12, 25]. In MTT targets can appear and disappear randomly in time and this results in a varying and unknown number of targets and their corresponding states. Furthermore, not all measurements received by sensors at each time instance are due to existing targets. The sensor may pick up detections as false alarms due to clutter or may even miss some detections. As a result, the measurements received

at each time step are corrupted and consist of indistinguishable measurements that may be either target-originated or due to clutter. Therefore, the main objective of MTT is to jointly estimate target states and number of targets from a set of corrupted measurements.

Furthermore, because there is no particular ordering between measurements received and target states at each time step in terms of association; both the received measurements and target states can be represented as finite sets [102–105]. The modelling of target states and measurements as a RFS allows for the use of the Bayesian filtering approach (as an optimal multi-target filter) to estimate the multi-target states in the presence of clutter, missed detections and association uncertainty [102–105]. Tractable alternatives to the optimal multi-target filters include the RFS based PHD filter, CPHD filter [100, 103, 105], the MeMBer filter[1] and its cardinality-balanced version, the CBMeMBer filter [103, 105, 144]. Both the CPHD in [100] and the CBMeMBer in [144] have been shown to have better performance than the MeMBer filter in [105]. The CBMeMBer filter was proposed specifically to address the pronounced bias in the cardinality estimate of the MeMBer filter. More details on other tractable RFS based MTT methods can be found in [22, 113, 137, 138].

The PHD filter is a recursion that propagates the posterior intensity of the RFS of targets in time [102]. The integral of the PHD is the expected number of targets in a measurable region, and the peaks of the PHD function provide the estimates of the target states [100, 103, 105]. The PHD filter is able to track time varying multiple targets without the need to explicitly associate measurements to tracks. In the literature, the PHD filter has been implemented in two distinct fashions; that is, as the Gaussian mixture PHD (GM-PHD) filter [140] and the Sequential Monte Carlo PHD (SMC-PHD) filter [141]. In the GM-PHD filter implementation, the PHD is assumed to be a Gaussian mixture (GM) while in the SMC-PHD filter implementation, the PHD is approximated by a set of weighted particles and does

[1]The MeMBer filter is a recursion that propagates (approximately) the multi-target posterior density and is based on the assumption that every multi-target posterior is a multi-target multi-Bernoulli process [105, 144].

not need any further assumptions. The SMC-PHD filter is therefore more suitable for tracking in non-linear and non-Gaussian environments.

In SMC filter design, the choice of importance density function from which samples are drawn to avoid sample degeneracy and impoverishment is of crucial importance [55]. Furthermore, in MTT which involves multiple modalities, if particles are in clusters representing the modes of the posterior, the iterative process of randomly drawing samples from proposal distributions results in random fluctuations in the total weight attributed to each mode [108]. In addition, the errors associated with the estimation of the weights of each mode will increase in magnitude with time [108]. These errors arise due to the stochastic nature of drawing samples from the proposal distribution and the stochasticity of the resampling process [108]. These two processes greatly influence performance of SMC filters. SMC filters are further affected by how well the state space of targets is populated with samples. Also, [142] argued that the mean squared error (MSE) of the SMC-PHD filter is inversely proportional to number of samples. In [55], it is shown that the optimal importance density function is the posterior. In many cases it is difficult to sample from the optimal importance density. As an attempt to solve the importance sampling problem, [108] proposed using an optimised proposal distribution for SMC filters with multiple modes in general. However, this approach tends to be problem specific. In [148], the authors proposed the Gaussian mixture unscented sequential Monte Carlo probability hypothesis density (GM-USMC-PHD) filter which uses the Gaussian mixture representation to approximate the importance sampling function and the predictive density functions via the unscented information filter (UIF). Additionally, [14] and [146] proposed the auxiliary SMC-PHD (ASMC-PHD) filter and its improved version, the auxiliary particle PHD (AP-PHD) filter respectively. Both try to use the auxiliary particle approach to incorporate the measurement into the importance sampling function. This however involves double computation on the measurement and more samples are required to populate the state space in order to make the importance sampling function more viable.

However, it is also possible to construct suboptimal approximations to the optimal importance density by using local linearisation techniques [55]. As a realisation of this, the unscented Kalman particle PHD filter (UK-P-PHD) was proposed in [109] for the joint tracking of multi-targets. It tries to use the unscented Kalman filter (UKF) in the prediction step. This allowed for inclusion of the latest measurement to draw particles. Similarly, [96] proposed the Kalman particle PHD filter for multi-target visual tracking which uses the Kalman filter to construct the proposal density also in the prediction step. Furthermore, [133] presented an improvement to the SMC-PHD filter which incorporates the latest measurements into the resampling step by using the UKF.

Additionally, in the literature are the combined implementation of the GM and particle PHD filter as a GM particle PHD (GMP-PHD) filter in [36, 147] and [152] and the Gaussian mixture SMC-PHD (GM-SMC-PHD) in [114]. These methods attempt to combine the advantages of both GM-PHD and SMC-PHD filters. The methods give some level of performance improvement without easing computational burden or the number of particles. Also, it may be possible to implement the Markov Chain Monte Carlo (MCMC) sampling method in the update stage of the SMC-PHD filter as a way of asymptotically approximating the posterior. However, this approach will require even more particles, as these extra particles will be used to perform some sort of random walk in order to achieve maximum a posteriori estimate of target states, but no guarantees exist about it yielding good point estimates [82]. Recently, [153] proposed a data driven SMC-PHD filter for multi-target tracking. The method tries to segment the measurements available at each time step into measurements due to persistent targets and measurements due to new born targets. Again, this does not help reduce the number of particles but rather, more particles are required to populate regions of interest.

It is desirable therefore to have an efficient filter that can provide for particle state correction for any proposal distribution using fewer particles. This gives the motivation for the contributions of Chapters 4 and 5.

2.2.2 Data Association

In MTT, not all measurements received by sensors at each time instance are from existing targets. The sensor may pick up spurious detections due to clutter or may miss detections. As a result, the measurements received at each time step are corrupted and consist of indistinguishable measurements that may be either target-originated or due to clutter. It is therefore crucial in MTT to ascertain which measurement is due to which target. Data association deals with the problem of assigning measurements-to-target or target-state-estimates to individual target tracks [9, 10].

In solving the MTT problem, the most common methods are: i) those that try to avoid explicit association techniques [128], and ii) those that apply explicit data association techniques to assign measurements to each track [11]. Those MTT techniques that avoid explicit associations between measurements and tracks include the sparse-grid quadrature non-linear filter [78], multi-target particle filters [131] and RFS method [100, 103, 105]. In the second case, data association techniques are used to assign measurements to each track and a single target tracker [9, 103, 105] (for example the Kalman filter (KF) or the particle filter (PF)) is used for that track. In this setting, the number of targets needs to be known and fixed. Several techniques are used to achieve data association. The most common data association techniques include the nearest neighbour (NN) [9], the multiple hypothesis tracker (MHT) [9], and the joint probabilistic data association (JPDA) filter [9, 59]. In NN, at each time step, the predicted target state is associated with the closest measurement. MHT however keeps track of, and carries forward, all the association hypotheses to the next time step and aggregates them over time. The JPDA finds the association probabilities during each time update by considering all the targets and the measurements simultaneously and merging many hypotheses to form a single track hypothesis following a validation process. However, NN, MHT and JPDA algorithms are more suited to linear update/linear measurement and Gaussian uncertainty scenarios [34].

However, in complex MTT scenarios the target dynamics can be non-linear and even non-Gaussian. For such scenarios, [34] and [35] proposed a measurement-to-track data association for MTT using game theory. In their approach, a known and fixed number of targets was considered, and the aim was to use game theory to assign measurements to individual single target trackers. This approach however is constrained because the number of targets need to be known.

Having a data association technique robust to nonlinearity in target dynamics and non-Gaussian scenarios is the focus of Chapter 6.

2.2.3 Extended Target Tracking

In MTT, the aim is to jointly estimate the number and state of multiple targets present within a tracking volume while maintaining target tracks/history (data association). This problem becomes even more challenging in the face of missed detections, false alarms and noisy or corrupted measurements. The MTT problem can be addressed under a Bayesian formulation where models are used to relate unobserved states to measurements. A common representation of such models is to assume that one target produces one measurement per time step, for example, see [8] and [9]. This is often referred to as the *standard* measurement or *point target* model.

However, with the increasing advances in sensor technology, the proliferation of high-resolution sensors (for example, video cameras, phased array radars, ground or marine radar and laser range sensors) in recent years, size of the targets, or proximity between targets and sensor, can be such that the targets occupy multiple resolution cells of the sensor giving rise to more than one measurement per time step. Such targets are termed extended targets (ET). Therefore, the point target assumption does no longer hold in such scenarios. Scenarios where ETs may appear include using marine or ground radar to track sufficiently close ships or aeroplanes, using automotive radar for vehicle tracking or using laser range sensors for person tracking [95]. Besides, modern applications require extensive and detailed physical information about targets to achieve tasks including target detection, tracking,

classification, recognition and identification. In such cases, the idea of ET becomes even more appealing and useful. Additionally, applications that require tracking a group of closely spaced targets in formation can benefit from the ET formulation [88]. This is because the knowledge of the size, shape, and orientation of the group formation can be crucial in practical applications where recognition and classification are of importance [88]. Hence, target extension model and other information (for example, kinematics) for ETs are required for tracking application.

When considering ET measurement models, two main aspects are usually required and these are i) a model to describe the number of measurements generated by each ET; ii) a model to capture the target's spatial distribution. These two components however depend very much on the type of ET being tracked. For instance, a target (for example, radar target) can generate measurements from different scatter points. Another target type may generate just a few measurements around a scatter point [20]. In any case, the measurements from an ET can be considered to be such that the detections are geometrically structured.

As for modelling the number of measurements generated by an ET, the authors in [61] and [62] proposed one such model where the number of ET measurements are modelled as an inhomogeneous Poisson distribution characterised by a rate parameter. Knowledge on the distribution of measurements and acquiring a good estimate of the measurement rate parameter especially in the case of spatially close extended targets are important to improve performance [64]. The work in [67] proposed a recursive Bayesian method with exponential forgetting factor to estimate the measurement rate. However, this method has two limitations. This method requires choosing an appropriate window size for the forgetting factor as this is application dependent.

With regards to modelling the target extent (i.e. shape and size) of an ET, this is possible even in the absence of a specific target structure. This can be achieved for example by methods including: i) assuming some general parametric shape such as an ellipse or a rectangle (see for example, [2, 16, 49, 68, 69, 84, 88, 118, 119, 126, 154]) or ii) assuming an arbitrary shape for the ET (see for example, [18, 30, 70, 75, 86, 87, 94, 145]). For the first approach mentioned (that is,

assuming a general parametric shape), the most common technique used is the random matrix method proposed in [84] where the ET extension was modelled as a symmetric positive definite matrix (the ET is assumed to be elliptical). This method has been applied in various scenarios in both LIDAR and marine radar tracking (see for example, [65] and [66]). However, this method has limitations as its performance depends inherently on the elliptic shape assumption. As for the approach were the ET shape is assumed to be arbitrary, one of the most common techniques used in the literature is the star-convex method. This method is based on the random hypersurface model (RHM) proposed in [15] and [17] or its alternative, the Gaussian process model of [75] and [145]. Although this approach provides a systematic way to model different target shapes from ellipses [16] to arbitrary star-convex shapes [18], it does so at the expense of increased computational cost.

Once the ET measurement model has been defined, a multi-object tracker can be implemented together with the ET measurement model to perform state and target number estimation under the Bayesian formulation. Among the promising techniques available in the literature to achieve this are the RFS based methods and the non-RFS based methods. Techniques for achieving ET MTT include use of the PHD filter (see for example, [66, 68, 101, 151]) and CPHD filter (see for example, [90, 95, 112]). The PHD filter recursively estimates the first order moment (intensity function) of a random finite set [105] while the CPHD filter, in addition to estimating the PHD of an RFS, estimates a truncated cardinality distribution. It provides a better cardinality estimate as compared to the PHD filter [6]. The cardinality-balanced multi-target multi-Bernoulli (CB-MeMBer) filter was proposed specifically to address the pronounced bias in the cardinality estimate of the MeMBer filter [105, 144]. The CB-MeMBer filter which is a recursion that propagates (approximately) the multi-target posterior density and is based on the assumption that every multi-target posterior is a multi-target multi-Bernoulli process is also RFS based and has been used in ET MTT (see for example, [93, 150]). However, the PHD, CPHD and CB-MeMBer filters do not formally estimate target trajectories (perform data association) in their basic forms.

A post processing step is required to achieve this. To alleviate this problem, the generalised labelled multi-Bernoulli (GLMB) filter [138] and its computationally efficient version the labelled multi-Bernoulli (LMB) filter [117] were proposed, all under the RFS framework. In their approach, they assign distinct labels to each element of the target set, so that trajectory history of each object can be naturally identified, without the need for post-processing. The GLMB filter in [138] and [137] was for solving the multi-object tracking problem under the standard point-detection likelihood model (that is, when targets generate at most one measurement per time step. Both filters can in addition to recursively estimating the target state and the number of targets, provide track association histories (data association).

As a proposed solution to ET MTT, both the GLMB filter [138] and the LMB filter [137] have been used to achieve ET MTT [20] and [21]. Recently, the authors in [20] and [21] proposed a method to achieve this through a recursive Bayesian rate estimator to compute the measurement rate of each target individually and sequentially. The authors used the random matrix approach to model the target extent and formulated expressions for achieving ET MTT under the framework of GLMB and LMB. This approach requires pre-setting a window size to perform the measurement rate estimation based on the rate estimation method proposed in [67]. The authors in [67] noted that the choice of the window size affects how fast or slow the estimated rate by their method changes to the true rate parameter. This requirement may mean parameter tuning to obtain the right window size in some applications. The ET extension model in this approach is restrictive in that not all ET can be modelled using the elliptical shape.

It is therefore desirable to have an ET multi-target tracker capable of incorporating models of measurement rate and target extent of arbitrary targets into a tracker that can estimate extended target states, number of targets and maintain track association in order to achieve improved tracking performance. This possibility is investigated in Chapter 7.

2.3 Summary

This chapter highlighted certain issues associated with MTT. In addition, the chapter presented a literature review of the cutting-edge techniques to addressing the MTT problem. Furthermore, some of the restrictions and limitations of these existing techniques were highlighted thereby paving way for the various contributions of this thesis.

The next chapter discusses some fundamental signal processing and mathematical concepts that are key to understanding the MTT problem.

Chapter 3

Key Concepts and Preliminaries of Target Tracking

In this chapter, some key concepts that are fundamental to the idea of MTT are presented and discussed. Specifically, the idea of Bayesian target estimation, that is, the Bayesian single/multi-object filter is introduced. This is followed by a discussion on optimal and suboptimal solutions to the Bayesian filter. Under the optimal category, the Kalman filter and the extended Kalman filter are presented. Under the suboptimal category, firstly, the idea of importance sampling is described followed by a description of the particle filter and its implementation. Thirdly, the random finite sets concept is introduced along with the mathematical framework used to handle random finite sets. This is followed by an introduction to the random finite sets-based probability hypothesis density and its particle implementation. Also featured in this chapter is the idea of labelled random finite sets.

3.1 Bayesian Target Estimation

The MTT problem relates to that of modelling a dynamical system. Two models are generally used, the state evolution model and the measurement model.

State Model

A non-linear system governed by the state evolution model is considered:

$$\mathbf{x}_k = \mathbf{f}_{k-1}(\mathbf{x}_{k-1}, \mathbf{v}_k), \tag{3.1}$$

where $\mathbf{x}_k$ denotes the m-th target state at discrete time k, $\mathbf{v}_k$ is an independent and identically distributed (i.i.d.) process noise vector and $\mathbf{f}_k(\cdot)$ is the nonlinear system transition function. Then the multi-target state at time k can be written as

$$\mathbf{X}_k = \{\mathbf{x}_{1,k}, ..., \mathbf{x}_{M,k}\} \in E_s, \tag{3.2}$$

where M is the number of targets present at each time k, and E_s denotes the state space.

Measurement Model

Let the multi-target cumulative measurement set upto time K be $\boldsymbol{Z}_K = \{\mathbf{Z}_1, \mathbf{Z}_2, ..., \mathbf{Z}_K\} \in E_o$. Measurements consist of both target-originated measurements and false alarms due to clutter. Then the multi-target measurement set at time k in the measurement space is:

$$\boldsymbol{Z}_k = \{\mathbf{z}_{1,k}, ..., \mathbf{z}_{\alpha,k}\} \bigcup \{\mathbf{c}_{1,k}, ...\mathbf{c}_{\beta,k}\} \in E_o, \tag{3.3}$$

where α denotes the number of target-originated measurements, β denotes the number of false measurements and E_o denotes the measurement space. The m-th target-originated non-linear measurement model is given as:

$$\mathbf{z}_k = \mathbf{h}_k(\mathbf{x}_k, \mathbf{n}_k), \tag{3.4}$$

where $\mathbf{h}_k(\cdot)$ is a nonlinear function, and $\mathbf{n}_k$ is an i.i.d. process noise vector.

3.1.1 Single Target Bayes Filter

The Bayesian approach to target tracking involves recursively computing the posterior distribution using two stages known as the *prediction* and *update* stages [47]. The prediction stage uses the system model to predict the state probability density function (pdf) forward from one measurement time to the next. While the update operation uses the latest measurement to modify the prediction pdf. It may be recalled from Bayes' theorem that given the likelihood and prior, the posterior can be computed. The tracking problem from a Bayesian perspective is to calculate recursively some degree of belief in the state $\mathbf{X}_k$ at time k. Assuming that the required pdf at time $k-1$, $p(\mathbf{x}_{k-1}|\mathbf{z}_{1:k-1})$ is available, using the system model in (3.1), the prediction stage requires computing the prior pdf at time k using the Chapman-Kolmogorov equation [3]

$$p(\mathbf{x}_k|\mathbf{z}_{1:k-1}) = \int p(\mathbf{x}_k|\mathbf{x}_{k-1})p(\mathbf{x}_{k-1}|\mathbf{z}_{1:k-1})d\mathbf{x}_{k-1}. \tag{3.5}$$

The fact that $p(\mathbf{x}_k|\mathbf{x}_{k-1}, \mathbf{z}_{1:k-1}) = p(\mathbf{x}_k|\mathbf{x}_{k-1})$ has been made use of in (3.5) above since (3.1) describes a Markov process of order one.

The update stage is where the posterior, $p(\mathbf{x}_k|\mathbf{z}_{1:k})$ is computed. This requires updating the $prior$ at time k when a measurement $\mathbf{z}_k$ becomes available. Applying Bayes' rule,

$$p(\mathbf{x}_k|\mathbf{z}_{1:k}) = \frac{p(\mathbf{z}_k|\mathbf{x}_k)p(\mathbf{x}_k|\mathbf{z}_{k-1})}{p(\mathbf{z}_k|\mathbf{z}_{k-1})}, \tag{3.6}$$

where

$$p(\mathbf{z}_k|\mathbf{z}_{k-1}) = \int p(\mathbf{z}_k|\mathbf{x}_k)p(\mathbf{x}_k|\mathbf{z}_{k-1})d\mathbf{x}_{k-1}, \tag{3.7}$$

is the normalising constant. The reoccurring relation of (3.5) and (3.6) gives rise to the $optimal\ Bayesian\ solution$. The optimal Bayesian solution solves the problem of recursively calculating the exact posterior density. The recursive propagation nature of the posterior density is a solution that is conceptual due to the fact

that in general, it cannot be analytically determined [3]. Techniques are however available as analytical solutions to the optimal Bayesian solution.

An optimal technique is an algorithm which analytically solves the optimal Bayesian solution. An example of such a method is the Kalman filter (KF) [3]. More on how the KF solves the optimal Bayesian solution is discussed in this chapter. The analytical solution to the Bayesian solution can become intractable. When this happens, approximation techniques to the optimal Bayesian solution are required. A $suboptimal\ Bayesian\ solution$ is a technique or algorithm that approximates the optimal Bayesian solution. Such techniques include the extended Kalman filter (EKF) and sequential Monte Carlo (SMC) methods [3].

3.1.2 Multi-Target Bayes Filter

In Bayesian multi-target estimation, the aim is to recursively estimate at each time k (using the *prediction* and *update* stages) the state of multi-targets $\mathbf{X}_k \subset \mathbb{X}$.

In the *prediction* stage, the multi-target state at time $k-1$ is assumed to be distributed according to the density $p_{k-1}(\cdot|\mathbf{Z}_{1:k-1})$, with $\mathbf{Z}_{1:k-1}$ denoting an array of finite sets of measurements received up to and including time $k-1$. Each $\mathbf{Z}_k$ is assumed to be generated through a process of thinning of mis-detected objects, Markov shifts of detected objects, and superposition of false measurements. The multi-target prediction to time k given $k-1$ is given by the Chapman-Kolmogorov equation

$$p_{k|k-1}(\mathbf{X}_k|\mathbf{Z}_{1:k-1}) = \int f_{k|k-1}(\mathbf{X}_k|\mathbf{X}_{k-1}) p_{k-1}(\mathbf{X}_{k-1}|\mathbf{Z}_{1:k-1}) \delta\mathbf{X}_{k-1}, \tag{3.8}$$

where $f_{k|k-1}(\cdot|\cdot)$ is the multi-target transition kernel, and the integral is the set integral [105],

$$\int f(X)\delta X = \sum_{i=0}^{\infty} \frac{1}{i!} \int_{\mathbb{X}^i} f(\{x_1, \cdots, x_i\}) d(x_1, \ldots, x_i). \tag{3.9}$$

At time k, a new set of measurements $\mathbf{Z}_k$ is available and modelled by a multi-target likelihood function $g_k(\mathbf{Z}_k|X_k)$. Thus, the *update* stage involves computing

the multi-target posterior at time k given by Bayes rule

$$p_k(\mathbf{X}_k|\mathbf{Z}_{1:k}) = \frac{g_k(\mathbf{Z}_k|\mathbf{X}_k)p_{k|k-1}(\mathbf{X}_k|\mathbf{Z}_{1:k-1})}{\int g_k(\mathbf{Z}_k|\mathbf{X})p_{k|k-1}(\mathbf{X}|\mathbf{Z}_{1:k-1})\delta\mathbf{X}}. \tag{3.10}$$

Both (3.8) and (3.10) above collectively form the multi-target Bayes filter. However, computing the exact multi-target posterior (that is, (3.10)) is in general numerically intractable, and therefore approximations are required in order to derive practical algorithms [105].

3.2 The Kalman Filter

The Kalman filter (KF) can be thought of as a sequential minimum mean square error (MMSE) estimator of a given signal that is embedded in noise, where the signal is characterised by a state model [81].

In order to implement the KF as an optimal Bayesian solution to the tracking problem and using the models in Section 3.1.1 the following highly restrictive assumptions must hold [3, 81]:

1. Both the state and measurement models of (3.1) and (3.4) must be linear, and

2. The posterior density of any target $\mathbf{x}_k$ at every time step k must be Gaussian.

From assumption 2 above, the posterior can then be characterised by a mean and covariance. And if $p(\mathbf{x}_{k-1}|\mathbf{z}_{1:k-1})$ is Gaussian, it can also be proven that $p(\mathbf{x}_k|\mathbf{z}_{1:k})$ is also Gaussian given that $\mathbf{n}_k$ and $\mathbf{v}_k$ are drawn from a Gaussian distribution with known parameters [3].

Following assumption 1 above, the state and measurement models of (3.1) and (3.4) can consequently be rewritten thus:

$$\mathbf{x}_k = \mathbf{F}_k\mathbf{x}_{k-1} + \mathbf{v}_k, \tag{3.11}$$

$$\mathbf{z}_k = \mathbf{H}_k\mathbf{x}_k + \mathbf{n}_k, \tag{3.12}$$

$\mathbf{F}_k$ and $\mathbf{H}_k$ are matrices that define the linear function and are known as state transition matrix and transformation matrix respectively. The covariance matrices of $\mathbf{n}_k$ and $\mathbf{v}_k$ are $\mathbf{C}_k$ and $\mathbf{Q}_{k-1}$respectively; $\mathbf{n}_k$ and $\mathbf{v}_k$ have zero mean and statistically are independent.

The prior, $p(\mathbf{x}_{k-1}|\mathbf{z}_{1:k-1})$, posterior given measurement up to time $k-1$, $p(\mathbf{x}_k|\mathbf{z}_{1:k-1})$, and posterior given measurement up to time k $p(\mathbf{x}_k|\mathbf{z}_{1:k})$, can now be determined as:

$$p(\mathbf{x}_{k-1}|\mathbf{z}_{1:k-1}) = \mathcal{N}(\mathbf{x}_{k-1}; \mathbf{s}_{k-1|k-1}, \mathbf{M}_{k-1|k-1}), \tag{3.13}$$

$$p(\mathbf{x}_k|\mathbf{z}_{1:k-1}) = \mathcal{N}(\mathbf{x}_k; \mathbf{s}_{k|k-1}, \mathbf{M}_{k|k-1}), \tag{3.14}$$

$$p(\mathbf{x}_k|\mathbf{z}_{1:k}) = \mathcal{N}(\mathbf{x}_k; \mathbf{s}_{k|k}, \mathbf{M}_{k|k}), \tag{3.15}$$

where $\mathcal{N}(x; \mathbf{s}, \mathbf{M})$ denotes a Gaussian density with argument x, mean $\mathbf{s}$ and covariance $\mathbf{M}$,

$$\mathbf{s}_{k|k-1} = \mathbf{F}_k \mathbf{s}_{k-1|k-1}, \tag{3.16}$$

$$\mathbf{M}_{k|k-1} = \mathbf{Q}_{k-1} + \mathbf{F}_k \mathbf{M}_{k-1|k-1} \mathbf{F}_k^T, \tag{3.17}$$

$$\mathbf{s}_{k|k} = \mathbf{s}_{k|k-1} + \mathbf{K}_k(\mathbf{z}_k - \mathbf{H}_k \mathbf{s}_{k|k-1}), \tag{3.18}$$

$$\mathbf{M}_{k|k} = \mathbf{M}_{k|k-1} - \mathbf{K}_k \mathbf{H}_k \mathbf{M}_{k|k-1}, \tag{3.19}$$

where

$$\mathbf{P}_k = \mathbf{H}_k \mathbf{M}_{k|k-1} \mathbf{H}_k^T + \mathbf{C}_k, \tag{3.20}$$

$$\mathbf{K}_k = \mathbf{M}_{k|k-1} \mathbf{H}_k^T \mathbf{P}_k^{-1}, \tag{3.21}$$

and $\mathbf{P}_k$ is covariance of the innovation term $\mathbf{z}_k - \mathbf{H}_k \mathbf{s}_{k|k-1}$, with $\mathbf{K}_k$ being the Kalman gain. For a matrix $\mathbf{B}$, $\mathbf{B}^T$ is its transpose.

The KF algorithm to analytically solve the optimal Bayesian solution can now be formulated thus:

Prediction

$$\begin{aligned}
\mathbf{s}_{k|k-1} &= \mathbf{F}_k \mathbf{s}_{k-1|k-1}, \\
\mathbf{M}_{k|k-1} &= \mathbf{Q}_{k-1} + \mathbf{F}_k \mathbf{M}_{k-1|k-1} \mathbf{F}_k^T, \\
\mathbf{P}_k &= \mathbf{H}_k \mathbf{M}_{k|k-1} \mathbf{H}_k^T + \mathbf{C}_k, \\
\mathbf{K}_k &= \mathbf{M}_{k|k-1} \mathbf{H}_k^T \mathbf{P}_k^{-1},
\end{aligned}$$

Update

$$\begin{aligned}
\mathbf{s}_{k|k} &= \mathbf{s}_{k|k-1} + \mathbf{K}_k(\mathbf{z}_k - \mathbf{H}_k \mathbf{s}_{k|k-1}), \\
\mathbf{M}_{k|k} &= \mathbf{M}_{k|k-1} - \mathbf{K}_k \mathbf{H}_k \mathbf{M}_{k|k-1}.
\end{aligned}$$

With the above recursive algorithm and the earlier restrictive assumptions, no algorithm can do better than KF in a linear environment [3]. When either of the two assumptions do not hold, the KF solution becomes intractable, and therefore an approximation to the optimal Bayesian solution is required [47].

3.2.1 Extended Kalman Filter

The extended Kalman filter (EKF) is an extension of the KF. The algorithm tries to approximate the optimal Bayesian solution; hence it is a suboptimal Bayesian solution.

The technique is used when either or both the state and measurement models of (3.1) and (3.4) are non-linear but assumption 2 for the KF above still holds. When this is the case, (3.11) and (3.12) will no longer hold and therefore a local linearisation of (3.11) and (3.12) will be required to describe the non-linearity. The EKF is based on this approximation and (3.13), (3.14), and (3.15) become:

$$p(\mathbf{x}_{k-1}|\mathbf{z}_{1:k-1}) \approx \mathcal{N}(\mathbf{x}_{k-1}; \mathbf{s}_{k-1|k-1}, \mathbf{M}_{k-1|k-1}), \tag{3.22}$$

$$p(\mathbf{x}_k|\mathbf{z}_{1:k-1}) \approx \mathcal{N}(\mathbf{x}_k; \mathbf{s}_{k|k-1}, \mathbf{M}_{k|k-1}), \tag{3.23}$$

$$p(\mathbf{x}_k|\mathbf{z}_{1:k}) \approx \mathcal{N}(\mathbf{x}_k; \mathbf{s}_{k|k}, \mathbf{M}_{k|k}), \tag{3.24}$$

where

$$\mathbf{s}_{k|k-1} = \mathbf{f}_k(\mathbf{s}_{k-1|k-1}), \tag{3.25}$$

$$\mathbf{M}_{k|k-1} = \mathbf{Q}_{k-1} + \hat{\mathbf{A}}_k \mathbf{M}_{k-1|k-1} \hat{\mathbf{A}}_k^T, \tag{3.26}$$

$$\mathbf{s}_{k|k} = \mathbf{s}_{k|k-1} + \mathbf{K}_k(\mathbf{z}_k - \mathbf{h}_k(\mathbf{s}_{k|k-1})), \tag{3.27}$$

$$\mathbf{M}_{k|k} = \mathbf{M}_{k|k-1} - \mathbf{K}_k \hat{\mathbf{H}}_k \mathbf{M}_{k|k-1}, \tag{3.28}$$

and $\mathbf{f}_k(.)$ and $\mathbf{h}_k(.)$ are non-linear functions, $\hat{\mathbf{A}}_k$ and $\hat{\mathbf{H}}_k$ are local linearisations of the non-linear functions. The matrices are defined below:

$$\hat{\mathbf{A}}_k = \left.\frac{d\mathbf{f}_k(x)}{dx}\right|_{\mathbf{x}=\mathbf{s}_{k-1|k-1}}, \tag{3.29}$$

$$\hat{\mathbf{H}}_k = \left.\frac{d\mathbf{h}_k(x)}{dx}\right|_{\mathbf{x}=\mathbf{s}_{k|k-1}}, \tag{3.30}$$

$$\mathbf{P}_k = \hat{\mathbf{H}}_k \mathbf{M}_{k|k-1} \hat{\mathbf{H}}_k^T + \mathbf{C}_k, \tag{3.31}$$

$$\mathbf{K}_k = \mathbf{M}_{k|k-1} \hat{\mathbf{H}}_k^T \mathbf{P}_k^{-1}. \tag{3.32}$$

The first term in a Taylor series expansion of the non-linear function is used in the EKF as described above. A recursive implementation of the EKF becomes:
$Prediction$

$$\begin{aligned}
\mathbf{s}_{k|k-1} &= \mathbf{f}_k(\mathbf{s}_{k-1|k-1}), \\
\mathbf{M}_{k|k-1} &= \mathbf{Q}_{k-1} + \hat{\mathbf{A}}_k \mathbf{M}_{k-1|k-1} \hat{\mathbf{A}}_k^T, \\
\mathbf{P}_k &= \hat{\mathbf{H}}_k \mathbf{M}_{k|k-1} \hat{\mathbf{H}}_k^T + \mathbf{C}_k, \\
\mathbf{K}_k &= \mathbf{M}_{k|k-1} \hat{\mathbf{H}}_k^T \mathbf{P}_k^{-1},
\end{aligned}$$

$Update$

$$s_{k|k} = s_{k|k-1} + \mathbf{K}_k(\mathbf{z}_k - \mathbf{h}_k(s_{k|k-1})),$$
$$\mathbf{M}_{k|k} = \mathbf{M}_{k|k-1} - \mathbf{K}_k\hat{\mathbf{H}}_k\mathbf{M}_{k|k-1},$$

Since the EKF depends on the linearisation of the KF, its performance depends on the accuracy of this linearisation and therefore has no optimality properties [81].

3.3 The Particle Filter

Sequential Monte Carlo (SMC) or particle filtering (PF) methods have proven useful within the past couple of decades in handling target tracking, especially when the measurements are represented by nonlinear state-space models with non-Gaussian noise models. The PF has been known by such names as: particle filter [32], survival of the fittest [80], condensation algorithm [97], sequential importance sampler [3], multinomial filter [63], and the interacting particle approximations filter [41, 50]. The filter achieves recursive Bayesian filtering through implementing MC simulations. The PF method has been applied in a diverse range of disciplines including control, wireless communications, surveillance, defence, space applications, oceanography, finance, autonomous vehicles, robotics, remote sensing, computer vision and biomedical research, see for example [3, 9, 26, 31, 33, 51, 55, 56, 85, 105–107, 132]. The main advantage of SMC methods lies in their ability to approximate states of non-linear dynamical models and non-Gaussian noise [54, 55].

When PF methods are used, for example in tracking applications, the goal is to track and estimate various distributions that emerge in the dynamic state-space models [89]. To this end, randomly generated samples (*particles*) are used to explore the states of the space. The generated samples along with associated weights are then used to approximate the distributions of interest [89].

The main idea in PF is to represent the required posterior density function with a weighted set of random samples and then compute estimates based on these samples and their weights [121].

3.3.1 PF Implementation

A set of particle $\{\mathbf{x}_k^i\}_{i=1}^{N_s}$ are introduced to represent the conditional state probability given by $p(\mathbf{x}_k|\mathbf{z}_{1:k})$. Each particle represents a potential state for the object [3].

$$p(\mathbf{x}_k|\mathbf{z}_{1:k}) \approx \sum_{i=1}^{N_s} w_k^i \delta(\mathbf{x}_k - \mathbf{x}_k^i), \tag{3.33}$$

where N_s is the number of particles at time instance k centred around $\mathbf{x}_k^i$ and w_k^i represents the particle weights. More weight is given to particles of more importance. The particles are sampled from an importance density $q(\mathbf{x}_k|\mathbf{x}_{k-1}^i, \mathbf{z}_k)$. More details on importance sampling are given in the next section. A new filtering distribution is approximated by a new set of particles with an importance weight which is given as:

$$w_k^i \propto \frac{p(\mathbf{z}_k|\mathbf{x}_k^i)p(\mathbf{x}_k^i|\mathbf{x}_{k-1}^1)}{q(\mathbf{x}_k|\mathbf{x}_{k-1}^i, \mathbf{z}_k)}. \tag{3.34}$$

In the prediction step of the PF, new particles are estimated by propagating the old samples $\left\{\mathbf{x}_{k-1}^i, w_{k-1}^i\right\}_{i=1}^{N_s}$ through the state space model. The correction step calculates the weights corresponding to the new samples. The samples are resampled each time the 'effective' number of importance weights $\hat{N}_{eff}$ falls below a predetermined threshold value.

$$\hat{N}_{eff} = \frac{1}{\sum_{i=1}^{N_s} \left(w_k^i\right)^2}. \tag{3.35}$$

The resampling is done such that particles with high weights are redistributed across the state space replacing particles with low weights to form the new state space. The new particles are then assigned equal weights. Once new samples have been obtained the estimated target location can be computed by taking the

expectation over the weighted samples.

$$\mathbb{E}\left[p(\mathbf{x}_k|\mathbf{z}_{1:k})\right] = N_s^{-1}\sum_{i=1}^{N_S} w_k^i \mathbf{x}_k^i. \tag{3.36}$$

The recursion then proceeds to the next time step $k+1$. A common problem associated with the PF is the degeneracy phenomenon, where after a few iterations, all but one particle will have negligible weight. Resampling techniques are however available to handle this [121] (see Section 4.4 for details.). Another important point to note is the choice of importance density to sample from. A wrong choice may lead to convergence issues with the filter [121]. A common choice of the importance density is to use the prior

$$q(\mathbf{x}_k|\mathbf{x}_{k-1}^i, \mathbf{z}_k) = p(\mathbf{x}_k|\mathbf{x}_{k-1}^i) \tag{3.37}$$

3.4 The Importance Density Function

In this section the focus is on proposal distributions and their role in SMC methods in general.

3.4.1 Importance Sampling

Monte Carlo (MC) methods for numerical integration deal with problems of the form

$$g = \int_{\Re^n} f(\mathbf{y})\pi(\mathbf{y})d\mathbf{y} \tag{3.38}$$

where $\pi(\mathbf{y})$ is such that $\pi(\mathbf{y}) \geq 0$ and integrates to unity,

$$\int_{\Re^n} \pi(\mathbf{y})d\mathbf{y} = 1 \tag{3.39}$$

is a pdf.

It is also the assumption that it is possible to generate $N \gg 1$ samples distributed according to the probability density $\pi(\mathbf{y})$. The MC estimate of the integral (3.38)

is formed by taking the average over the set of samples

$$\hat{g} = \frac{1}{N}\sum_{i=1}^{N} f(\mathbf{y}_i) \tag{3.40}$$

where N is assumed to be large. However, $\pi(\mathbf{y})$ is not usually a familiar density and so it is difficult to generate samples directly from it. When the latter is the case, the integral of (3.38) can be solved by letting $q(\mathbf{y})$ be a *proposal distribution* or *importance density* which is easy to generate samples and with the assumption that $\pi(\mathbf{y}) > 0 \Rightarrow q(\mathbf{y}) > 0$ for all $\mathbf{y} \in \Re^n$. Under this assumption, (3.38) becomes:

$$g = \int_{\Re^n} f(\mathbf{y})\pi(\mathbf{y})d\mathbf{y} = \int_{\Re^n} f(\mathbf{y})\frac{\pi(\mathbf{y})}{q(\mathbf{y})}q(\mathbf{y})d\mathbf{y} \tag{3.41}$$

An MC estimate is then computed by generating $N \gg 1$ samples from $q(\mathbf{y})$ instead of $\pi(\mathbf{y})$ and forming a weighted sum

$$\hat{g} = \frac{1}{N}\sum_{i=1}^{N} f(\mathbf{y}_i)w(\mathbf{y}_i), \tag{3.42}$$

where $w(\mathbf{y}_i) \propto \frac{\pi(\mathbf{y}_i)}{q(\mathbf{y}_i)}$ are the associated weights [23]. To sum up, importance sampling makes it possible to sample, with associated weights, from a distribution, $\pi(\mathbf{y})$ difficult to sample from by sampling from an alternate distribution, $q(\mathbf{y})$ known as the proposal distribution.

3.4.2 Importance Densities

Some common choices of importance density in SMC methods are given below:

3.4.2.1 The Transitional Prior (TP)

This is the most popular choice of suboptimal proposal distribution for SMC-PHD filters and particle filters in general because its implementation is easy and straightforward [121]. This choice requires sampling from the dynamic prior,

$$q(\mathbf{x}_k|\mathbf{x}_{k-1}^l, \mathbf{z}_k) = p(\mathbf{x}_k|\mathbf{x}_{k-1}^l) \tag{3.43}$$

3.4.2.2 Extended Particle Filter (EPF)

Given that the measurement model of (3.4) is non-linear, but Gaussian, it is possible to use a proposal distribution that exploits a linear approximation to the posterior [108] in the same way as the extended Kalman filter uses a local linearisation about its estimates. The proposal distribution is then given as:

$$q(\mathbf{x}_k|\mathbf{x}_{k-1}^l, \mathbf{z}_k) = \mathcal{N}(\mathbf{x}_k; \mathbf{u}_k, \mathbf{A}_k) \tag{3.44}$$

where

$$\mathbf{u}_k = \mathbf{f}_{k-1}(\mathbf{x}_{k-1}) + \mathbf{A}_k\mathbf{H}_k^T\mathbf{R}_k^{-1}(\mathbf{z}_k - \mathbf{h}(\mathbf{f}_{k-1}(\mathbf{x}_{k-1}))) \tag{3.45}$$

$$\mathbf{H}_k = \left.\frac{\partial \mathbf{h}}{\partial \mathbf{x}_k}\right|_{\mathbf{f}_{k-1}(\mathbf{x}_{k-1})} \tag{3.46}$$

where $\mathbf{A}_k$ and $\mathbf{R}_k$ denote state and measurement covariances respectively, and $\mathbf{H}_k$ is the measurement transformation matrix.

3.4.2.3 Unscented Particle Filter (UPF)

As an alternative to the EPF, an unscented transform can be used to calculate the mean $\mathbf{h}(\mathbf{f}_{k-1}(\mathbf{x}_{k-1}))$ and covariance $\mathbf{H}_k$ by generating sigma points and applying a transform such that the new generated samples have $\mathbf{f}_{k-1}(\mathbf{x}_{k-1})$ as mean and $\mathbf{P}_{k-1}$ as covariance. $\mathbf{h}(\mathbf{f}_{k-1}(\mathbf{x}_{k-1}))$ is then evaluated at each sigma point and $\mathbf{H}_k$ is computed from these samples [108].

3.5 Random Finite Sets

In the multi-target case, varying number of targets are present. Moreover, the targets can appear and disappear randomly in the state-space. $\mathbf{X}_k$ of (3.2) holds for all targets present in the state space E_S at time step k and $\mathbf{Z}_k$ in (3.3) holds for all measurements received in the measurement space E_O at time k. However, some measurements $\mathbf{z}_{k,j} \in \mathbf{Z}_k$ may not necessarily originate from $\mathbf{x}_{k,i} \in \mathbf{X}_k$ and may be

due to clutter. Such spurious measurements can be modelled using specific clutter models [102].

A Random finite set (RFS) Ξ is a finite-set valued random variable, which can be described by a discrete probability distribution and a family of joint probability densities [102, 105, 103]. RFS are models used to represent the uncertainty about the number of elements in multiple target state $\mathbf{X}_k$ and measurement state $\mathbf{Z}_k$ [102, 105, 103]. With an RFS formulation, both the multi-target states X_k and multi-target measurements $Z_k \subset \mathbb{Z}$ are modelled as RFS. A framework for dealing with RFSs is known as finite sets statistics [105] which is based on the notion of integration/density that is consistent with point process theory [142].

Consider $\Gamma_k = \left\{\mathbf{X}_{1,(k)}, \mathbf{X}_{2,(k)}, ..., \mathbf{X}_{M,(k)}\right\}$, where M is the total number of targets present at time k; and

$$\mathbf{X}_k = \boldsymbol{S}_k(\mathbf{X}_{k-1}) \bigcup \boldsymbol{B}_k(\mathbf{X}_{k-1}) \tag{3.47}$$

where $\boldsymbol{S}_k(\mathbf{X}_{k-1})$ and $\boldsymbol{B}_k(\mathbf{X}_{k-1})$ denote persistent and new born targets respectively.

And $\Sigma_{(k)} = \left\{\mathbf{Z}_{1,(k)}, \mathbf{Z}_{2,(k)}, ..., \mathbf{Z}_{N,(k)}\right\}$,where N is the total number of targets present at time k, with

$$\mathbf{Z}_k = \Omega(\mathbf{X}_k) \bigcup \boldsymbol{C}_k \tag{3.48}$$

where $\Omega(\mathbf{X}_k)$ denotes the RFS measurement generated by $\mathbf{X}_k$ and $\mathbf{C}_k$ denotes measurement due to clutter.

The multiple target Bayesian posterior density can be formulated as:

$$p_{\Gamma_k|\Sigma_{1:k}}(\mathbf{X}_k|\mathbf{Z}_{1:k}) \propto p_{\Sigma_k|\Gamma_k}(\mathbf{Z}_k|\mathbf{X}_k) p_{\Gamma_k|\Sigma_{1:k-1}}(\mathbf{X}_k|\mathbf{Z}_{1:k-1}) \tag{3.49}$$

where $p_{\Gamma_k|\Sigma_{1:k}}(\mathbf{X}_k|\mathbf{Z}_{1:k})$ is the multiple target posterior density, $p_{\Sigma_k|\Gamma_k}(\mathbf{Z}_k|\mathbf{X}_k)$ is the likelihood and $p_{\Gamma_k|\Sigma_{1:k-1}}(\mathbf{X}_k|\mathbf{Z}_{1:k-1})$ the prior density. These densities can be described using a mathematical framework known as finite-set statistics [102, 105, 103].

3.5.1 Finite-Set Statistics

Finite-set statistics (FISST) represent a mathematical framework which transforms multisensor-multitarget problems into single-sensor single-target problems. It bundles all sensors, targets and measurements into a single meta-sensor, single meta-target and single meta-measurement respectively [104].

3.6 Probability Hypothesis Density

3.6.1 The PHD Filter

The probability hypothesis density (PHD), D_Λ, of a given RFS, Λ, is the first order moment of Λ and is given by [102, 105, 103]:

$$D_\Lambda(\mathbf{x}) = \mathbb{E}\left\{\delta_\Lambda(\mathbf{x})\right\} = \int \delta_{\mathbf{X}}(\mathbf{x}) P_\Lambda(d\mathbf{X}) \tag{3.50}$$

where $\mathbb{E}\{\cdot\}$ is the statistical expectation operator and $\delta_\Lambda(\mathbf{x}) = \sum_{\mathbf{y}\in\Lambda} \delta_{\mathbf{y}(\mathbf{x})}$ is the random density representation of Λ. P_Λ is the probability measure of the RFS. The PHD filter is a recursion of the PHD, $D_{k|k}$ that is associated with the multi-target posterior density $p(\mathbf{X}_k|\mathbf{Z}_k)$, and

$$p(\mathbf{X}_k|\mathbf{Z}_k) \propto p(\mathbf{Z}_k|\mathbf{X}_k) p(\mathbf{X}_k|\mathbf{Z}_{k-1}) \tag{3.51}$$

where $p(\mathbf{Z}_k|\mathbf{X}_k)$ and $p(\mathbf{X}_k|\mathbf{Z}_{k-1})$ denote the multi-target likelihood and prior density respectively.

The prediction formula of the PHD, $D_{k|k}$ is given as [105, 103]:

$$D_{k|k-1}(\mathbf{x}_k|\mathbf{Z}_{k-1}) = \gamma_k(\mathbf{x}_k) + \int \phi_{k|k-1}(\mathbf{x}_k, \mathbf{x}_{k-1}) D_{k-1|k-1}(\mathbf{x}_{k-1}|\mathbf{Z}_{k-1}) d\mathbf{x}_{k-1}, \tag{3.52}$$

with the factor

$$\phi_{k|k-1}(\mathbf{x}_k, \mathbf{x}_{k-1}) = p_S(\mathbf{x}_{k-1}) f_{k|k-1}(\mathbf{x}_k, \mathbf{x}_{k-1}) + b_{k|k-1}(\mathbf{x}_k, \mathbf{x}_{k-1}), \tag{3.53}$$

where $\gamma_k(\cdot)$ is the PHD of the spontaneous birth, $p_S(\cdot)$ is the probability of the target survival, $f_{k|k-1}(\mathbf{x}_k, \mathbf{x}_{k-1})$ is the single target motion model, and $b_{k|k-1}(\mathbf{x}_k, \mathbf{x}_{k-1})$ is the PHD of the spawned targets.

The update formula is given as:

$$D_{k|k}(\mathbf{x}_k|\mathbf{Z}_k) = \left[\nu(\mathbf{x}_k) + \sum_{\mathbf{z}\in\mathbf{Z}_k} \frac{\psi_{k,\mathbf{z}}(\mathbf{x}_k)}{\kappa_k(\mathbf{z}) + \langle D_{k|k-1}, \psi_{k,\mathbf{z}}\rangle}\right] D_{k|k-1}(\mathbf{x}_k|\mathbf{Z}_{k-1}) \tag{3.54}$$

with $\nu(\mathbf{x}_k) = 1 - p_D(\mathbf{x}_k)$, $\psi_{k,\mathbf{z}}(\mathbf{x}_k) = p_D(\mathbf{x}_k)g(\mathbf{z}|\mathbf{x}_k)$, and $\kappa_k(\mathbf{z}) = \lambda_k c_k(\mathbf{z})$; where $p_D(\mathbf{x}_k)$ and $\nu(\mathbf{x}_k)$ denote the probability of target detection and non-detection for a given $(\mathbf{x}_k)$ respectively, $g(\mathbf{z}|\mathbf{x}_k)$ is the measurement likelihood function for the single target, $\kappa_k(\mathbf{z})$ is the clutter intensity, λ_k is the average number of Poisson clutter points per scan, and $c_k(\mathbf{z})$ is the probability density over the state-space of the clutter point; $\langle\cdot,\cdot\rangle$ denotes inner product and is computed as [105, 103]:

$$\langle D_{k|k-1}, \psi_{k,\mathbf{z}}\rangle = \int D_{k|k-1}(\mathbf{x}_k|\mathbf{Z}_{k-1})\psi_{k,\mathbf{z}}(\mathbf{x}_k)d\mathbf{x}_k. \tag{3.55}$$

3.6.2 The Standard SMC-PHD Filter

The PHD filter can be implemented either as in the sequential Monte Carlo (SMC) fashion (particle-PHD) or as the Gaussian mixture PHD (GM-PHD). The SMC-PHD filter approximates the PHD using random samples and is more specifically an effective scheme in non-linear and non-Gaussian scenarios as well as different noise models [71]. For comparison purposes, the standard SMC-PHD filter of [141] is briefly presented. The implementation of the standard SMC-PHD filter usually requires four stages. These stages are briefly presented in Algorithm 1. From Algorithm 1, L_{k-1} and J_k denotes number of particles for existing targets and new born targets respectively; $\mathcal{L}_k = L_{k-1} + J_k$, $q_k(\cdot|\cdot)$ and $p_k(\cdot|\cdot)$ denotes the proposal distributions for persistent and new born targets respectively; $\gamma_k(\cdot)$ is the PHD of the spontaneous birth, $p_S(\cdot)$ is the probability of target survival and $\phi_{k|k-1}(\tilde{\mathbf{x}}_k^l, \tilde{\mathbf{x}}_{k-1}^l)$ is as defined in (3.53).

Fig. 3.1 illustrates how particles are used to represent and track targets in the standard SMC-PHD filter. The state space of two targets populated with particles

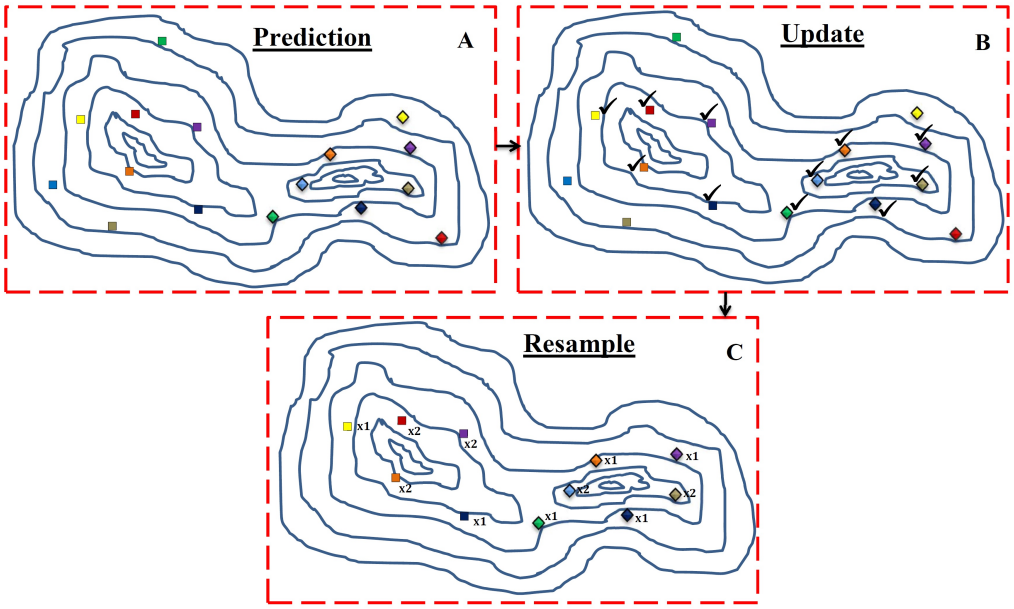

Figure 3.1 Schematic representation of the standard SMC-PHD filter showing the 2D state space of the PHD of two targets populated with particles. The contours represent the state space of targets. The contour centres and number of centres represent the mode and cardinality of targets respectively. Boxes **A**, **B** and **C** represent various stages of the filter. The square shaped and diamond shaped particles are for target 1 and target 2 respectively. The colours stand for different particle states. The particles marked with "$\surd$" in **B** denote particles with higher weight for when the latest measurement arrives.

at k=0, ***Initialise*** $\left[\left\{\mathbf{x}_k^l, w_k^l\right\}_{l=1}^{L_k}\right]$.
for $k = 1 : K$ **do**
  Prediction
  for $l = 1 : L_k$ **do**
    Draw samples for existing targets, $\tilde{\mathbf{x}}_{k|k-1}^l \sim q_k(\cdot|\tilde{\mathbf{x}}_{k-1}^l, \mathbf{Z}_k)$,
    ▷ and compute weights, $\tilde{w}_{k|k-1}^l = \frac{\phi_{k|k-1}(\tilde{\mathbf{x}}_k^l, \tilde{\mathbf{x}}_{k-1}^l)}{q_k(\tilde{\mathbf{x}}_{k|k-1}|\tilde{\mathbf{x}}_{k-1}^l, \mathbf{Z}_k)} w_{k-1}^l$
  end for
  for $l = L_k + 1 : \mathcal{L}_k$ **do**
    Draw samples for newborn targets, $\tilde{\mathbf{x}}_{k|k-1}^l \sim p_k(\cdot|\mathbf{Z}_k)$,
    ▷ and compute weights, $\tilde{w}_{k|k-1}^l = \frac{\gamma_k(\tilde{\mathbf{x}}_k^l)}{J_k p_k(\tilde{\mathbf{x}}_{k|k-1}|\mathbf{Z}_k)}$
  end for
  Update
  for $\mathbf{z} \in \mathbf{Z}_k$ **do**
    $C_k(\mathbf{z}) = \sum_{l=1}^{\mathcal{L}_k} p_D(\tilde{\mathbf{x}}_{k|k-1}^l) g(\mathbf{z}|\tilde{\mathbf{x}}_{k|k-1}^l) \tilde{w}_{k|k-1}^l$
    for $l = 1 : \mathcal{L}_k$ **do**
      update weight,
      $\tilde{w}_k^i = \left[\nu + \sum_{\mathbf{z}\in\mathbf{Z}_k} \frac{p_D(\tilde{\mathbf{x}}_{k|k-1}^l) g(\mathbf{z}|\tilde{\mathbf{x}}_{k|k-1}^l)}{\kappa_k(\mathbf{z}) + C_k(\mathbf{z})}\right] \tilde{w}_{k|k-1}^l$
        ▷ $\nu = 1 - p_D(\tilde{\mathbf{x}}_{k|k-1}^i)$
    end for
  end for
  Resample
  Compute estimated number of targets, $\hat{T}_{k|k} = \text{round}\left(\sum_{l=1}^{\mathcal{L}_k} \tilde{w}_k^l\right)$
  Resample L_k particles using resampling techniques such as in [121].
  return $\left\{\tilde{\mathbf{x}}_{k|k-1}^l, \frac{\hat{T}_{k|k}}{L_k}\right\}_{l=1}^{L_k} \equiv \left\{\mathbf{x}_k^l, w_k^l\right\}_{l=1}^{L_k}$
end for

Algorithm 1: The Standard SMC-PHD Filter

at time k is shown. In **A**, during the prediction stage, the PHD is represented with eight equally weighted particles. In **B**, as the latest measurement arrives, the particle weights are updated accordingly. Particles with higher weights are chosen for resampling. As seen in **B**, the highly weighted particles are marked with "$\surd$" respectively, five particles for the first target and six particles for the second target. To ensure that the number of particles remains eight for each target, the particles marked with "$\surd$" are resampled depending on the size of their weights as seen in **C**. Notice that the particle positions remain unchanged and the particles corresponding to high weights are retained and those with lower weights are discarded. The estimated state of the targets or the posterior at time k is derived

from the resampled particles. It is true that populating the state space of the targets with many more particles will result in more particles falling near the modes of the state space. This will translate to higher weighted particles and a more accurate posterior. However, doing this will increase computational complexity.

3.7 Labelled Random Finite Sets

In loose terms, a labelled random finite set is an RFS with corresponding set of labels. The following notations and definitions are useful concepts in the study of labelled random finite sets.

Notation 1

For a real-valued function h, its multi-object exponential is

$$h^X \triangleq \prod_{x \in X} h(x) \tag{3.56}$$

with $h^{\emptyset} = 1$ by convention. The elements in set X can be of any type for example, sets, scalars or vectors so long as the function $h(\cdot)$ accepts such arguments.

Notation 2

The generalised Kronecker delta function, and the set inclusion function are respectively defined as

$$\delta_Y(X) = \begin{cases} 1, & \text{if } X = Y \\ 0, & \text{otherwise,} \end{cases} \qquad 1_Y(X) = \begin{cases} 1, & \text{if } X \subseteq Y \\ 0, & \text{otherwise,} \end{cases} \tag{3.57}$$

where both, X and Y can be of any type for example, sets, scalars or vectors.

Definition 1

A labelled RFS $\mathbf{X}$ with state space $\mathbb{X}$ and discrete label space $\mathbb{L}$, is an RFS on $\mathbb{X} \times \mathbb{L}$, such that the labels within each realisation are always distinct. That is, if $\mathcal{L}(\mathbf{X})$ is

the set of unique labels in $\mathbf{X}$, and the distinct label indicator function is defined as

$$\Delta(\mathbf{X}) = \begin{cases} 1, & \text{if } |\mathcal{L}(\mathbf{X})| = |\mathbf{X}| \\ 0, & \text{if } |\mathcal{L}(\mathbf{X})| \neq |\mathbf{X}|, \end{cases} \tag{3.58}$$

a labelled RFS $\mathbf{X}$ always satisfies $\Delta(\mathbf{X}) = 1$ [137, 138].

Definition 2

A generalised labelled multi-Bernoulli (GLMB) RFS is a labelled RFS with state space $\mathbb{X}$ and discrete label space $\mathbb{L}$, and is distributed according to [137, 138]

$$\zeta(\mathbf{X}) = \Delta(\mathbf{X}) \sum_{c \in \mathbb{C}} w^{(c)}(\mathcal{L}(\mathbf{X}))[p^{(c)}(\cdot)]^{\mathbf{X}}, \tag{3.59}$$

where $\mathbb{C}$ is a discrete index set, and $w^{(c)}(\mathcal{L})$ and $p^{(c)}(x, \ell)$ satisfy the following

$$\sum_{L \subseteq \mathbb{L}} \sum_{c \in \mathbb{C}} w^{(c)}(L) = 1, \tag{3.60a}$$

$$\int_{x \in \mathbb{X}} p^{(c)}(x, \ell) dx = 1. \tag{3.60b}$$

Definition 3

A labelled multi-Bernoulli (LMB) RFS is a cheaper approximation of the GLMB RFS. The LMB is a labelled RFS having a state space $\mathbb{X}$ and a discrete label space $\mathbb{L}$, which is distributed according to [117]

$$\zeta(\mathbf{X}) = \Delta(\mathbf{X}) w(\mathcal{L}(\mathbf{X}))[p(\cdot)]^{\mathbf{X}}, \tag{3.61a}$$

where

$$w(L) = \prod_{\ell \in \mathbb{L}} \left(1 - r^{(\ell)}\right) \prod_{\ell \in L} \frac{1_L(\ell) r^{(\ell)}}{1 - r^{(\ell)}}, \tag{3.61b}$$

$$p(x, \ell) = p^{(\ell)}(x), \tag{3.61c}$$

with $x \in X$ denoting for example, a target state, $p^{(\ell)}(\cdot)$ and $r^{(\ell)}$ denoting the probability density and existence probability respectively of the track corresponding to label $\ell \in \mathbb{L}$.

3.8 Summary

The KF can solve analytically the optimal Bayesian solution by calculating the exact posterior density. This provides the overall best performance for tracking in a linear environment. However, there are some limitations of KF that have been highlighted in this chapter. These limitations lead to the discussion on EKF as an approximation to the optimal Bayesian solution (suboptimal Bayesian solution). The pros and cons of EKF were highlighted. The KF was chosen for implementation in the STT case while the EKF was not due to reasons already mentioned.

In the next chapter, a new technique is proposed for the effective and efficient tracking of multiple targets in clutter.

Chapter 4

Kalman-Gain Aided Particle PHD Filter with Improved Resampling for Multiple Target Tracking

4.1 Introduction

In this chapter, a new particle filtering technique for efficient MTT is proposed. In this new method, an SMC-PHD filter with a validation threshold is designed to select promising particles and to guide them to regions of high likelihood using the Kalman-gain, irrespective of the importance density function. This method seeks to minimise the MSE between the estimated measurements due to selected particles and the actual measurements to achieve a more efficient SMC-PHD filter with less computational complexity. This allows fewer particles to be used to populate the state space and at the same time achieve improved tracking performance as opposed to the standard SMC-PHD filter. Furthermore, the Kalman gain SMC-PHD filter presented in this chapter is particle filter (PF) based and as with PFs, it requires a process known as resampling to avoid the problem of degeneracy. To this end, an improved resampling method for use with SMC methods is also proposed in this chapter. The new resampling scheme addresses a problem with the *systematic resampling* method which causes a high tendency of resampling very

low weight particles especially when a large number of resampled particles are required; which in turn affect state estimation.

The remainder of this chapter is organised as follows. In Section 4.2 the multi-target tracking problem is presented in terms of process and measurement models. Section 4.3 presents the proposed KG-SMC-PHD filter. Section 4.4 discusses the new resampling method. Simulation results demonstrating performance improvements of the new multi-target tracker and the new resampling method together with discussions are presented in Section 4.5. Finally, conclusions are drawn in Section 4.6.

4.2 Multi-target Tracking Problem Formulation

The MTT problem relates to that of modelling a dynamical system. Two models are generally used, the state evolution model and the measurement model.

4.2.1 State Model

A non-linear system governed by the state evolution model is considered:

$$\mathbf{x}_k = \mathbf{f}_{k-1}(\mathbf{x}_{k-1}, \mathbf{v}_k) \tag{4.1}$$

where $\mathbf{x}_k$ denotes the t-th target state at discrete time k, $\mathbf{v}_k$ is an independent and identically distributed (i.i.d.) process noise vector and $\mathbf{f}_{k-1}(\cdot)$ is the non-linear system transition function. Then the multi-target state at time k can be written as

$$\boldsymbol{X}_k = \{\mathbf{x}_{1,k}, ..., \mathbf{x}_{T,k}\} \in E_s \tag{4.2}$$

where T is the number of targets present at time k, and E_s denotes the state space.

4.2.2 Measurement Model

Let the multi-target cumulative measurement sequence up to time K be $\boldsymbol{Z}_{1:K}$: $\mathbf{Z}_1, \mathbf{Z}_2, ..., \mathbf{Z}_K \subset E_o$. Measurements consist of both target-originated measurements

and false alarms due to clutter. Then the multi-target measurement set at time k in the measurement space is:

$$\boldsymbol{Z}_k = \{\mathbf{z}_{1,k}, ..., \mathbf{z}_{\alpha,k}\} \bigcup \{\mathbf{c}_{1,k}, ...\mathbf{c}_{\beta,k}\} \subset E_o \tag{4.3}$$

where $\{\mathbf{z}_{1,k}, ..., \mathbf{z}_{\alpha,k}\}$ denotes the target-originated measurement set with number of measurements, α; $\{\mathbf{c}_{1,k}, ...\mathbf{c}_{\beta,k}\}$ denotes the false measurement set with the number of measurements, β and E_o denotes the measurement space. The t-th target-originated non-linear measurement model is given as:

$$\mathbf{z}_k = \mathbf{h}_k(\mathbf{x}_k, \mathbf{n}_k) \tag{4.4}$$

where $\mathbf{h}_k(\cdot)$ is a non-linear function, and $\mathbf{n}_k$ is an i.i.d. process noise vector.

In the next section, the proposed SMC-PHD filter is presented.

4.3 The Proposed SMC-PHD Filter

In the standard SMC-PHD filter, the particles appear to be scattered and it is difficult to guide particles to regions of interest. The filter's ability to estimate the posterior at a given time depends on how densely the state space is populated with samples and how well the estimated measurements match the actual measurements received in that time frame. The weights are then updated accordingly. The SMC-PHD filter does not provide for particle state correction to achieve particle improvement. In other words, it does not seek to reduce the error between the actual measurement and the estimated measurements irrespective of the importance density chosen. The proposed method seeks to address this problem. The novelty of our approach lies in the technique behind the Kalman filter. The Kalman filter is a minimum MSE (MMSE) estimator, which in effect seeks to recursively minimise the mean square error between the estimated measurements and actual measurements using the Kalman-gain [81]. The Kalman-gain computes the required correction from the measurement and transforms the correction of the measurement back to the correction of state. The proposed approach tries

to apply particle state correction/improvement using the Kalman-gain to guide validated particles in the SMC-PHD filter to the region of higher likelihood to better approximate the posterior at each time step.

4.3.1 Measurement Set Partition

Given that T_k targets exist at time k, the measurements received at k may consist of target-originated measurements (that is, measurements due to persistent target or new born targets) and clutter. In the standard SMC-PHD filter, all measurements are used to compute weights to show the significance of all particles with no attempt to check for errors. Therefore, a measurement set partition is needed to separate the measurement set into target-originated measurements and measurements due to clutter. A statistical distance measure and gating technique is used to achieve this. The second step is to identify promising particles from the predicted target state using a validation threshold and improve their states using the Kalman-gain while updating weights as measurement arrives.

At time k, measurements assumed to originate from persistent targets are identified by computing the square Mahalanobis distance between elements in the measurement set $\boldsymbol{Z}_{k-1}$ at time $k-1$ and $\boldsymbol{Z}_k$ at time k from (4.3) as

$$d^2_{i,j,k} = (\mathbf{z}^i_k - \mathbf{z}^j_{k-1})^T \boldsymbol{\Sigma}^{-1}_k (\mathbf{z}^i_k - \mathbf{z}^j_{k-1}), \tag{4.5}$$

for $i = 1, ..., |\boldsymbol{Z}_k|$ and $j = 1, ..., |\boldsymbol{Z}_{k-1}|$. $\boldsymbol{\Sigma}_k$ is the measurement covariance matrix. For target originated measurements $\mathbf{z}^i_k$ and $\mathbf{z}^j_{k-1}$ belonging to the same target, the square Mahalanobis distance $d^2_{i,j,k}$ is χ^2 distributed with degree of freedom equal to the dimension of the measurement vector. Therefore, a unit-less threshold $\tilde{d}$ can be computed for a given probability using the inverse cumulative χ^2 function such that the Pr$[d^2_{i,j,k} \leq \tilde{d}]$ falls within a given confidence region [11].

Assuming that measurement noise is not too great, and the time increment is not too large, a target generated measurement in $\boldsymbol{Z}_k$ will usually be nearby some measurement in $\boldsymbol{Z}_{k-1}$. Assuming that clutter is not too dense and is uncor-

related frame to frame, a clutter measurement in $\boldsymbol{Z}_k$ will usually not be near any measurement in $\boldsymbol{Z}_{k-1}$.

Thus $d^2_{i,j,k}$ as defined in (4.5) will tend to be small for some j if $\mathbf{z}^i_k$ is due to a target. Likewise, it will tend to be large for all j if $\mathbf{z}^i_k$ is a clutter measurement. So for a given i, the measurement $\mathbf{z}^i_k$ is recorded as a valid target-originated measurement, $\dot{\mathbf{z}}^n_k$ if,

$$\min_j d^2_{i,j,k} \leq \tilde{d} \tag{4.6}$$

is satisfied or, otherwise, regarded either as clutter or a potential new born target. Therefore, the clutter free measurement set at time k is

$$\dot{\boldsymbol{Z}}_k = \bigcup_{n=1}^{n_s} \{\dot{\mathbf{z}}^n_k\}, \tag{4.7}$$

where $n = 1, \cdots, n_s$ and $n_s = \left|\dot{\boldsymbol{Z}}_k\right|$, that is, the total number of measurements in Z_k satisfying (4.6).

4.3.2 Validated Particle Selection and Correction

Once the measurement set is partitioned, the selection and correction step follow. In order to identify those particles to correct, a validation threshold, τ, is used, which selects particles from the predicted target state that fall under a given measurement for correction. A predicted particle, $\tilde{\mathbf{x}}^l_{k|k-1}$ is selected for correction if, for each clutter free measurement $\dot{\mathbf{z}}^n_k \in \dot{\boldsymbol{Z}}_k$,

$$g(\dot{\mathbf{z}}^n_k | \tilde{\mathbf{x}}^l_{k|k-1}) \geq \tau, \quad \text{for } l = 1, ..., \mathcal{L}_k \tag{4.8}$$

where $g(\dot{\mathbf{z}}^n_k | \tilde{\mathbf{x}}^l_{k|k-1})$ is the measurement likelihood function; τ is chosen to be inversely proportional to the total number of samples per persistent target ρ, that is,

$$\tau \propto \frac{1}{\rho} \tag{4.9}$$

Each particle satisfying (4.8) is assumed to be a reasonable candidate for correction given the current measurement. A large τ will lead to a tighter particle selection while a smaller value of τ will result in wider particle selection, that is, more particles will be selected for correction. Once a reasonable candidate $\tilde{\mathbf{x}}^l_{k|k-1}$ has been identified, it's state is corrected as

$$\tilde{\mathbf{x}}^l_k = \tilde{\mathbf{x}}^l_{k|k-1} + \mathcal{K}_k(\dot{\mathbf{z}}^n_k - f(\tilde{\mathbf{x}}^l_{k|k-1})) \tag{4.10}$$

$$\mathcal{K}_k = \mathbf{P}_{k-1}\mathbf{H}^T_k\mathbf{S}^{-1}_k \tag{4.11}$$

$$\mathbf{S}^{-1}_k = \mathbf{R}_k + \mathbf{H}_k\mathbf{P}_{k-1}\boldsymbol{H}^T_k \tag{4.12}$$

$$\mathbf{P}_k = \mathbf{P}_{k-1} - \mathcal{K}_k\mathbf{H}_k\mathbf{P}_{k-1} \tag{4.13}$$

where $f(\tilde{\mathbf{x}}^l_{k|k-1})$ is the projection of the predicted state $\tilde{\mathbf{x}}^l_k$ on to the measurement, $\mathcal{K}_k$ is the Kalman-gain, **H** is the measurement transformation matrix and **P** is the state estimation covariance matrix, **R** is the measurement error covariance matrix, and **S** is the innovation covariance matrix.

Therefore, given that the t-th target generated the clutter free measurement $\dot{\mathbf{z}}_{t,k}$ at time k, and its state is represented by particles $\{\mathbf{x}_{t,k}\}^{\rho}_{t=1}$ from the predicted target state, then, only those particles, $\{\mathbf{x}_{t,k}\}^{s}_{t=1}$ satisfying (5.13) will be selected for correction according to (5.15) where $s \leq \rho$. Fig. 4.1 illustrates how particles representing the state of the PHD of targets are selected for correction as the measurement originating from the t-th target arrives at time k. From the figure, in **A**, during the prediction stage, each of the target states is represented with eight equally weighted particles. As the latest measurement for each target arrives, particles with high likelihood are marked with "$\surd$" as seen in **B**. The validation threshold τ of (5.13) is then applied to the likelihood of particles with "$\surd$". Each particle whose likelihood satisfies the threshold condition is selected for correction. The selected particles are shown with "*" in **B**. The particle weights are updated accordingly. Notice from **B** that for the first target, five particles have high likelihood but only three from the five were chosen for state correction. Similarly, for the second target, six particles gave high likelihood but out of which only four were selected for state correction. The selected particles from **B** are then corrected

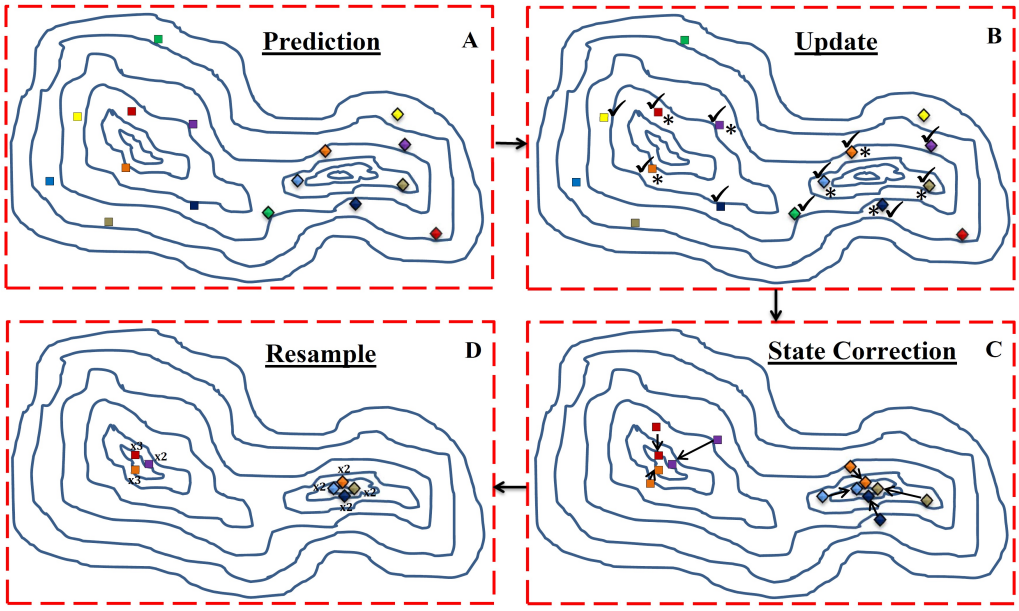

Figure 4.1 Schematic representation of the proposed SMC-PHD filter showing the 2D state space of the PHD of two targets populated with particles. The contours represent the state space of targets. The contour centres and number of centres represent the mode and number of targets respectively. Boxes **A**, **B**, **C** and **D** represent various stages of the filter. The square shaped and diamond shaped particles are for target 1 and target 2 respectively. The colours stand for different particle states. The particles with "$\surd$" stand for particles with higher weight for when latest the measurement arrives. Particles with "*" denote particles selected for state correction.

using (5.15) and (5.16) as shown in **C**. The corrected particles are then resampled to ensure the number of particles remains eight for each target.

Note, the above measurement set partition approach can be applied under the following assumptions: that new born targets exist for at least two consecutive time steps, the manoeuvring of targets is not too abrupt, the sample period δt is not too large, measurement noise is not too large, clutter is not too dense, and clutter is not time correlated.

Furthermore, it is emphasised that the proposed KG-SMC-PHD is different from the GM-PHD in [140] even with the application of the gating technique as will be demonstrated in the simulation section. This is primarily because the strict assumption of linearity and Gaussianity condition of [140] is not used.

4.3.3 KG-SMC-PHD Implementation of the PHD Filter

This section presents the initialisation, prediction, update and resample steps of the KG-SMC-PHD filter.

4.3.3.1 Initialisation Step

At time $k = 0$, initialise the PHD, $D_{k|k}$ by a number of particles with associated weights $\left\{\mathbf{x}_k^l, w_k^l\right\}_{l=1}^{L_k}$. A particle approximation of the intensity function at time step, $k > 0$, can be obtained from a particle distribution at the previous time step using *prediction* and *update* stages.

4.3.3.2 Prediction Step

The predicted PHD, $D_{k|k-1}$ is:

$$D_{k|k-1}(\tilde{\mathbf{x}}_k|\dot{\mathbf{Z}}_{k-1}) = \sum_{l=1}^{\mathcal{L}_k} \tilde{w}_{k|k-1}^l \delta(\mathbf{x} - \tilde{\mathbf{x}}_{k|k-1}^l). \tag{4.14}$$

L_{k-1} and J_k particles are drawn from two proposal densities (chosen from the possibilities discussed in Sec. 3.4, that is, TP, EPF or UPF) to represent persistent

and new born targets respectively as:

$$\tilde{\mathbf{x}}_{k|k-1}^{l} \approx \begin{cases} q_k(\cdot|\tilde{\mathbf{x}}_{k-1}^{l}, \dot{\mathbf{Z}}_k), & l = 1, ..., L_{k-1} \\ p_k(\cdot|\dot{\mathbf{Z}}_k), & l = L_{k-1}+1, ..., \mathcal{L}_k \end{cases} \tag{4.15}$$

with corresponding weights:

$$\tilde{w}_{k|k-1}^{l} = \begin{cases} \frac{\phi_{k|k-1}(\tilde{\mathbf{x}}_k^l, \tilde{\mathbf{x}}_{k-1}^l)}{q_k(\tilde{\mathbf{x}}_{k|k-1}|\tilde{\mathbf{x}}_{k-1}^l, \mathbf{Z}_k)} w_{k-1}^{l}, & l = 1, ..., L_{k-1} \\ \frac{\gamma_k(\tilde{\mathbf{x}}_k^l)}{J_k p_k(\tilde{\mathbf{x}}_{k|k-1}|\mathbf{Z}_k)}, & l = L_{k-1}+1, ..., \mathcal{L}_k \end{cases} \tag{4.16}$$

with the term

$$\phi_{k|k-1}(\mathbf{x}_k, \mathbf{x}_{k-1}) = p_S(\mathbf{x}_{k-1}) f_{k|k-1}(\mathbf{x}_k, \mathbf{x}_{k-1}) + b_{k|k-1}(\mathbf{x}_k, \mathbf{x}_{k-1})$$

where $\mathcal{L}_k = L_{k-1} + J_k$, $q_k(\cdot|\cdot)$ and $p_k(\cdot|\cdot)$ denote the proposal distributions for persistent and new born targets respectively; $\gamma_k(\cdot)$ is the PHD of the spontaneous birth, $p_S(\cdot)$ is the probability of target survival, $f_{k|k-1}(\mathbf{x}_k, \mathbf{x}_{k-1})$ is the single target motion model, and $b_{k|k-1}(\mathbf{x}_k, \mathbf{x}_{k-1})$ is the PHD of spawned targets; J_k is the number of particles for new born targets.

4.3.3.3 Update Step

For each $\dot{\mathbf{z}}_k^n \in \dot{\mathbf{Z}}_k$ where $\dot{\mathbf{Z}}_k$ is the clutter free measurement set at time k obtained using (4.5) and (4.6), let

$$\mathcal{H}(\dot{\mathbf{z}}_k^n) = \kappa(\dot{\mathbf{z}}_k^n) + C_k(\dot{\mathbf{z}}_k^n) \tag{4.17}$$

$$C_k(\dot{\mathbf{z}}_k^n) = \sum_{l=1}^{\mathcal{L}_k} p_D(\tilde{\mathbf{x}}_{k|k-1}^{l}) g(\dot{\mathbf{z}}_k^n|\tilde{\mathbf{x}}_{k|k-1}^{l}) \tilde{w}_{k|k-1}^{l}, \tag{4.18}$$

then, for $l = 1, ..., \mathcal{L}_k$, compute the likelihood $g(\dot{\mathbf{z}}_k^n|\tilde{\mathbf{x}}_{k|k-1}^{l})$ and verify if (5.13) is true, correct predicted state by computing $\tilde{\mathbf{x}}_k^l$ using (5.15) then compute (4.18)

and update the weights using:

$$\tilde{w}_k^l = \left[\nu + \sum_{\dot{\mathbf{z}}\in\dot{\mathbf{Z}}_k} \frac{p_D(\tilde{\mathbf{x}}_{k|k-1}^l) g(\dot{\mathbf{z}}_k^n|\tilde{\mathbf{x}}_{k|k-1}^l)}{\mathcal{H}(\dot{\mathbf{z}}_k^n)}\right] \tilde{w}_{k|k-1}^l \tag{4.19}$$

where $\nu = 1 - p_D(\tilde{\mathbf{x}}_{k|k-1}^l)$. However, if (5.13) is not satisfied, the predicted state is not corrected; $\tilde{\mathbf{x}}_k^l$ is computed as $\tilde{\mathbf{x}}_k^l = \tilde{\mathbf{x}}_{k|k-1}^l$ and (4.17) and (6.7) are computed immediately.

The updated PHD, $D_{k|k}$ is then given as:

$$D_{k|k}(\tilde{\mathbf{x}}_k|\dot{\mathbf{Z}}_k) = \sum_{l=1}^{\mathcal{L}_k} \tilde{w}_k^l \delta(\mathbf{x} - \tilde{\mathbf{x}}_k^l) \tag{4.20}$$

4.3.3.4 Resampling Step

i The expected number of targets $\hat{T}_{k|k}$ is computed as:

$$\hat{T}_{k|k} = \text{round}\left(\sum_{l=1}^{\mathcal{L}_k} \tilde{w}_k^l\right) \tag{4.21}$$

where $\text{round}(\cdot)$ denotes round to the nearest integer.

ii $L_k = \rho\hat{T}_{k|k}$ particles are resampled (ρ corresponds to the number of particles per existing target) according to the modified systematic resampling technique below:

- Find all noncontributing weights $\bar{w}_k$ from $\tilde{w}_k$ such that $\bar{w}_k \in \tilde{w}_k$ and replace with ϖ where $0 < \varpi \ll \frac{1}{\rho}$. This is to ensure that only weights belonging to corrected particles are chosen for resampling.
- Then compute cumulative probability $c_1 = 0$, $c_l = c_{l-1} + (\frac{\tilde{w}_k^l}{\hat{T}_{k|k}})$, $l = 2, ..., L_k + J_k$
- Draw a starting point u_1 from $U[0, \frac{1}{L_k}]$
- For $j = 1, ..., L_k$,

$$u_j = u_1 + L_k^{-1}(j-1)$$

while $u_j > c_i$, $l = l + 1$. End while

$$\mathbf{x}_k^j = \tilde{\mathbf{x}}_k^j$$
$$w_k^j = \frac{1}{L_k}$$

iii) Rescale (multiply) the weights by $\hat{T}_{k|k}$ to get $\left\{\mathbf{x}_k^l, \frac{\hat{T}_{k|k}}{L_k}\right\}_{l=1}^{L_k}$ where $w_k^l = \frac{\hat{T}_{k|k}}{L_k}$ therefore $\left\{\mathbf{x}_k^l, \frac{\hat{T}_{k|k}}{L_k}\right\}_{l=1}^{L_k} \equiv \left\{\mathbf{x}_k^l, w_k^l\right\}_{l=1}^{L_k}$.

The pseudo code of the proposed KG-SMC-PHD filter is described in Algorithm 2.

Initialisation
Initialise filter parameters as in Sec. 4.3.3.1.
Prediction
Follow the prediction technique as in Sec. 4.3.3.2.
Update
Obtain clutter free measurement $\dot{\boldsymbol{Z}}_k$ at time k using (4.5) and (4.6) by computing:
for all $\mathbf{z}_k^i \in \mathbf{Z}_k$ and $\mathbf{z}_{k-1}^j \in \mathbf{Z}_{k-1}$ **do**
  if $(\mathbf{z}_k^i - \mathbf{z}_{k-1}^j)^T \Sigma^{-1} (\mathbf{z}_k^i - \mathbf{z}_{k-1}^j) \leq \tilde{d}$ **then**
    $\dot{\mathbf{z}}_k^n = \mathbf{z}_k^i$
  end if
end for
$\dot{\mathbf{Z}}_k = \bigcup_{n=1}^{n_s} \{\dot{\mathbf{z}}_k^n\}$
for all $\dot{\mathbf{z}}_k^n \in \dot{\mathbf{Z}}_k$ **do**
  for $l = 1 : \mathcal{L}_k$ **do**
    if $g(\dot{\mathbf{z}}_k^n | \tilde{\mathbf{x}}_{k|k-1}^l) \geq \tau$ **then**
      $\tilde{\mathbf{x}}_k^l = \tilde{\mathbf{x}}_{k|k-1}^l + \mathcal{K}_k(\dot{\mathbf{z}}_k^n - f(\tilde{\mathbf{x}}_{k|k-1}^l))$
      Compute (4.17)
    else
      $\tilde{\mathbf{x}}_k^l = \tilde{\mathbf{x}}_{k|k-1}^l$
      Only compute (4.17)
    end if
    Compute (6.7)
  end for
end for
Resample
Resample according to the resampling method described in Section 4.4.

Algorithm 2: KG-SMC-PHD filter

4.4 Improved Resampling Approach for SMC Methods

Most PF (or SMC) methods generally involve a process for generating and propagating particles, weight assignment and computation and resampling of particles [53]. The resampling process replaces certain set of particles with another (usually depending on the particle weights) [53]. The resampling process is crucial in PF methods in order to avoid a situation where a few set of particles dominate other particles with their weights; a process known as degeneracy [3, 53, 121]. Having a degenerate set of particles is undesired as this will cause large variances in the obtained state estimates. Several methods of resampling in PF methods have been proposed in the literature. These include residual resampling [19, 91], multinomial resampling [63], stratified resampling [83], systematic resampling (SR) [32, 53, 83], branching corrections [42], resampling with rejection control [92]. For more details on surveys and review of resampling methods, the reader is referred to [28, 52, 53, 76, 89]. The resampling methods listed are sequential algorithms and the most common are the multinomial, residual, systematic and stratified resampling techniques [89]. In these algorithms, resampling is performed from the approximating distributions utilising the latest weights [89]. Among the most common algorithms listed, the SR method is often more desired due to its ease of implementation, less computational complexity and less random number generation [89]. The stratified resampling has the same order of complexity as the SR (in the order of number of resampled particles required N) but requires N number of random number generation during implementation while the SR requires only one random number generation.

In PF methods, very low weight particles are less likely to contribute to the estimates of an approximating distribution. Therefore, allowing very low weights to contribute-during resampling-to the approximating distribution estimates could add to estimation variance leading to poor state estimates especially when the required number of resampled particles is large. The SR method, despite its

desirable properties, has a tendency to resample very low weight particles especially when the required number of resampled particles is large.

The reason for the occurrence of this phenomenon in the SR algorithm is discussed next and a way to address the problem is explained. The proposed method is namely the improved systematic resampling (ISR) method.

4.4.1 Problem Formulation

Firstly, a brief overview of the PF stages preceding the resampling stage is given in order to set a scene for presenting the new algorithm.

Consider a tracking context (either single or multiple target tracking) where at time k we have a single target state and measurement model respectively given by:

$$x_k = f(x_{k-1}, n_k), \tag{4.22}$$

$$z_k = g(x_k, v_k), \tag{4.23}$$

where $f(\cdot)$ and $g(\cdot)$ are nonlinear functions; $x_k \in \mathbb{X}$ is the state of the model and $z_k \in \mathbb{Z}$ is the measurement with state and measurement space $\mathbb{X}$ and $\mathbb{Z}$ respectively; n_k and v_k are independent and identically distributed white noises. Assume that an alternate representation of the state, (4.22) is the probability distribution, $p(x_k|x_{k-1})$ and that of the measurement, (4.23) is the distribution, $p(z_k|x_k)$. We aim to sequentially estimate the filtering distribution $p(x_k|z_{1:k})$ in a recursive manner by computing

$$p(x_k|z_{1:k}) \propto \int p(z_k|x_k)p(x_k|x_{k-1})p(x_{k-1}|z_{1:k-1})dx_{k-1}. \tag{4.24}$$

Generally, the above cannot be solved analytically therefore approximations (such as PF methods) are required.

In PF, the distribution $p(x_{k-1}|z_{1:k-1})$ is approximated by a set of particles with assigned weights $\{x^i_{k-1}, w^i_{k-1}\}^M_{i=1}$ where M is the number of particles, such that:

$$p(x_{k-1}|z_{1:k-1}) \approx \sum_{i=1}^{M} w^i_{k-1}\delta(x_{k-1} - x^i_{k-1}), \tag{4.25}$$

where $\delta(\cdot)$ is the Dirac delta operator. The weights are normalised such that they all sum up to one. This approximation makes it possible to solve (3), so that

$$p(x_k|z_{1:k}) \propto p(z_k|x_k) \sum_{i=1}^{M} w_{k-1}^i p(x_k|x_{k-1}^i). \tag{4.26}$$

The expression of (4.26) shows how the approximating distribution of $\{x_{k-1}^i, w_{k-1}^i\}_{i=1}^M$ can be obtained. This is the particle propagation stage as the particle x_{k-1}^i is propagated in time to give x_k^i through importance sampling (see for example, [3] for more details).

As for weight computation, we draw equally weighted particles from $p(x_k|z_{1:k})$. However, since this is not possible in most cases, we resort to sampling from an alternate distribution called the *proposal/importance* distribution, $q(x_k)$ [3, 121, 124]. An example of such distribution is $p(x_k|x_{k-1})$ [121, 124]. Since $q(x_k)$ is different from $p(x_k|z_{1:k})$, the particles drawn from $q(x_k)$ need to be weighted in order to have a correct inference [121, 124]. This can be acheived by recursively computing

$$w_k^i \propto \frac{p(z_k|x_k^i)p(x_k^i|x_{k-1}^i)}{q(x_k^i)} w_{k-1}^i. \tag{4.27}$$

Eq. (4.27) is usually followed by a normalisation to ensure all weights sum to one. A recursive progression of this expression can lead to degeneracy. This is an undesired situation where one or few particles have large weights and others have negligible weights. This in turn causes an increase in weight variances as measurements are processed. This will lead to a very poor approximation of the filtering distribution $p(x_k|z_{1:k})$ [89]. This is why the resampling stage is needed in PF methods. Following particle propagation and weight computation for the filtering distribution, we now have the approximating distribution at time k given by $\{x_k^i, w_k^i\}_{i=1}^M$.

4.4.2 Systematic Resampling

In this section, the SR algorithm is described. An explanation to why the phenomenon described earlier exists is also given.

SR and sequential resampling methods in general require particles from an approximating distribution with associated weights. These particles are resampled (usually depending on the weights) to give an estimate of the approximate distribution.

Assume we have an approximating distribution represented by a set of particles and associated weights $\{x_k^i, w_k^i\}_{i=1}^M$. We aim to resample N particles from these set of particles such that the outcome is the set $\{x_k^j, w_k^j\}_{j=1}^N$. N can be greater than the number of propagated particles M but for most applications, it is kept constant, this means, $N = M$ [89]. The SR method achieves this in what is described next.

The SR method [32, 53, 83] first computes the cumulative sum of the weights

$$\begin{aligned} Q^1 &= w_k^1, \\ Q^i &= Q^{i-1} + w_k^i, \quad i = 2, \cdots, M. \end{aligned} \tag{4.28}$$

The whole particle set is divided into subpartitions called *strata*. The first *strata* is a random number, U^1 generated from the uniform distribution $\mathcal{U}[0, \frac{1}{N}]$. The rest are updated by $U^n = U^{n-1} + \frac{1}{N}$ for $n = 1, \cdots, N$. SR compares the cumulative sum Q^i with the updated uniform number U^n. A possible implementation of the SR method is shown in Algorithm 3. The number of times the i-th particle is

Data: $\left(\{x_k^i, w_k^i\}_{i=1}^M, N\right)$
Result: $\{x_k^j, w_k^j\}_{j=1}^N$
Normalise weight;
Generate random number $U \sim \mathcal{U}[0, \frac{1}{N}]$;
Compute cumulative sum of weights Q;
for $i = 1 : M$ **do**
  $t = 0$;
  while $Q^i > U$ **do**
    $t = t + 1$;
    $U = U + \frac{1}{N}$;
  end
  $N(i) = t$
end

Algorithm 3: A sample SR algorithm

replicated (resampled) depends on how many times the updated uniform number

U^n falls within the range of $(Q^{i-1}, Q^i]$. For a very low weight, its contribution to the cumulative sum Q will be small and if the required number of resampled particles N is small, the increment to the uniform number update $\frac{1}{N}$ will be large. Hence the probability of the i-th particle being resampled is very low if the i-th particle is very small. Similarly, if the weight of the i-th particle is very small but N is large, the increment term $\frac{1}{N}$ will be very small. Hence the probability of the uniform number U^n falling within the range $(Q^{i-1}, Q^i]$ increases. This presents a high tendency of the very low i-th particle being resampled. Allowing very low weight particles to contribute to the approximating distribution estimates could add to estimation variance and this could lead to poor state estimates.

4.4.3 The Improved Systematic Resampling

In the previous section the SR method was introduced. A phenomenon that causes it to yield poor state estimates of the approximating distribution particularly when large number of resampled particles is required was also described. This section presents the proposed improvement to the SR algorithm.

Given that in PF methods, a particle having very low weight is less likely to contribute (improvement wise) to the estimate of an approximating distribution; we then propose that, for a very low weight w_k^i, we want to be able to reduce the possibility of the updated uniform number U^n falling within the range $(Q^{i-1}, Q^i]$ given the increment term $\frac{1}{N}$ for a large N.

To this end, a sort of *weight-relowering* technique is performed where very low weights $\tilde{w}_k \subset w_k$ are identified and reassigned to a much lower value, ρ such that $0 < \rho \ll 1$. This is so that for a very low weight $\tilde{w}_k^i$, its contribution to the cumulative sum of weights Q of (4.28) will be very small. A weight is classed as being very low if the condition

$$w_k^i < \tau, \quad \forall i \tag{4.29}$$

is satisfied, where $i = 1, \cdots, M$. The threshold τ is chosen such that $\Pr(w_k^i > \tau) = 99\%$. A possible implementation of the ISR method is shown in Algorithm 4.

Data: $\left(\{x_k^i, w_k^i\}_{i=1}^M, N, \rho, \tau\right)$
Result: $\{x_k^j, w_k^j\}_{j=1}^N$
Check that (4.29) is satisfied in order to identify $\tilde{w}_k$;
Apply *weight-relowering* to $\tilde{w}_k$ by assigning then the value ρ;
Normalise weight;
Generate random number $U \sim \mathcal{U}[0, \frac{1}{N}]$;
Compute cumulative sum of weights Q;
for $i = 1 : M$ **do**
  $t = 0$;
  while $Q^i > U$ **do**
    $t = t + 1$;
    $U = U + \frac{1}{N}$;
  end
  $N(i) = t$
end

Algorithm 4: A sample ISR algorithm

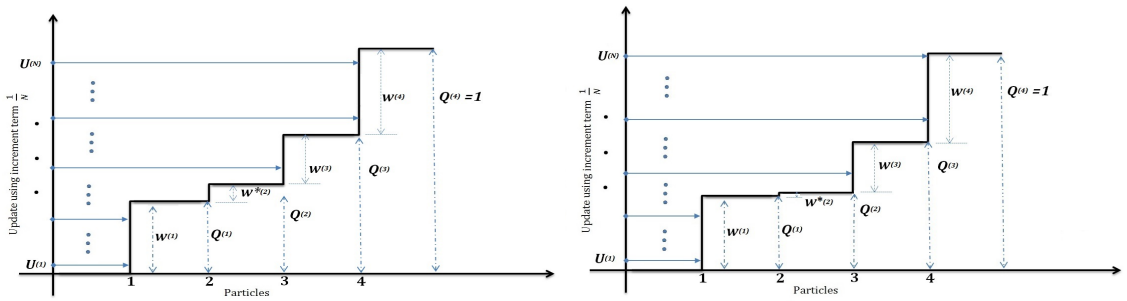

(a) SR (b) ISR

Figure 4.2 An illustration of the SR and ISR method. There are four particles with respective weights w. The very low weight is indicated as $w^{*(2)}$.

The proposed method is further illustrated and contrasted with the SR method as shown in Fig. 4.2 for the same set of weights as input. The SR and ISR method are depicted in Fig. 4.2a and Fig. 4.2b respectively. From Fig. 4.2a, the weight marked with '$*$' is the very low weight. So depending on number of resampled particles required, N, the increment term, $\frac{1}{N}$ can cause the updated uniform number U^n to fall in the range $(Q^1, Q^2]$. This become even more likely especially when N is large. In Fig. 4.2b, after the *weight-relowering* technique is applied, we see that the height of the very low weight indicated by '$*$' has reduced, hence the updated uniform number U^n, given the increment term, $\frac{1}{N}$ is much less likely to fall in the range $(Q^1, Q^2]$ even for large N.

4.5 Simulation Results

This section features two simulation studies. Firstly, the non-linear tracking performance of the proposed KG-SMC-PHD filter is shown. Lastly, the performance improvement offered by the new resampling technique, the ISR method is demonstrated.

4.5.1 The KG-SMC-PHD Filter Performance

4.5.1.1 Simulation Context and Filter Parameters

In this simulation, a two-dimensional non-linear range and bearing scenario with unknown and varying number of targets observed over a cluttered region is considered. A total of 10 targets enter and exit the scene at various times throughout the simulation scenario. The measurement region is a half disc of radius 2000m. A plot of the ground truth (true trajectories) of the targets along with the start and end positions of each track is shown in Fig. 4.3. The start and end positions are indicated by a circle and a triangle respectively. The non-linear target dynamics are described by a nearly constant turn state model driven by white noise acceleration

$$\hat{\mathbf{x}}_k = \mathbf{F}(\omega_{k-1})\hat{\mathbf{x}}_{k-1} + \Gamma\mathbf{v}_k \tag{4.30}$$

$$\omega_k = \omega_{k-1} + \delta t u_{k-1} \tag{4.31}$$

where

$$\mathbf{F}(\omega) = \begin{bmatrix} 1 & \frac{\sin\omega\delta t}{\omega} & 0 & -\frac{1-\cos\omega\delta t}{\omega} \\ 0 & \cos\omega\delta t & 0 & -\sin\omega\delta t \\ 0 & \frac{1-\cos\omega\delta t}{\omega} & 1 & \frac{\sin\omega\delta t}{\omega} \\ 0 & \sin\omega\delta t & 0 & \cos\omega\delta t \end{bmatrix}, \ \Gamma = \begin{bmatrix} \frac{\delta t^2}{2} & 0 \\ \delta t & 0 \\ 0 & \frac{\delta t^2}{2} \\ 0 & \delta t \end{bmatrix}.$$

$\mathbf{F}(\omega)$ is the transition matrix for nearly constant turn rate, δt denotes the sample period which is assumed to be $1s$ in this simulation and Γ denotes the input matrix. The target state vector $\mathbf{x}_k = [\hat{\mathbf{x}}_k, \omega_k]^{\bar{T}}$ comprises the planar positions and velocities given as $\hat{\mathbf{x}}_k = [x_k, \dot{x}_x, y_k, \dot{y}_k]^{\bar{T}}$ along with turn rate ω_k. The variables (x_k, y_k) represent the position of the target and $(\dot{x}_k, \dot{y}_k)$ represent the velocities.

$\mathbf{v}_k = \mathcal{N}(\cdot, 0, \sigma_v^2 I)$ and $u_{k-1} = \mathcal{N}(\cdot, 0, \sigma_u^2 I)$ with $\sigma_v = 10$ m/s^2 and $\sigma_u = \pi/180$ rad/s. $[\cdot]^{\bar{T}}$ denotes transpose operation.

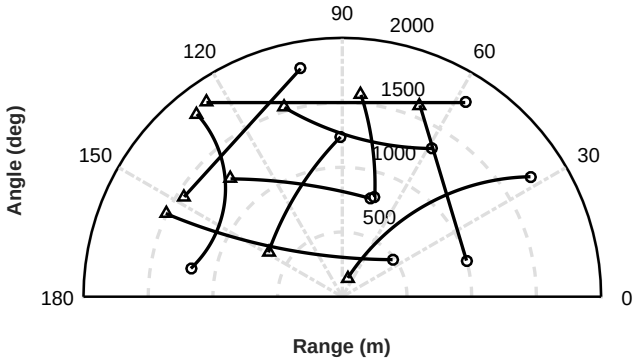

Figure 4.3 True target trajectories in the range-bearing plane with start/end positions for each track shown with $\bigcirc/\triangle$.

Targets can appear and disappear in the tracking volume at any time. Target spawning is not considered in this example. Each persistent target has a probability of survival, $p_S(\mathbf{x}_{k-1}) = 0.9$. The target birth process is modelled as a Poisson point process with intensity function $\gamma_k(\mathbf{x}_k) = 0.3\mathcal{N}(\cdot, \acute{\mathbf{x}}_1, \acute{\mathbf{Q}}) + 0.3\mathcal{N}(\cdot, \acute{\mathbf{x}}_2, \acute{\mathbf{Q}}) + 0.3\mathcal{N}(\cdot, \acute{\mathbf{x}}_3, \acute{\mathbf{Q}}) + 0.3\mathcal{N}(\cdot, \acute{\mathbf{x}}_4, \acute{\mathbf{Q}}) + 0.3\mathcal{N}(\cdot, \acute{\mathbf{x}}_5, \acute{\mathbf{Q}})$, where $\acute{\mathbf{x}}_1 = [-1000, 0, 200, 0]^{\bar{T}}$, $\acute{\mathbf{x}}_2 = [1000, 0, 1500, 0]^{\bar{T}}$, $\acute{\mathbf{x}}_3 = [0, 0, 1500, 0]^{\bar{T}}$, $\acute{\mathbf{x}}_4 = [500, 0, 500, 0]^{\bar{T}}$, $\acute{\mathbf{x}}_5 = [1500, 0, 1000, 0]^{\bar{T}}$ and covariance matrix, $\acute{\mathbf{Q}} = \mathrm{diag}([200, 50, 200, 50, 6(\pi/180)]^{\bar{T}})$.

The target-originated measurements are given by the non-linear model

$$\boldsymbol{z}_k = \begin{bmatrix} r_k \\ \theta_k \end{bmatrix} + \mathbf{n}_k \tag{4.32}$$

with

$$r_k = \left\| \begin{bmatrix} 1 & 0 & 0 & 0 \\ 0 & 0 & 1 & 0 \end{bmatrix} \mathbf{x}_k - \begin{bmatrix} x_s \\ y_s \end{bmatrix} \right\|, \tag{4.33}$$

and

$$\theta_k = \arctan\left(\frac{[0\ 0\ 1\ 0]\mathbf{x}_k + y_s}{[1\ 0\ 0\ 0]\mathbf{x}_k + x_s} \right) \tag{4.34}$$

where the measurement noise, $\mathbf{n}_k$ is a zero-mean Gaussian white noise vector with covariance matrix $\mathbf{R}$ =diag($[\sigma_r^2, \sigma_\theta^2]$) with $\sigma_r = 10m$ and $\sigma_\theta = 0.5$ rad. The measurement sensor's location, $[x_s, y_s]^T$ is at the origin. Clutter is uniformly distributed over the measurement region of $[0, \pi] \times [0, 2000]$ with a Poisson point process on the clutter region with a uniform intensity function $\kappa_k = 3.2 \times 10^{-3}$(radm)$^{-1}$ (giving an average of $\lambda = 20$ clutter points per scan). The total number of particles at time k is

$$\mathcal{L}_k = L_k + J_k, \qquad \text{and} \qquad L_k \cong \rho \hat{T}_{k|k} \tag{4.35}$$

where $\hat{T}_{k|k}$ denotes the expected number of targets, L_k is the number of particles for all persistent tracks, ρ denotes number of particles per persistent track and $J_k = \frac{\varrho}{5}$ is the number of samples per new born track. The probability of detection $p_D(\mathbf{x}_k)$ is 0.9.

To analyse the estimation error of the filter, the optimal subpattern assignment (OSPA) proposed in [125] and computation time (CT) are used. The CT is the time taken to run one iteration of the filter. The OSPA is a standard and well accepted metric in the MTT literature for evaluating performance of MTT techniques. The OSPA distance metric enables us to compare multi-target filtering algorithms [125]. The OSPA distance between two arbitrary finite sets, the state set $\mathbf{A} = \{\mathbf{a}_1, ..., \mathbf{a}_m\}$ and the ground truth state set $\mathbf{B} = \{\mathbf{b}_1, ..., \mathbf{b}_n\}$ is

$$\bar{d}_{\acute{p}}^{(\acute{c})}(\mathbf{A}, \mathbf{B}) = \begin{cases} 0 & \text{if} \quad \acute{m} = \acute{n} = 0 \\ \Theta(\mathbf{A}, \mathbf{B}) & \text{if} \quad \acute{m} \leq \acute{n} \\ d^{(\acute{c})}(\mathbf{A}, \mathbf{B}) & \text{if} \quad \acute{m} > \acute{n} \end{cases} \tag{4.36}$$

where

$$\Theta(\mathbf{A}, \mathbf{B}) \triangleq \left(\frac{1}{\acute{n}} \left(\min_{\pi \in \prod_{\acute{n}}} \sum_{i=1}^{\acute{m}} d^{(\acute{c})}(a_i, b_{\pi(i)})^{\acute{p}} + \acute{c}^{\acute{p}}(\acute{n} - \acute{m}) \right) \right)^{\frac{1}{\acute{p}}} \tag{4.37}$$

$\prod_{\acute{n}}$ is the set of permutations with length $\acute{m}$ on the set $\{1, ..., \acute{n}\}$. $d^{(\acute{c})}(\mathbf{a}, \mathbf{b}) := \min\{\acute{c}, \| \mathbf{a} - \mathbf{b} \|\}$ is the distance between single target vectors $\mathbf{a}$ and $\mathbf{b}$. $\acute{c} > 0$ is the

cut-off parameter and $\acute{p} \geq 1$ is a unit-less real number. Parameters $\acute{c} = 300$ and $\acute{p} = 1$ were chosen. The cut-off parameter $\acute{c}$ determines the relative weighting of the penalties assigned to localisation and cardinality errors, and $\acute{p}$ determines the sensitivity to outliers.

4.5.1.2 Effect of Proposal Distributions

Here, different importance sampling functions, TP, EPF and UPF of Sec. 3.4 are applied to the SMC-PHD and KG-SMC-PHD filters to observe the effects of each choice on filter performance. The results obtained are shown in Tables 4.1 and 4.2. The number of particles used in each of the two clutter cases is $\rho = 1000$. Tables 4.1 and 4.2 show results averaged over 1000 MC trials for $\lambda = 20$ and $\lambda = 30$ with measurement set partition respectively. Overall, using the UPF as a proposal distribution gives better performance for both filters in terms of low OSPA distance, but this method incurs the most computational load. This is primarily due to the generation of sigma points for each particle and the computation that follows during the unscented transform process. Using both EPF and UPF to construct the proposal distributions give better performance in terms of yielding lower OSPA, when compared to using TP. This is because both EPF and UPF helps to place generated samples 'under' measurements as soon as measurements become available. However, the improvement of using the UPF over EPF is not too significant in terms of OSPA distance. As a result, the EPF will be used as the importance sampling function for both filters in our subsequent discussion.

Table 4.1 Filter performance comparison in terms of OSPA distance, computation time (CT) and PD for $\lambda = 20$ and $\rho = 1000$ with measurement partition.

Filter	PD	OSPA (m)	CT (s)
SMC-PHD	TP (from Sec. 3.4.2.1)	94.85	9.50
	EPF (from Sec. 3.4.2.2)	83.17	11.67
	UPF (from Sec. 3.4.2.3)	81.72	12.85
KG-SMC-PHD	TP (from Sec. 3.4.2.1)	22.19	10.43
	EPF (from Sec. 3.4.2.2)	19.64	13.40
	UPF (from Sec. 3.4.2.3)	18.69	14.51

Table 4.2 Filter performance comparison in terms of OSPA distance, CT and PD for $\lambda = 30$ and $\rho = 1000$ with measurement partition.

Filter	PD	OSPA (m)	CT (s)
SMC-PHD	TP (from Sec. 3.4.2.1)	111.76	10.63
	EPF (from Sec. 3.4.2.2)	105.46	12.15
	UPF (from Sec. 3.4.2.3)	103.78	13.40
KG-SMC-PHD	TP (from Sec. 3.4.2.1)	31.56	11.77
	EPF (from Sec. 3.4.2.2)	21.70	14.90
	UPF (from Sec. 3.4.2.3)	20.15	15.76

4.5.1.3 Varying Number of Particles

For this case, the EPF was chosen as the importance sampling density for both filters. This is because as discussed earlier, using the EPF gives a lower CT. Tables 5.1 and 4.4 show results of filter performance in terms of number of particles, OSPA distance and CT obtained for both filters averaged over 1000 MC simulations for different ρ values when clutter is present with measurement partition. It can be observed from both tables that the performance of the SMC-PHD filter appears to deteriorate further with more position and cardinality mismatch (high OSPA distance) as clutter density increases while the proposed filter is seen to maintain a consistent performance with improved accuracy in position and cardinality (low OSPA distance). The CT of the proposed filter however is seen to be higher than the SMC-PHD filter for a given ρ value. This is due to the particle state correction step of the proposed filter. However, the number of particles required in terms of performance level (i.e. low OSPA) by the proposed filter is far less when compared to the SMC-PHD filter making the proposed filter more efficient.

Fig. 4.4 depicts the average of 1000 MC runs of the true and estimated number of targets for $\rho = 500$ with average number of clutter per scan, $\lambda = 20$. This result shows that the KG-SMC-PHD filter is able to estimate properly the number of targets under such high clutter condition. Fig. 4.5 shows the x and y components (versus time) of the true trajectories and the KG-SMC-PHD filter estimates. The plots indicate that the proposed filter with $\rho = 500$ particles per existing track is able to properly track all targets and in addition to being able to identify all target

Table 4.3 Filter performance in terms of number of particles, OSPA distance and CT for $\lambda = 20$ with measurement partition.

Filter	ρ	OSPA (m)	CT (s)
SMC-PHD	50	149.31	0.42
	100	100.36	0.86
	500	86.38	5.19
	1000	83.17	11.67
KG-SMC-PHD	50	44.70	0.72
	100	33.29	1.26
	500	22.11	6.29
	1000	19.64	13.40

Table 4.4 Filter performance in terms of number of particles, OSPA distance and CT for $\lambda = 30$ with measurement partition.

Filter	ρ	OSPA (m)	CT (s)
SMC-PHD	50	154.82	0.47
	100	117.88	0.93
	500	106.19	5.99
	1000	105.46	12.15
KG-SMC-PHD	50	47.15	0.87
	100	39.30	1.36
	500	25.79	7.02
	1000	21.70	14.90

births and deaths while successfully accommodating non-linearities under high clutter condition.

4.5.1.4 Other Filters

To further demonstrate the performance of the KG-SMC-PHD filter, the proposed filter was evaluated along with the GM-PHD filter of [140], the GM-USMC-PHD filter of [148] and the AP-PHD filter in [14] in addition to the standard SMC-PHD filter. The evaluation is in terms of OSPA distance and CT. For this comparison, the EPF was used to construct the importance sampling function for both the KG-SMC-PHD filter and the SMC-PHD filter. The KG-SMC-PHD filter was evaluated at 500 and $\frac{500}{5}$ particles for existing and newborn tracks respectively while 1000

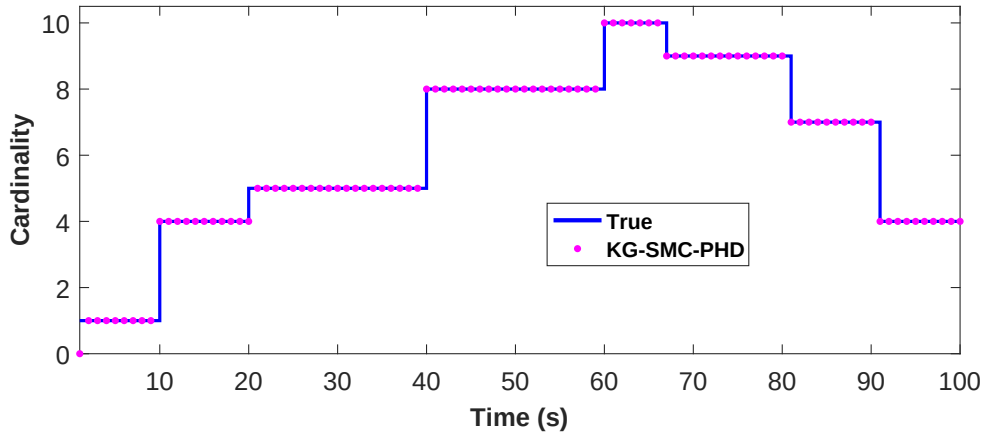

Figure 4.4 True and KG-SMC-PHD filter cardinality estimates of targets time averaged over 1000 MC trials with $\rho = 500$ particles per existing track.

and $\frac{1000}{5}$ particles for existing and newborn tracks respectively were used for the SMC-PHD filter.

The GM-PHD filter was implemented with an extended Kalman filter (EKF). The maximum number of Guassian terms was set to 100, with the merging (T_m) and pruning threshold (T_p) set at 10m and 10^{-3} respectively. A Gaussian component is considered target-originated if its weight is above 0.4. The estimated number of targets is given by the sum of weights of the Gaussian mixture.

In the AP-PHD filter implementation, 1000 particles were used per existing track and $\frac{1000}{5}$ particles were used for the newborn track. Each new track initialisation is measurement driven and each current measurement is associated with the corresponding highest bidder if the bid is greater than 0.4. The auxiliary importance sampling [14] process starts with the selection of the measurements that are well described by the targets' states extracted from the estimated PHD and this is achieved using the auction algorithm. Both auctioning and state extraction is done as in [14].

The GM-USMC-PHD filter uses a Gaussian mixture to approximate the IS function. The GM implementation of the GM-USMC-PHD filter is similar to the GM-PHD filter in terms of number of Gaussian components and pruning and merging thresholds. The number of samples per GM component is set to 1000. The

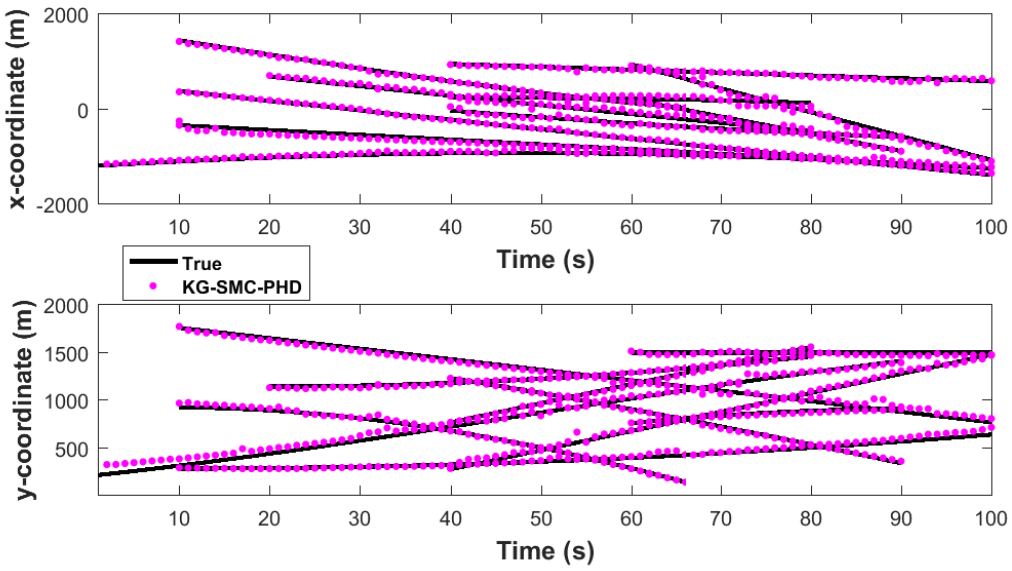

Figure 4.5 x and y components (versus time) of the true target trajectories and the KG-SMC-PHD filter estimates for $\rho = 500$ particles per existing track.

newborn track initialisation, resampling and state extraction steps follow [148] and the mean and the covariance of Gaussian is computed using the unscented information filter [11].

Tables 4.5 and 4.6 show filter performance results averaged over 1000 MC runs with and without measurement set partition respectively. In both tables, measurement partition was applied to the KG-SMC-PHD filter. The effect of the measurement partitioning process can be seen in Table 4.5 as the OSPA distance improved for the other filters. This is because measurements due to clutter were discarded and not used in the weight update stages of the filters. Notice also there is a slight increase in CT from Table 4.5 as compared to 4.6. This reflects the added CT during the partitioning process. Overall, under high clutter, the KG-SMC-PHD filter gives a better performance as it maintains low OSPA[1] distance. This is mainly due to our particle state correction technique. Also, in Table 4.5, it can be observed that with just 500 particles per existing track, the KG-SMC-PHD filter outperformed all other filters by having lower OSPA distance.

[1]The OSPA [125] metric measures the combination of both localisation and cardinality distance.

Figure 4.6 plots the time averaged OSPA distances for all the five filters over 1000 MC trials with measurement set partition. Here, 1000 particles were used per existing track for the KG-SMC-PHD filter while the parameters of the other four filters were maintained. As shown in Fig. 4.6, high values of OSPA distance occurs when new targets are born around time indices $k = 10, 20, 40$ and 60. It is observed from the Figure that the SMC-PHD filter gave the least performance while the proposed filter shows superior performance in terms of average OSPA distance per target when compared to the other filters under high clutter condition. The proposed filter achieved this good performance level due to our selective particle correction technique. Fig. 4.6 further suggests that for our simulation example, there isn't a significant difference performance wise between the GM-PHD, GM-USMC-PHD and the AP-PHD filters as all three filters gave similar level of performance in terms of average miss-distance per target.

Table 4.5 Filter performance comparison in terms of OSPA distance and CT for $\lambda = 20$ with measurement set partition.

Filter	OSPA (m)	CT (s)
KG-SMC-PHD	22.11	6.29
SMC-PHD	83.17	11.67
GM-PHD	38.05	2.59
GM-USMC-PHD	35.38	13.58
AP-PHD	33.19	16.99

Table 4.6 Filter performance comparison in terms of OSPA distance and CT for different filters for $\lambda = 20$ without measurement set partition.

Filter	OSPA (m)	CT (s)
KG-SMC-PHD	22.11	6.29
SMC-PHD	94.66	10.11
GM-PHD	44.93	1.90
GM-USMC-PHD	47.23	12.25
AP-PHD	39.01	14.22

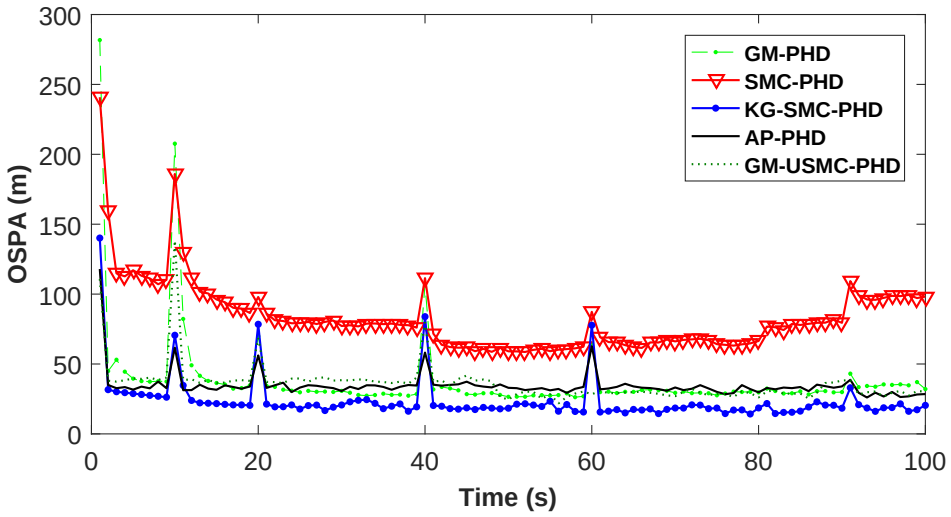

Figure 4.6 OSPA distance averaged over 1000 MC runs for clutter rate of 20 Poisson clutter ($\lambda = 20$) per scan ($\acute{c} = 300$, $\acute{p} = 1$)

4.5.1.5 Further Evaluation

The filter limitations in terms of OSPA distance and number of clutter points, number of particles and CT as well as general filter performance are now discussed. Fig. 4.7 plots time averaged 1000 MC trials of the OSPA distance for the SMC-PHD filter and the KG-SMC-PHD filter against clutter intensities from $\kappa_k = 0$ (radm)$^{-1}$ to $\kappa_k = 8 \times 10^{-3}$(radm)$^{-1}$, that is, from $\lambda = 0$ to $\lambda = 50$. Both filters were implemented with measurement set partition with $\rho = 1000$. It is observed that the miss-distance increases for both filters as clutter intensity increases. However, this increase in OSPA distance is more significant in the SMC-PHD filter implementation compared to the proposed filter. Fig. 4.7 clearly shows that the proposed filter outperforms the SMC-PHD filter as it maintains an average OSPA distance of less than 51m up to clutter intensity of $\kappa_k = 8 \times 10^{-3}$(radm)$^{-1}$ due to the particle state correction technique in our approach while the SMC-PHD filter starts to exhibit breakdown from about $\kappa_k = 6.4 \times 10^{-3}$(radm)$^{-1}$ ($\lambda = 40$). For this simulation example, the proposed filter performed well up to $\lambda = 60$ and started exhibiting breakdown at about $\lambda = 65$. Note that this time-averaging result is intended as a guide to provide a broad indication of the performance of the filter and can vary depending on the application scenario.

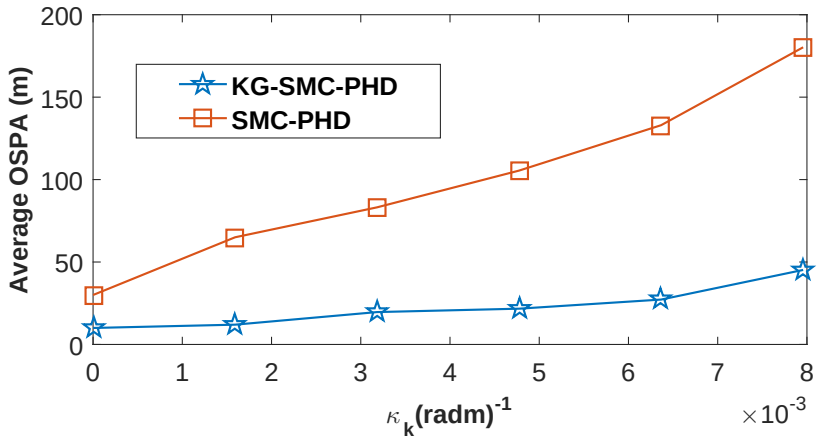

Figure 4.7 Averaged OSPA distances versus varying clutter intensity over 1000 Monte Carlo (MC) trials.

Fig. 4.8 shows the effect of the choice of number of particles on OSPA distance and CT. As expected, on the right side of the y-axis, the CT increases for both filters as number of particles increases. It is also observed that for the same number of particles, the CT of the SMC-PHD filter is always lower when compared to the proposed approach and the difference in CT for both filters increases with increase in number of particles. The extra computation load for the proposed filter is due to the extra particle state correction step of our approach. However, on the left side of the y-axis, the miss-distance of the proposed technique is seen to be significantly lower compared to the SMC-PHD filter. Although the performance of the SMC-PHD filter is seen to improve with increase in number of particles, the filter did not achieve the accuracy level of the proposed filter even with 10000 particles. In terms of miss-distance, Fig. 4.8 also suggests that the proposed filter is more efficient as only few a particle (less than 1000) are required to achieve an OSPA distance of less than 50m while the SMC-PHD filter requires about 10000 particles.

4.5.2 ISR Performance Demonstration

The performance of the proposed ISR method against the SR resampling method is demonstrated. A 2-D MTT scenario where a total of four targets are tracked using

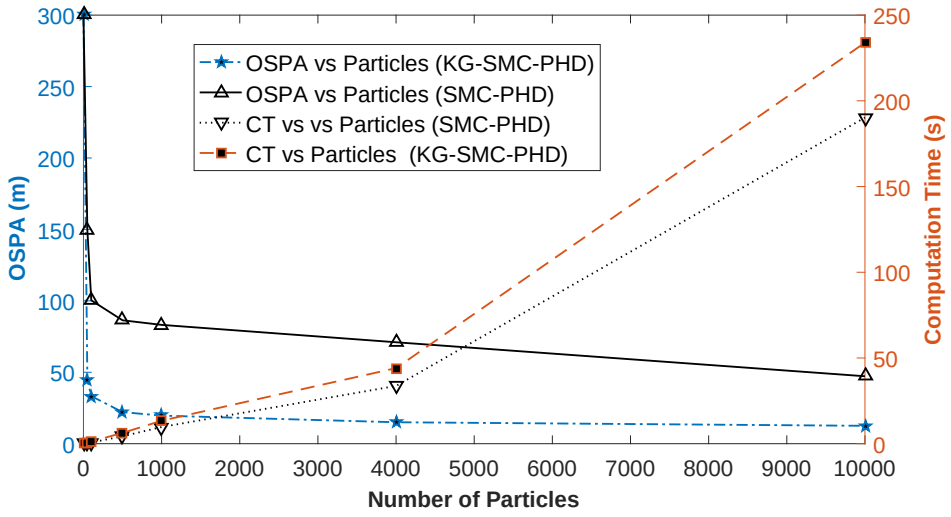

Figure 4.8 KG-SMC-PHD and SMC-PHD filter performance evaluation in terms of OSPA distance and CT versus varying number of particles time averaged over 1000 MC trials for $\lambda = 20$.

a nonlinear measurement model is considered. The targets were observed for 100 discrete time steps, that is, $k = 1, \cdots, 100$. The true trajectories of the targets are shown in Fig. 4.9. The start and end positions are indicated by a triangle and a square respectively. Filter parameters as in Section 4.5.1.1 are maintained.

The new KG-SMC-PHD filter is used to achieve MTT. The new filter‘s tracking result is shown in Fig. 4.10. So that at each time k the multiple target approximating distributions can be obtained and both the SR and ISR can be applied to perform resampling. After resampling, state estimation and estimation error are computed before proceeding to the next time $k + 1$. The OSPA metric described in Section 4.5.1.1 is used to evaluate the error in the estimation of the approximating distribution for using the ISR and the SR methods. A high OSPA measure translates to high estimation error while a lower OSPA measure means lower estimation error, hence higher accuracy. In addition, the OSPA for each of the methods for various number of resampled particles required N is observed.

Fig. 4.11a shows OSPA measures versus measurement time. The results were averaged over 100 Monte Carlo (MC) runs of the tracking filter. The number of particles used for the tracking filter is 10,000 particles per existing target. Both ISR and SR methods were implemented concurrently during each MC run. This

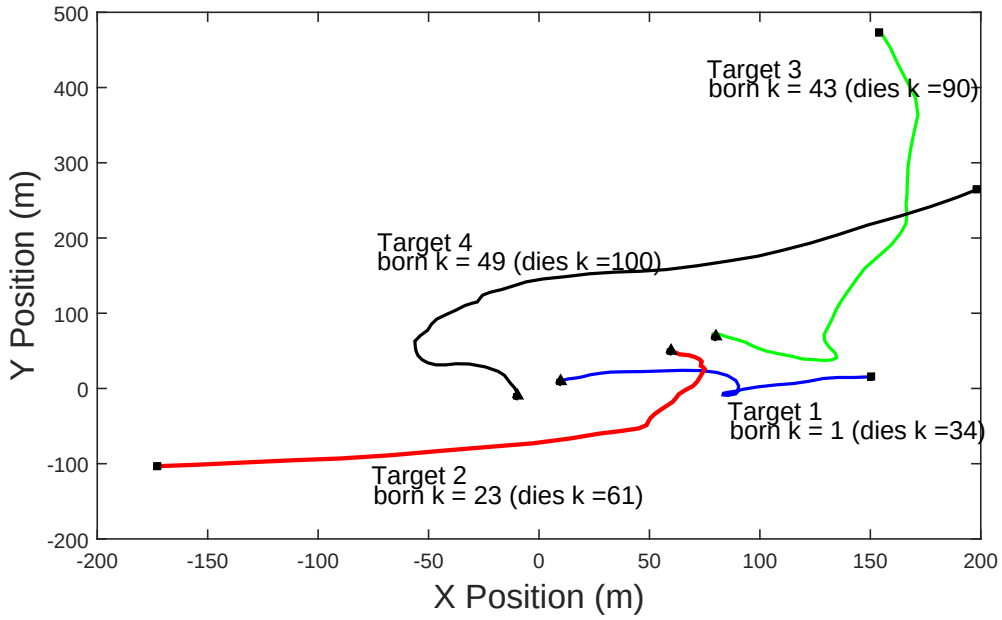

Figure 4.9 Ground truth for target trajectories of four tracks superimposed on the xy plane over 100 time steps

means that the same approximating distributions were fed into to both resampling methods at each time k before state estimates were extracted and OSPA computed. From Fig. 4.11a, it is seen that the ISR method outperforms the SR method by giving a lower OSPA measure compared to the SR throughout the measurement time. The poor state estimation for when the SR method is used can be attributed to very low weights being resampled. Furthermore, with the *weight-relowering* technique, the state estimation accuracy is improved for when the ISR resampling method was used.

Fig. 4.11b shows OSPA measures versus number of resampled particles required. The results were averaged over 100 MC runs of the tracking filter. The result shows that both techniques give similar level of performance for when the number of resampled particles required, N is around 1000 or less. But for larger values of N, the proposed method performs better than the SR method by having a lower OSPA measure when compared to the SR method. The result further confirms the hypothesis that when the SR method is used, the state estimation error is likely to increase especially for large values of N.

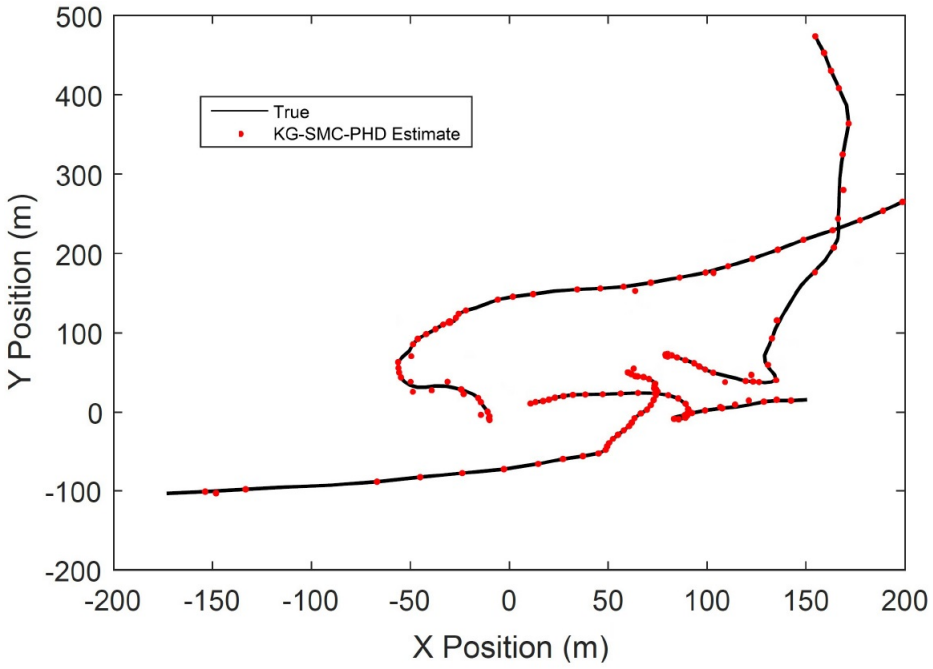

Figure 4.10 Ground truth for target trajectories of four tracks superimposed on the xy plane over 100 time steps

4.5.3 Overall Performance Contribution

Comparing the contributions of this chapter, firstly, a partitioning technique was used on consecutive measurement sets to separate existing targets from clutter and new born targets. This process primarily serves the function of reducing the number candidate measurements to use in the weight update stage in the presence of clutter. A reduced computational burden is thus achieved as the unnecessary computation on measurements due to clutter is avoided during weight update. Secondly, the Kalman-gain as a correction technique seeks to achieve minimal variance and thereby gives better accuracy (in approximating the posterior). Additionally, an improved resampling method is utilised in resapmling to further improve the posterior accuracy. As a result, fewer particles are required to populate regions of interest. Furthermore, the effect of the partitioning process is not apparent in the no clutter to partition. However, the correction step is needed with or without clutter. As a whole, the use of the Kalman-gain correction method is the contribution which gives the main improvement.

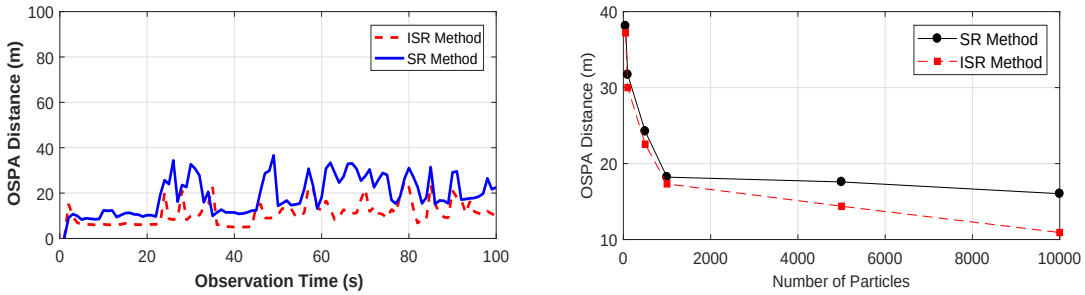

(a) (b)

Figure 4.11 (a) Performance in terms of OSPA distance against measurement time for $N = M$. (b) Performance in terms of OSPA measure against increasing number of particles for a constant $M = 1000$ and varying N from 50 to 10,000.

4.6 Summary

In this chapter, a new and efficient SMC filter, namely the KG-SMC-PHD filter for MTT which seeks to minimise the MSE between received and estimated measurements at any given time has been proposed. This was achieved by first partitioning the measurement set into target-originated measurements and clutter for weight computation and applying the Kalman-gain to selected particles for state correction. Furthermore, an improved resampling method was proposed to address a resamping problem that lead to the possibility of poor state estimates in SMC methods. The overall tracking performance of the KG-SMC-PHD filter was improved because, i) only target-originated measurements were used for weight computation and ii) the MSE at each time step was reduced resulting in fewer number of particles for state estimation. Simulation studies demonstrate that the KG-SMC-PHD filter algorithm outperforms the standard SMC-PHD filter as well as other alternative implementations of the PHD filter. Additionally, simulation results showed that the proposed ISR resampling method outperforms the standard systematic resampling method particularly when large number of resampled particles are required.

The standard SMC-PHD filter described in Section 3.6.2 and the KG-SMC-PHD filter proposed in this chapter are able to perform multiple target state estimation as well as estimate number of targets. However, when the number of targets large, the variance in the estimated number of targets by both filters increases. Addressing this problem will mean an even more accurate multi-target tracker

that can track more targets with better performance when the Kalman-gain aided technique is applied. The next chapter introduces a multi-target tracker that achieves this.

Chapter 5

Multiple Target Tracking Using the Kalman-Gain Particle CPHD Filter

5.1 Introduction

In the previous chapter, a new and efficient SMC-PHD filter for multiple target tracking was developed. Besides the improvement in tracking accuracy offered by this method, fewer number of particles are used to achieve this performance improvement. However, the KG-SMC-PHD filter developed in Chapter 4 and PHD filters in general can give a high variance in target number. This is because the PHD recursion propagates cardinality information with only a single parameter (i.e. mean of the cardinality distribution), and as a result it effectively approximates the cardinality distribution by a Poisson distribution. So as the number of target gets higher, so does the mean and consequently the variance since the mean and variance of a Poisson distribution are equal. As a solution to this problem, the cardinalised PHD (CPHD) filter was proposed by authors in [100]. The CPHD filter not only propagates the first order moment of an RFS but also the probability distribution of the number of targets. Hence, the CPHD filter not only has the advantages of the PHD filter but also provides a better estimate of the target number (cardinality).

In this chapter, a cardinalised version of the work in Chapter 4 is proposed. By doing so, an MTT technique that not only offers improved tracking performance with fewer particles but also improved cardinality estimate is developed. This new filter is named as the Kalman-gain aided cardinalised SMC-PHD (KG-SMC-PHD) filter. This technique is applied to track multiple targets in nonlinear target dynamics setting to demonstrate its performance.

5.2 Preliminaries

Assume that the multi-target state is given by $\mathbf{X}_k = \{\boldsymbol{x}_{1,k}, ..., \boldsymbol{x}_{T,k}\} \in \mathbb{X}$, where $\mathbb{X}$ denotes the state space. In addition, at each time step, a new target may enter the tracking scene, and/or an existing target may disappear from the scene or evolve to another state.

Furthermore, let the set $\mathbf{Z}_k \in \mathbb{Z}$ be the multi-target measurement state at time k where $\mathbb{Z}$ denotes the measurement space. The measurement set $\mathbf{Z}_k$ consists of measurements due to targets and measurements due to clutter or false alarms. Since the evolution of the targets and the origin of measurements are uncertain, both $\mathbf{X}_k$ and $\mathbf{Z}_k$ can be modelled as RFS [102] and [105]. Under the RFS model, the uncertainty can be handled using finite set statistics (FISST) [102].

In the recursive Bayes multi-target filter, the goal is to use the *prediction* and *update* steps to evaluate the posterior pdf $p_{k|k}(\mathbf{X}_k|\mathbf{Z}_{1:k})$ given the corrupted sets of measurements up to and including time k ($\mathbf{Z}_{1:K} : \mathbf{Z}_1, \mathbf{Z}_2, ..., \mathbf{Z}_K$). As this is difficult to achieve, Mahler proposed in [102] to propagate only the first-order moments of the posterior $p_{k|k}(\mathbf{X}_k|\mathbf{Z}_{1:k})$, known as the PHD $D_{k|k}(\mathbf{x} \mid \mathbf{Z}_{1:k})$. Taking the integral of $D_{k|k}$ over the state space $\mathbb{X}$ yields the expected target number under the state space [102]. However, authors in [57] highlighted that the PHD filter suffers from a problem known as target-death where even a single missed detection can lead to the apparent disappearance of a target. Therefore, they argued for the need for a PHD type filter which remains first-order in the estimate of states of individual targets, but which is higher-order in target number. To this end, the work in [100] proposed a technique which jointly propagates the PHD $D_{k|k}$ alongside the

cardinality distribution $\rho(n) = \Pr(|\ \mathbf{X}\ | = n)$ where

$$\rho(n) = \frac{1}{n!} \int p_{k|k}(\{\boldsymbol{x}_1, \ldots, \boldsymbol{x}_n\}|\mathbf{Z}_{1:k}) d\boldsymbol{x}_1 \ldots \boldsymbol{x}_n. \tag{5.1}$$

where $p_{k|k}(\cdot|\cdot)$ is the multi-target state posterior probability density. This then forms the basis for the CPHD filter.

5.3 The CPHD Filter

The CPHD filter is a generalisation of the PHD filter $D_{k|k}$ where both the cardinality distribution $\rho_{k|k}(n)$ and the PHD $D_{k|k}$ are jointly propagated to achieve better performance but with a higher computational complexity [100]. Part of the computational complexity of the CPHD filter is in the computation of an elementary symmetric function in the update stage (as will be seen later). However, methods such as the Newton-Girard formulae have been used to achieve this thereby facilitating the CPHD filter implementation. From here on, the alternative form of the CPHD proposed in [139] is used. The prediction and update stages of the CPHD filter are presented next.

5.3.1 Prediction

The CPHD prediction involves computing the predicted PHD $D_{k|k-1}$ in the same manner as the PHD filter (see [102]) alongside the predicted cardinality distribution $\rho_{k|k-1}(n)$, which is the convolution of the birth cardinality distributions $\rho_{\Gamma,k}$:

$$\rho_{k|k-1}(n) = \sum_{i=0}^{n} \rho_{\Gamma,k}(n-i)\rho_{S,k|k-1}(i) \tag{5.2}$$

and surviving target cardinality distribution

$$\rho_{S,k|k-1}(i) = \sum_{\ell=i}^{\infty} \frac{\ell!}{i!(l-i)!} p_S^i (1-p_S)^{\ell-i} \rho_{k-1|k-1}(\ell) \tag{5.3}$$

where p_S is the probability of survival.

5.3.2 Update

The CPHD update equations for both the PHD $D_{k|k}$ and the cardinality distribution $\rho_{k|k}(n)$ are given by [100], [139]

$$\rho_{k|k}(n) = \frac{\Upsilon_k^0[D_{k|k-1}; \mathbf{Z}_k](n)\rho_{k|k-1}(n)}{\langle \Upsilon_k^0[D_{k|k-1}; \mathbf{Z}_k], \rho_{k|k-1} \rangle} \tag{5.4}$$

$$\begin{aligned} D_{k|k}(\boldsymbol{x}) = & \frac{\langle \Upsilon_k^1[D_{k|k-1}; \mathbf{Z}_k], \rho_{k|k-1} \rangle (1 - p_D(\boldsymbol{x})) D_{k|k-1}(\boldsymbol{x})}{\langle \Upsilon_k^0[D_{k|k-1}; \mathbf{Z}_k], \rho_{k|k-1} \rangle} \\ & + \sum_{\boldsymbol{z} \in \mathbf{Z}_k} \frac{\langle \Upsilon_k^1[D_{k|k-1}; \mathbf{Z}_k \backslash \{\boldsymbol{z}\}], \rho_{k|k-1} \rangle \psi_{k,\boldsymbol{z}}(\boldsymbol{x}) D_{k|k-1}(\boldsymbol{x})}{\langle \Upsilon_k^0[D_{k|k-1}; \mathbf{Z}_k], \rho_{k|k-1} \rangle} \end{aligned} \tag{5.5}$$

where $\langle \cdot, \cdot \rangle$ denote the dot product operator. The sequence $\Upsilon_k^u[D, \mathbf{Z}](n)$ for $u \in \{0, 1\}$ is defined as:

$$\begin{aligned} \Upsilon_k^u[D, \mathbf{Z}](n) = & \sum_{i=0}^{\min(|\mathbf{Z}|, n)} (|\mathbf{Z}| - i)! \rho_{C,k}(|\mathbf{Z}| - i) P_{j+u}^n \\ & \times \frac{\langle 1 - p_{D,k}, D \rangle^{n-(i+u)}}{\langle 1, D \rangle^n} e_i \left(\Xi_k(D, \mathbf{Z}) \right) \end{aligned} \tag{5.6}$$

with

$$\psi_{k,z}(\boldsymbol{x}) = \frac{\langle 1, \kappa_k \rangle}{\kappa_k(\boldsymbol{z})} g_k(\boldsymbol{z}|\boldsymbol{x}) p_{D,k}(\boldsymbol{x}) \tag{5.7}$$

$$\Xi_k(D, \mathbf{Z}) = \{ \langle D, \psi_{k,z} \rangle : \boldsymbol{z} \in \mathbf{Z} \} \tag{5.8}$$

$$e_i(\mathbf{Z}) = \sum_{\mathrm{W} \subseteq \boldsymbol{z}, |\mathrm{W}| = i} \left(\prod_{\xi \in w} \zeta \right) \tag{5.9}$$

$$P_\ell^n = \frac{n!}{(n - l)!}. \tag{5.10}$$

where $e_i(z)$ is the elementary symmetric function (ESF) of order i for a finite set $\boldsymbol{z}$ [105], $\mathbf{Z}_k$ is the measurement set at time k, $g_k(\cdot|\boldsymbol{x})$ is the single-target measurement likelihood function given current state $\boldsymbol{x}$, $p_{D,k}(\boldsymbol{x})$ is the probability of detection, $\kappa_k(\cdot)$ denotes the intensity of clutter measurements, while $\rho_{C,k}(n)$ is the cardinality distribution of clutter at time k.

The CPHD filter recursion above has been implemented in two distinct fashions. The first one is a Gaussian mixture CPHD (GM-CPHD) filter [139] which assumes

linear Gaussian dynamics in target states and birth process. The second one is the particle CPHD filter [120] which is more suited to non-linear non-Gaussian target dynamics. The improvement proposed in this chapter is towards the particle implementation of the CPHD filter.

5.4 The Kalman-Gain-Aided SMC-CPHD Filter

The KG-SMC-CPHD filter seeks to achieve a more accurate posterior by applying particle state correction in the update stage of the standard SMC-CPHD filter. This is achieved by using the Kalman gain technique alongside a validation threshold. The validation threshold is used to identify promising particles belonging to a target and moving them to regions of higher likelihoods in order to arrive at a more accurate posterior. To this end, the prediction stage of the KG-SMC-CPHD filter is first presented followed by the update stage.

5.4.1 Prediction

The KG-SMC-CPHD filter prediction stage is similar to the standard SMC-CPHD filter (see for example, [120]). Assume at time $k-1$ that the cardinality distribution is $\rho_{k-1|k-1}(n)$ and that the PHD $D_{k-1|k-1}$ is given by a set of particles with associated weights $\left\{\boldsymbol{x}_{k-1}^{j}, w_{k-1}^{j}\right\}_{j=1}^{L_{k-1}}$.

Predict the cardinality distribution according to (5.2). Predict the PHD $D_{k|k-1}$ by drawing L_k and J_k samples with associated weights for existing and new born targets respectively from two proposal distribution using:

$$\begin{aligned}
\boldsymbol{x}_{k|k-1}^{j} &\approx \begin{cases} q_k(\cdot|\boldsymbol{x}_{k-1}^{j}, \mathbf{Z}_k), & j = 1, ..., L_k \\ p_k(\cdot|\mathbf{Z}_k), & j = L_k+1, ..., \mathcal{L}_k \end{cases} \\
w_{k|k-1}^{j} &= \begin{cases} \frac{p_S(\boldsymbol{x}_{k-1}) f_{k|k-1}(\boldsymbol{x}_k, \boldsymbol{x}_{k-1})}{q_k(\boldsymbol{x}_{k|k-1}|\boldsymbol{x}_{k-1}^{j}, \mathbf{Z}_k)} w_{k-1}^{j}, & j = 1, ..., L_k \\ \frac{\gamma_k(\boldsymbol{x}_k^{j})}{J_k p_k(\boldsymbol{x}_{k|k-1}|\mathbf{Z}_k)}, & j = L_k+1, ..., \mathcal{L}_k \end{cases}
\end{aligned} \tag{5.11}$$

such that

$$D_{k|k-1}(\boldsymbol{x}|\mathbf{Z}_{k-1}) = \sum_{j=1}^{\mathcal{L}_k} w_{k|k-1}^{j} \delta(\boldsymbol{x}_{k|k-1}^{j}). \tag{5.12}$$

where $q_k(\cdot|\cdot)$ and $p_k(\cdot|\cdot)$ denote proposal distributions for surviving and new born targets respectively, $p_S(\cdot)$ is the probability of target survival, $\mathcal{L}_k = L_k + J_k$, $\gamma_k(\cdot)$ is the PHD of the spontaneous birth and $f_{k|k-1}(\cdot,\cdot)$ is the single target motion model.

5.4.2 Update

Our proposed technique is applied during this stage. In this stage, the PHD is updated by computing (5.5) and then the cardinality distribution (5.4). To this end, predicted particles for state correction are identified and selected. A predicted particle, $\boldsymbol{x}_{k|k-1}^{j}$ is selected for correction if, for each clutter free measurement $\mathbf{z}_k \in \boldsymbol{Z}_k$, the condition below is satisfied:

$$g(\dot{\mathbf{z}}_k^n|\boldsymbol{x}_{k|k-1}^{j}) \geq \tau, \quad \text{for } j = 1, ..., \mathcal{L}_k \tag{5.13}$$

where $g(\cdot|\cdot)$ is the measurement likelihood function; τ is chosen to be inversely proportional to the total number of samples per persistent target [46]. The term $\dot{\mathbf{z}}_k^n$ is the clutter free measurement such that

$$\dot{\boldsymbol{Z}}_k = \bigcup_{n=1}^{n_s} \{\dot{\mathbf{z}}_k^n\}, \tag{5.14}$$

where $\dot{\boldsymbol{Z}}_k \subset \boldsymbol{Z}_k$ is the set of clutter free measurements obtained using a measurement set partitioning method as in [46]; $n = 1, \cdots, n_s$ and $n_s = \left|\dot{\boldsymbol{Z}}_k\right|$. Each particle satisfying (5.13) is assumed to be a reasonable candidate for correction given the current measurement. The state of each particle satisfying (5.13) is corrected as

follows:

$$\boldsymbol{x}_k^j = \boldsymbol{x}_{k|k-1}^j + \mathbf{K}_k(\dot{\mathbf{z}}_k^n - h(\boldsymbol{x}_{k|k-1}^j)) \tag{5.15}$$

$$\mathbf{K}_k = \mathbf{M}_{k-1}\mathbf{H}_k^T\mathbf{P}_k^{-1} \tag{5.16}$$

$$\mathbf{P}_k^{-1} = \mathbf{R}_k + \mathbf{H}_k\mathbf{M}_{k-1}\boldsymbol{H}_k^T \tag{5.17}$$

$$\mathbf{M}_k = \mathbf{M}_{k-1} - \mathbf{K}_k\mathbf{H}_k\mathbf{M}_{k-1} \tag{5.18}$$

where $\mathbf{K}_k$ and $\mathbf{H}$ denotes the Kalman-gain and the measurement transformation matrix respectively, $h(\boldsymbol{x}_{k|k-1}^l)$ is the projection of the predicted state $\boldsymbol{x}_k^j$ on to the measurement, $\mathbf{R}$ is the measurement error covariance matrix, $\mathbf{M}$ is the state estimation covariance matrix, , and $\mathbf{P}$ is the innovation covariance matrix.

For each $\mathbf{z}_k \in \boldsymbol{Z}_k$, following particle state correction, (5.8), (5.9), and (5.6) are computed. Afterwards, the estimated cardinality distribution $\rho_{k|k}(n)$ is updated according to (5.4) and particle weights $w_{k|k}^j$ updated according to (5.5). The estimated number of targets is obtained as:

$$N_k = \sum_j^{\mathcal{L}_k} w_{k|k}^j \tag{5.19}$$

and the particle representation of the PHD $D_{k|k}$ is given as:

$$D_{k|k}(\boldsymbol{x}_k|\mathbf{Z}_k) = \sum_{j=1}^{\mathcal{L}_k} w_k^j \delta(\boldsymbol{x}_k^j). \tag{5.20}$$

5.5 Simulation Results

In this section, the performance of the KG-SMC-CPHD filter is compared with the SMC implementation of the CPHD filter of [100] and [139] which is tagged the standard SMC-PHD filter, using simulated data.

Assume a sensor $[x_s, y_s]^{\bar{T}}$ located at the origin of the x-y Cartesian coordinate which generates noisy range-bearing measurements of the targets with false alarms.

The target-originated measurements are given by the nonlinear model

$$\boldsymbol{z}_k = \begin{bmatrix} r_k \\ \theta_k \end{bmatrix} + \mathbf{n}_k \tag{5.21}$$

with

$$r_k = \left\| \begin{bmatrix} 1 & 0 & 0 & 0 \\ 0 & 1 & 0 & 0 \end{bmatrix} \mathbf{x}_k - \begin{bmatrix} x_s \\ y_s \end{bmatrix} \right\|, \tag{5.22}$$

and

$$\theta_k = \arctan\left(\frac{[0\ 1\ 0\ 0]\mathbf{x}_k + y_s}{[1\ 0\ 0\ 0]\mathbf{x}_k + x_s} \right) \tag{5.23}$$

where the measurement noise, $\mathbf{n}_k$ is a zero-mean Gaussian white noise vector with covariance matrix $\mathbf{R}$ =diag$([\sigma_r^2, \sigma_\theta^2])$ with $\sigma_r = 9m$ and $\sigma_\theta = 0.45$ rad. Clutter is uniformly distributed over the measurement region with a Poisson point process giving an average of $\lambda = 20$ clutter points per scan; $[\cdot]^{\bar{T}}$ denotes transpose operation.

A total of 8 targets entering and exiting the tracking scene with multiple crossings are considered for a duration of 100 time steps. A plot of the ground truth (true trajectories) of the targets along with the start and end positions of each track is shown in Fig. 5.1. The start and end positions are indicated by a circle and a triangle respectively. The non-linear dynamics of the targets are described using a nearly constant turn state model given by

$$\mathbf{x}_k = \begin{bmatrix} 1 & 0 & \frac{\sin\omega\Delta t}{\omega} & -\frac{1-\cos\omega\Delta t}{\omega} \\ 0 & 1 & \frac{1-\cos\omega\Delta t}{\omega} & \frac{\sin\omega\Delta t}{\omega} \\ 0 & 0 & \cos\omega\Delta t & -\sin\omega\Delta t \\ 0 & 0 & \sin\omega\Delta t & \cos\omega\Delta t \end{bmatrix} \mathbf{x}_{k-1} + \begin{bmatrix} \frac{\Delta t^2}{2} & 0 \\ 0 & \frac{\Delta t^2}{2} \\ \Delta t & 0 \\ 0 & \Delta t \end{bmatrix} \mathbf{v}_k \tag{5.24}$$

where $\omega_k = \omega_{k-1} + \Delta t u_{k-1}$, Δt denotes the sample period which is assumed to be $1s$. The target state vector $\boldsymbol{x}_k = [\mathbf{x}_k, \omega_k]^{\bar{T}}$ comprises of planar positions and velocities given as $\mathbf{x}_k = [x_k, y_k, \dot{x}_x, \dot{y}_k]^{\bar{T}}$ along with turn rate ω_k. The variables (x_k, y_k) represent the position of the target and $(\dot{x}_k, \dot{y}_k)$ represent the velocities.

$\mathbf{v}_k = \mathcal{N}(\cdot, 0, \sigma_v^2 I)$ and $u_{k-1} = \mathcal{N}(\cdot, 0, \sigma_u^2 I)$ with $\sigma_v = 10$ m/s^2 and $\sigma_u = \pi/180$ rad/s.

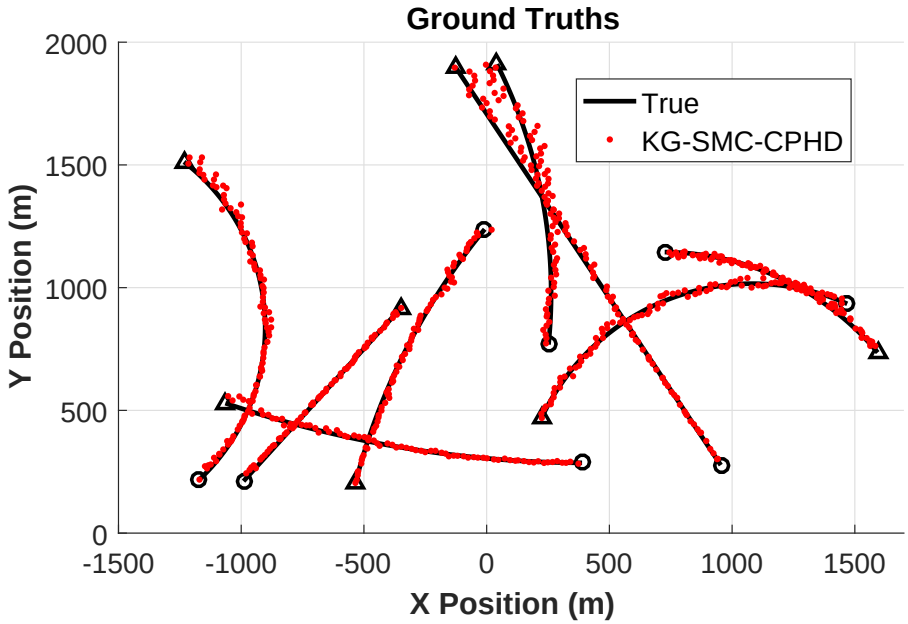

Figure 5.1 Plots showing the KG-SMC-CPHD filter estimates superimposed on the true target trajectories. The true start/end positions of the targets are indicated by ◯/△.

Fig. 5.1 show results from a single MC run of the proposed filter estimates superimposed on the true target tracks. The figure shows that the filter is able to track the targets correctly even with multiple target crossings. Fig. 5.3 shows the plot of target cardinality statistics for the KG-SMC-PHD filter (Fig. 5.3a) and the KG-SMC-CPHD filter (Fig. 5.3b). It is seen from Fig. 5.3a that although the KG-SMC-PHD filter is able to correctly estimate the number of targets, the standard deviation is high. From (Fig. 5.3b), as expected, the KG-SMC-CPHD filter, in addition to being able to correctly estimate the number of targets, it also had a much lower standard deviation. This is due to the propagation of the cardinality distribution jointly with PHD of the targets as opposed to only estimating the PHD of the targets as in the case of the KG-SMC-PHD filter.

Furthermore, to compare estimation error of the filter to the standard SMC-CPHD filter, the optimal subpattern assignment (OSPA) proposed in [125] and execution time (ET) are used. Table 5.1 show filter performance obtained for both

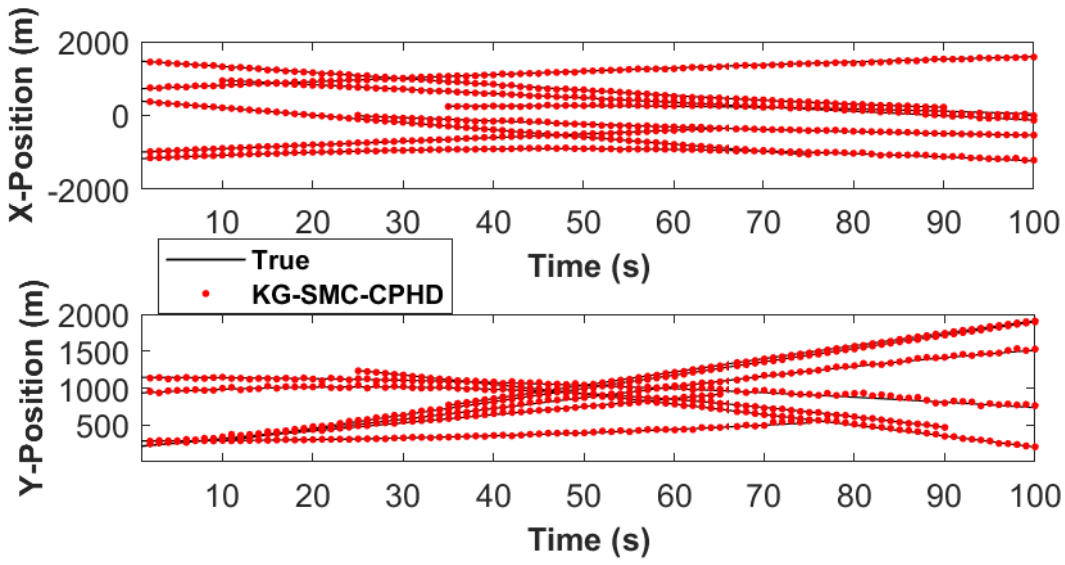

Figure 5.2 *x* and *y* components (versus time) of the true target trajectories and the KG-SMC-CPHD filter estimates.

filters in terms of number of particles, OSPA distance and ET averaged over 100 MC simulations for different values of η in the presence of clutter. It can be observed from table that the accuracy of both the proposed filter and the SMC-CPHD filter improves as number of particles per existing target increases. This is evident by the decrease in their respective OSPA distances. The ET of the proposed filter however is seen to be higher than the SMC-CPHD filter for a given η value. This is due to the extra particle state correction step of the proposed filter. However, the number of particles required in terms of performance level (i.e. low OSPA) by the proposed filter is far less when compared to the SMC-CPHD filter making the proposed filter more efficient.

Fig. 5.4a shows the OSPA plot (for $c = 100$ and $p = 1$) of the KG-SMC-CPHD filter (red-dashed-line) and the SMC-CPHD filter (solid black line) for the same targets shown in Fig. 5.1. The parameter c of the OSPA metric is the cut-off parameter and determines the relative weighting of the penalties assigned to localisation and cardinality errors, and p determines the sensitivity to outliers. The number of particles per existing target was set to $\eta = 1000$ and the number of particles for new born target set to $\frac{\eta}{5}$. The proposed filter had lower OSPA distance measure throughout the tracking time as compared to the SMC-CPHD

filter. This indicates that the proposed filter has higher accuracy. In Fig. 5.4b the evaluation of both the filters in terms of number of particles per existing target and the code execution time is provided. As the number of particles increases, the ET for both filters increases; which was an expected outcome. However, in this simulation example, it was noted that for fewer number of particles (< 1000), the ET of the KG-SMC-CPHD filter was higher than that of the SMC-CPHD filter. This is perhaps due to the extra computation on the selected particles for state correction. But for larger number of particles (> 1000), the proposed filter seems to have a competitive ET when compared to the SMC-CPHD filter. This result suggests that effect of the extra computation needed for the selective particle correction on the overall ET of the proposed filter is minimal especially for larger number of particles.

Table 5.1 Filter performance in terms of number of particles, OSPA distance and CT for $\lambda = 20$.

Filter	η	OSPA (m)	ET (s)
SMC-CPHD	50	57.00	1.1
	100	41.41	1.5
	500	32.13	4.7
	1000	28.49	8.4
KG-SMC-CPHD	50	38.36	2.0
	100	33.77	2.4
	500	20.79	5.3
	1000	15.04	9.0

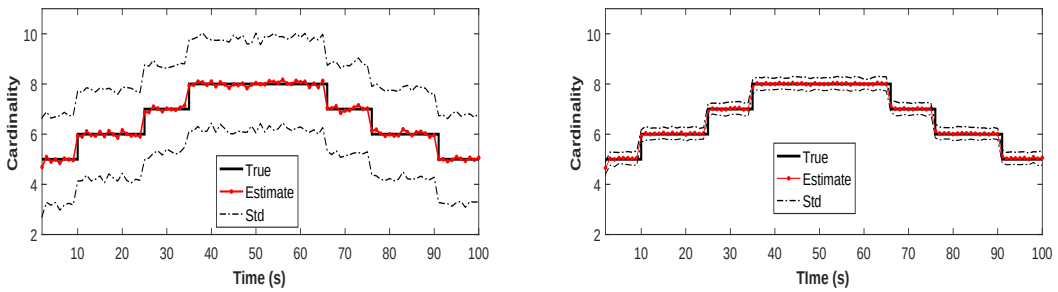

(a) (b)

Figure 5.3 True and estimated cardinality statistics vs time averaged over 100 MC trials. (a) KG-SMC-PHD filter (b) KG-SMC-CPHD filter. The red-dot-line denote the mean cardinality estimates to one decimal place and Std is the standard deviation.

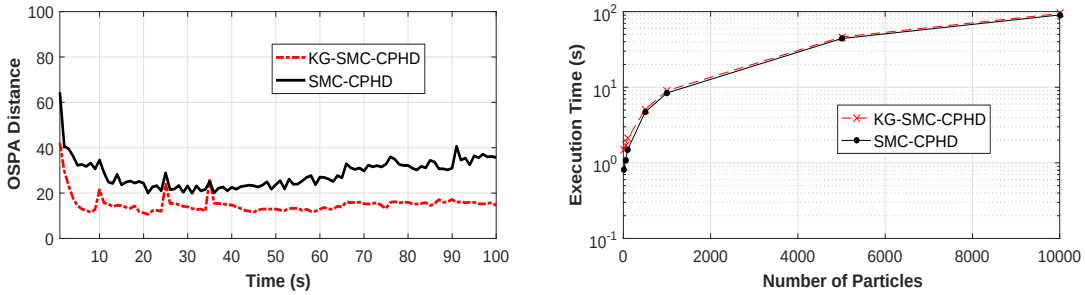

(a) (b)

Figure 5.4 (a) OSPA distance measure against tracking time (b) Execution time against number of particles per target. Results shown are averaged over 100 MC trials.

5.6 Summary

This chapter introduced the cardinalised version (KG-SMC-CPHD) of the proposed SMC-PHD filter of chapter 4 which was called the KG-SMC-PHD filter [46]. The KG-SMC-CPHD filter was applied to simulated data and results show that the KG-SMC-CPHD filter had improved cardinality estimate (both in mean and standard deviation) when compared to the KG-SMC-PHD filter. Furthermore, results showed that the KG-SMC-CPHD filter when compared to the standard SMC-CPHD filter is more efficient in terms of the number of particles needed for tracking, execution time for higher number of particles and accuracy as indicated by the OSPA distance.

Chapters 4 and 5 featured two new and improved point target multi-target tracking techniques capable of jointly estimating multiple target states and number of targets. However, these techniques do not provide for explicit data association of successive target state estimates. To achieve data association with these techniques, a post processing is required. To this end, the next chapter presents a new approach to achieving data association for multi-target tracking.

Chapter 6

Game Theoretic Data Association for Multi-target Tracking with Application to Passive Radar

6.1 Introduction

In the two preceding chapters, two MTT techniques were proposed for the tracking of multiple point targets in clutter environment. These techniques are able to estimate multiple target states as well as number of targets. These techniques however do not have a framework to associate successive target state estimates. As a solution to this drawback, this chapter investigates the use of game theory to develop a data association technique that can be deployed alongside the proposed KG-SMC-(C)PHD filter of Chapters 4 and 5.

To find target state-estimate-to-track associations, the problem of data association as a game between multiple and varying number of tracks is formulated. The strategies and utility function of each track are specified. A regret-based learning algorithm with a forgetting factor or memory is then used to find the equilibrium of this game. Correlated equilibrium is used as a stable operating point. Also, the set of correlated equilibria is a generalisation of Nash equilibria and correlated equilibria are preferable than Nash equilibria since they directly

consider the ability of agents to coordinate their actions and this coordination leads to better performance [72].

The game theoretic approach in this chapter involves firstly, using the KG-SMC-(C)PHD filter to track targets utilising all available measurements to obtain target state estimates. Then the proposed game theoretic method is used to perform target state estimate-to-track data association. The key differences between the proposed approach and [34, 35] are: i) a varying number of targets by using the SMC-PHD filter is considered, ii) a forgetting factor to avoid accumulating and keeping the regrets of each player is used. The use of a game theoretic approach allows for data association, for non-linear, non-Gaussian scenarios. Also, using game theory, data association is simultaneous rather than sequential as opposed to other data association algorithms [34, 35].

In addition, the developed game theoretic data association technique in this chapter is applied to simulated data and deployed in a passive radar application to demonstrate its performance.

6.2 Problem Formulation

This section presents the MTT problem for varying number of targets. Firstly, the multi-target state and measurement models are described followed by how target state estimates are obtained using the KG-SMC-(C)PHD filter.

6.2.1 State Model

Let the non-linear state evolution model of a target be:

$$\mathbf{x}_k = \mathbf{f}(\mathbf{x}_{k-1}, \mathbf{v}_k) \tag{6.1}$$

where $\mathbf{x}_k$ denotes target state at discrete time k, $\mathbf{v}_k$ is an independent and identically distributed (i.i.d.) process noise vector and $\mathbf{f}(\cdot)$ is the non-linear system transition function. Then the multi-target state at time k can be written as

$\boldsymbol{X}_k = \{\mathbf{x}_{1,k}, ..., \mathbf{x}_{M,k}\} \in E_s$ where M is the number of targets present at time k, and E_s denotes the state space.

6.2.2 Measurement Model

The target-originated non-linear measurement model is given as:

$$\mathbf{z}_k = \mathbf{h}_k(\mathbf{x}_k, \mathbf{n}_k) \tag{6.2}$$

where $\mathbf{h}_k(\cdot)$ is a non-linear function, and $\mathbf{n}_k$ is an i.i.d. process noise vector. Measurements consist of both target-originated measurements and false alarms. The multi-target measurement set at time k in the measurement space is: $\boldsymbol{Z}_k = \{\mathbf{z}_{1,k}, ..., \mathbf{z}_{a,k}\} \bigcup \{\mathbf{c}_{1,k}, ...\mathbf{c}_{b,k}\} \in E_o$ where a denotes the number of target-originated measurements, b denotes the number of false measurements and E_o denotes the measurement space. Then the multi-target cumulative measurement set at time K is $\boldsymbol{Z}_{1:K} = \{\mathbf{Z}_1, \mathbf{Z}_2, ..., \mathbf{Z}_K\} \in E_o$.

6.2.3 MTT Using KG-SMC-(C)PHD Filter

6.2.3.1 Initialisation

In the KG-SMC-(C)PHD filter proposed in Chapters 4 and 5, at time $k = 1$ the PHD $D_{k|k}$ is represented by a number of particles with associated weights $\{\mathbf{x}_k^i, w_k^i\}_{i=1}^{L_k}$. L_k is the number of all surviving particles at time k. A particle approximation of the intensity function at time step, $k > 1$, can be obtained from a particle distribution at the previous time step using *prediction* and *update* stages.

6.2.3.2 Prediction

Apply importance sampling to generate L_{k-1} and J_k particles from two proposal densities ($q_k(\cdot|\cdot)$ and $p_k(\cdot|\cdot)$) to represent persistent and new born targets with

associated weights respectively, with $\mathcal{L}_k = L_{k-1} + J_k$, that is,

$$\tilde{\mathbf{x}}_{k|k-1}^{l} \approx \begin{cases} q_k(\cdot|\tilde{\mathbf{x}}_{k-1}^{l}, \dot{\mathbf{Z}}_k), & l = 1, ..., L_{k-1} \\ p_k(\cdot|\dot{\mathbf{Z}}_k), & l = L_{k-1}+1, ..., \mathcal{L}_k \end{cases} \tag{6.3}$$

$$\tilde{w}_{k|k-1}^{l} = \begin{cases} \frac{\phi_{k|k-1}(\tilde{\mathbf{x}}_k^l, \tilde{\mathbf{x}}_{k-1}^l)}{q_k(\tilde{\mathbf{x}}_{k|k-1}|\tilde{\mathbf{x}}_{k-1}^l, \mathbf{Z}_k)} w_{k-1}^{l}, & l = 1, ..., L_{k-1} \\ \frac{\gamma_k(\tilde{\mathbf{x}}_k^l)}{J_k p_k(\tilde{\mathbf{x}}_{k|k-1}|\mathbf{Z}_k)}, & l = L_{k-1}+1, ..., \mathcal{L}_k \end{cases} \tag{6.4}$$

where $\phi_{k|k-1}(\tilde{\mathbf{x}}_k, \tilde{\mathbf{x}}_{k-1}) = p_S(\tilde{\mathbf{x}}_{k-1}) f_{k|k-1}(\tilde{\mathbf{x}}_k, \tilde{\mathbf{x}}_{k-1}) + b_{k|k-1}(\tilde{\mathbf{x}}_k, \tilde{\mathbf{x}}_{k-1})$, $\gamma_k(\cdot)$ is the PHD of the spontaneous birth, $p_S(\cdot)$ is the probability of the target survival, $f_{k|k-1}(\tilde{\mathbf{x}}_k, \tilde{\mathbf{x}}_{k-1})$ is the single target motion model, and $b_{k|k-1}(\tilde{\mathbf{x}}_k, \tilde{\mathbf{x}}_{k-1})$ is the PHD of spawned targets.

6.2.3.3 Update

For each $\dot{\mathbf{z}}_k^n \in \dot{\mathbf{Z}}_k$, compute:

$$\mathcal{H}(\dot{\mathbf{z}}_k^n) = \kappa(\dot{\mathbf{z}}_k^n) + C_k(\dot{\mathbf{z}}_k^n) \tag{6.5}$$

$$C_k(\dot{\mathbf{z}}_k^n) = \sum_{l=1}^{\mathcal{L}_k} p_D(\tilde{\mathbf{x}}_{k|k-1}^{l}) g(\dot{\mathbf{z}}_k^n|\tilde{\mathbf{x}}_{k|k-1}^{l}) \tilde{w}_{k|k-1}^{l}, \tag{6.6}$$

where $p_D(\tilde{\mathbf{x}}_{k|k-1}^{l})$ is the probability of detection, $g(\dot{\mathbf{z}}_k^n|\tilde{\mathbf{x}}_{k|k-1}^{l})$ is the measurement likelihood function for the single target, and $\kappa(\dot{\mathbf{z}}_k^n) = \lambda_k c_k(\mathbf{z})$ is the clutter intensity, λ_k is the average number of Poisson clutter points per scan, and $c_k(\mathbf{z})$ is the probability density over the state-space of the clutter point

Then, for $i = 1, ..., \mathcal{L}_k$, update the weights using:

$$\tilde{w}_k^l = \left[\nu(\tilde{\mathbf{x}}_{k|k-1}^{l}) + \sum_{\dot{\mathbf{z}} \in \dot{\mathbf{Z}}_k} \frac{p_D(\tilde{\mathbf{x}}_{k|k-1}^{l}) g(\dot{\mathbf{z}}_k^n|\tilde{\mathbf{x}}_{k|k-1}^{l})}{\mathcal{H}(\dot{\mathbf{z}}_k^n)} \right] \tilde{w}_{k|k-1}^{l} \tag{6.7}$$

where $\nu(\tilde{\mathbf{x}}_{k|k-1}^{l}) = 1 - p_D(\tilde{\mathbf{x}}_{k|k-1}^{l})$ is the probability of target non-detection.

6.2.3.4 Resample and Clustering

The number of targets at time k is computed as $T_k = \text{round}\left(\sum_{l=1}^{\mathcal{L}_k} \tilde{w}_k^l\right)$. $L_k = \rho T_k$ particles are resampled according to the ISR resampling method proposed in Chapter 4 to avoid degeneracy. Clustering is performed on resampled particles to obtain the target state estimates, $\tilde{\boldsymbol{x}}_k$.

Therefore, at time k, the output of the KG-SMC-(C)PHD filter is a set of target state estimates given as: $\tilde{\boldsymbol{x}}_k = \{\tilde{\boldsymbol{x}}_{1,k}, \tilde{\boldsymbol{x}}_{2,k}, \cdots, \tilde{\boldsymbol{x}}_{T_k,k}\}$, where $\tilde{\boldsymbol{x}}_{t,k} = [x_{t,k}, \dot{x}_{t,k}, y_{t,k}, \dot{y}_{t,k}]^{\bar{T}}$, $x_{t,k}$ and $y_{t,k}$ are the x and y positions at time k and $\dot{x}_{t,k}$ and $\dot{y}_{t,k}$ are the velocity in x and y directions for the tth target respectively. It is the assumption that, each target, when present generates at most one measurement. Also, most false alarms have been filtered out during the KG-SMC-(C)PHD filtering. This implies that the output of the KG-SMC-(C)PHD filter are target state estimates only with no false alarm. In the case where a false alarm was not filtered, it will be recorded as a new target. Figure 6.1 shows the different stages in the proposed approach.

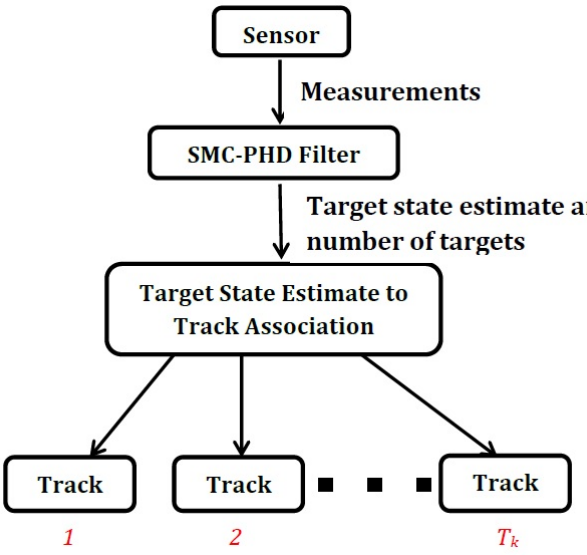

Figure 6.1 Block diagram showing various stages of the data association process.

Both target-originated measurements and clutter are obtained from a sensor. The KG-SMC-(C)PHD filter tracks the targets using these measurements while filtering out clutter to obtain target state estimates. The proposed game theoretic approach is then used to associate these target state estimates to various target tracks.

6.3 Data Association for Varying Number of Targets Using Game Theory

In this section, how the game between the different tracks is played at each iteration of the KG-SMC-(C)PHD filter output is explained.

6.3.1 The Game

Consider a game at time k with a set, Ω_k of $\mathcal{P}_k$ players. The players, $\mathcal{P}_k$ are the tracks for different targets and can vary depending on the estimated number of targets by the KG-SMC-(C)PHD filter, T_k. Each player wants to assign a new target state estimate to its existing track. It is said that a new player has joined the game at time k when $T_k > T_{k-1}$ and a player has left when $T_k < T_{k-1}$. The strategy set $\mathcal{S}_{p,k} = \{0, 1, 2, \cdots, T_k\}$ of each player corresponds to the set of target state estimates from the KG-SMC-(C)PHD filter and they are known to all of the players at time k. The strategy $s_{p,k} \in \mathcal{S}_{p,k}$ allows the player to choose one target state estimate from the set of all target state estimates or 0 in the case that the corresponding target does not produce any tracks or disappears from the tracking scene. $\mathcal{P}_k$ is the number of players at time k and corresponds to T_k. For each player, a utility function is defined as $u_{p,k}(s_{p,k}, s_{-p,k}) : \mathcal{S} \longrightarrow \mathbb{R}$, with $\mathcal{S} = \mathcal{S}_1 \times \cdots \times \mathcal{S}_{\mathcal{P},k}$ where $-p_k$ refers to all players except player p_k. $\mathcal{U}_k$ denotes the set of utility functions of all the players, that is, $\mathcal{U}_k = \{u_{p_k}\}_{p_k=1}^{\mathcal{P}_k}$. The game $\Gamma_k(\Omega_k, \mathcal{S}_k, \mathcal{U}_k)$ defined by the set of players Ω_k, the strategy set $\mathcal{S}_k$, and the utility functions $\mathcal{U}_k$ is a one shot game played at the end of each iteration of the MTT tracker and is called the MTT data association game for varying number of targets.

6.3.2 Utility Functions

For the pth player at time k, the utility function similar to [34] is defined as follows:

$$u_{p,k}(s_{p,k}, s_{-p,k}) = \begin{cases} d_{p,k}(s_{p,k}) + \mu_1 g_{p,k}(s_{p,k}, s_{-p,k}), & s_{p,k} \neq 0 \\ \mu_2, & s_{p,k} = 0 \end{cases} \tag{6.8}$$

where

$$d_{p,k}(s_{p,k}) = -\left[(\boldsymbol{x}_{s_p,k} - \tilde{\boldsymbol{x}}_{p,k})^T \boldsymbol{\Sigma}^{-1} (\boldsymbol{x}_{s_p,k} - \tilde{\boldsymbol{x}}_{p,k}) - d_{max}\right] \tag{6.9}$$

is the scaled Mahalonobis distance between the track of the pth target at previous time step, $\boldsymbol{x}_{s_p,k} := \mathbf{F}\boldsymbol{x}_{s_{p,k-1}}$ and the output of the KG-SMC-(C)PHD filter, $\tilde{\boldsymbol{x}}_{p,k}$; d_{max} is a constant and it specifies the boundary for the Mahalanobis distance and $-d_{max} \leq d_{p,k} \leq d_{max}$, $\mu_1 > 0$ and $\mu_2 > 0$ are constants and

$$\mathbf{F} = \begin{bmatrix} 1 & 1 & 0 & 0 \\ 0 & 1 & 0 & 0 \\ 0 & 0 & 1 & 1 \\ 0 & 0 & 0 & 1 \end{bmatrix}.$$

The function $g_{p,k}(s_{p,k}, s_{-p,k})$ is defined as

$$g_{p,k}(s_{p,k}, s_{-p,k}) = \begin{cases} \frac{1}{\mathcal{P}_k - 1} \sum_{\substack{l=1 \\ l \neq p}}^{\mathcal{P}_k} \parallel s_{p,k} - s_l \parallel_{l_0}, & T_k > 1 \\ 1, & T_k = 1 \end{cases} \tag{6.10}$$

6.3.3 Equilibrium Points: Correlated Equilibria

In order to find the equilibrium of the MTT data association game for varying number of targets, correlated equilibrium (CE) [4] as considered in [35] is used. CE is a generalisation of the Nash Equilibrium, (NE). A probability distribution φ is called a CE if for all players $p \in \Omega$ and all strategies $i, j \in \mathcal{S}_p$, [72]

$$\sum_{s \in \mathcal{S}: s_p = i} \varphi(s)[u_p(j, s_{-p}) - u_p(s)] \leq 0. \tag{6.11}$$

A CE, φ can be considered as a recommendation each player receives 'privately' from a trusted source. If this source draws a strategy profile s from φ and announces to each player p its own component separately and privately, then the player p will have no incentive to choose another strategy, assuming that the other players also conform to the recommendation provided by the source [72]. The CE

for the MTT data association game for varying number of targets can be reached using a learning mechanism called regret matching.

6.3.4 Regret Matching with Forgetting Factor

Regret matching (RM) is a type of learning algorithm used in fully distributed learning [72]. At each time instant, a player may either continue to play the same strategy as in the previous time instant, or switch to other strategies, with probabilities that are proportional to how much its regret would have been had it always made that change in the past. Specifically, let $s_{p,k} \in \mathcal{S}_k$ denote the strategy of the pth player in the kth iteration and let the index of $s_{p,k}$ within $\mathcal{S}_k$ be n such that $n \in \{1, \cdots, T_k\}$. Also, let $s_{p,k-1} \in \mathcal{S}_{k-1}$ be the strategy of the pth player at the $k-1$ iteration and let $s_{p,k-1}$ have index l such that $l \in \{1, \cdots, T_{k-1}\}$. Each player computes the average regret for choosing the nth strategy in the kth iteration using:

$$R_{p,n}(k) = \frac{1}{k-1} \sum_{l=1}^{k-1} [u_{p,k}(n, s_{-p,k}(l)) - u_{p,k}(s(l))] \tag{6.12}$$

$$r_{p,n}(k) = \max \{0, R_{p,n}(k)\}, \tag{6.13}$$

Each player p_k can recursively compute the nth component of $R_{p,k}$ using the recursion:

$$R_{p,n}(k) = \left(\frac{k-2}{k-1}\right) R_{p,n}(k-1) + \frac{1}{k-1} [(n, s_{-p,k}(k-1)) - u_{p,k}(s(k-1))] \tag{6.14}$$

Since the number of players changes with time, the regret in the distant past becomes irrelevant. As a result, an exponential forgetting factor is introduced, λ_f in (6.12) to obtain the regret matching with forgetting factor (RMFF) equation:

$$\tilde{R}_{p,n}(k) = \frac{1}{k-1} \sum_{l=1}^{k-1} \lambda_f^{(k-1)-l} [u_{p,k}(n, s_{-p,k}(l)) - u_{p,k}(s(l))] \tag{6.15}$$

and (6.13) becomes:

$$\tilde{r}_{p,n}(k) = \max\left\{0, \tilde{R}_{p,n}(k)\right\} \tag{6.16}$$

where $\tilde{R}_{p,n}(k)$ represent the average pay-off (with exponential forgetting factor) for the pth player at time k for not having played a different strategy n each time the strategy l was played in the past; $0 < \lambda_f \leq 1$ is the forgetting factor. The memory of the RMFF equation is given as $\Lambda = \frac{1}{1-\lambda_f}$. The expression $\tilde{r}_{p,n}(k)$ in (6.16) has an interpretation as the measure of the average regret at kth iteration for not having played the strategy n up to time k. Let $\beta_{p,n}(k)$ denote the probability that the p_kth player chooses nth strategy. Each player then chooses the nth strategy that satisfies

$$\arg\max_n \beta_{p,n}(k) \tag{6.17}$$

where the distribution $\beta_{p,n}(k)$ is given by

$$\beta_{p,n}(k) = \begin{cases} \dfrac{1}{\alpha}\tilde{r}_{p,n}(k), & \text{if } l \neq n \\ 1 - \sum_{\substack{n\in\{0,1,\cdots,T_k\} \\ n\neq l}} \beta_{p,n}(k), & l = n. \end{cases} \tag{6.18}$$

The constant $\alpha > 0$ is a large enough number such that $\beta_{p,n}(k) > 0$ and this ensures that there is always a positive probability of playing the same strategy as in the previous step [72]. When a new player, p^+ joins the game, that is, when $T_k > T_{k-1}$, its own distribution, $\beta_{p^+}(k)$ is started such that $\beta(k) = \cup\beta_{p^+}(k)$ at that instance. In regret matching, the correlation in the plays of different players arises from the commonly observed history. Thus, the history serves as a signal in giving the private recommendation to each player [72].

6.4 The Passive Bi-static Radar System

In order to demonstrate the performance of the game theoretic data association (GTDA) method described in the preceding sections, it is applied to real data ob-

tained from a passive bi-static radar (PBR) experiment. The aim of PBR experiment was to detect, track and associate target state estimates of moving aeroplanes. The PBR system was set-up using the NI USRP software defined radio platform with necessary hardware to record detections from moving aeroplanes. But firstly, some key steps in setting up the PBR system for the detection of moving aerial targets are discussed.

6.4.1 System Architecture

The PBR system implementation relies on exploiting a software-defined radio platform (SDR). The computationally demanding part of the passive radar signal processing chain is implemented on the software-defined radio FPGA, and the rest of the radar processing chain, such as target detection, multi-target tracking and data association have been implemented on the host CPU, (see Fig. 6.2).

6.4.2 Signal Reconstruction and Disturbance Cancellation

The SDR platform is the NI-USRP-2950R, and contains two RF channels that can be configured as two synchronised receivers that provide the reference signal (as input from a reference antenna) and surveillance signal (as input from a surveillance antenna). The antenna for the reference signal has been pointed towards the direction an FM transmitter. Since the surveillance antenna will not completely suppress the strong direct signal, a disturbance cancellation operation is performed on the surveillance signal using least mean square (LMS) adaptive algorithm. After that, the surveillance and reference signals have been used to perform the two-dimensional cross-correlation function (2D-CCF) to obtain range -Doppler map.

6.4.3 Two-Dimensional Cross-Correlation Function (2D-CCF)

The evaluation of the bi-static range-Doppler 2D-CCF is the key step in the PBR processing chain. It corresponds to the implementation of a bank of matched

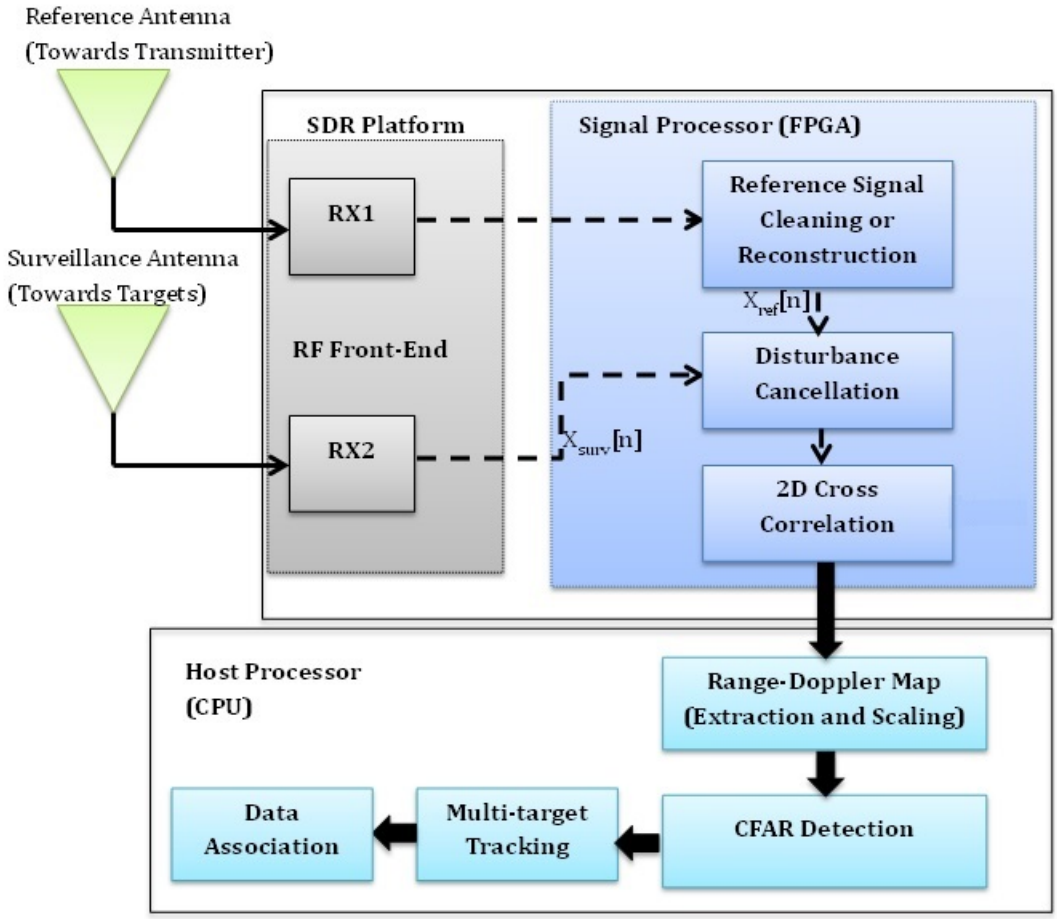

Figure 6.2 PBR System Architecture.

filters, each one tuned to a specific target bi-static Doppler frequency shift.

$$\chi(u,m) = \sum_{n=0}^{N-1} x_{surv}[n] x^*_{ref}[n-u] e^{-j2\pi \frac{mn}{N}} \tag{6.19}$$

where $x^*_{ref}[u]$ denotes the sampled reference signal, $x^*_{surv}[u]$ denotes the sampled surveillance signal and $\chi(u,m)$ denote the 2D-CCF. N is Number of integrated samples, u is the time bin corresponding to time delay $\tau = \frac{u}{f_s}$;where f_s is sampling rate and m is Doppler bin corresponding to Doppler shift $f_d = \frac{mf_s}{N}$.

The 2D-CCF stage serves two important purposes: the generation of sufficient signal processing gain to allow the targets to be detected above the noise floor and the estimation of the bi-static range and Doppler shift of the target echoes.

6.4.4 Target Detection (Order Statistic CFAR)

Having calculated the 2D-CCF correlation surface, target detection is performed by comparing the magnitude of each range Doppler bins to a threshold. The threshold for different range Doppler bins will vary according to the estimate of disturbance and noise for each range - Doppler bin in order to maintain a constant false alarm rate. The Constant false alarm rate (CFAR) algorithm of choice was the order

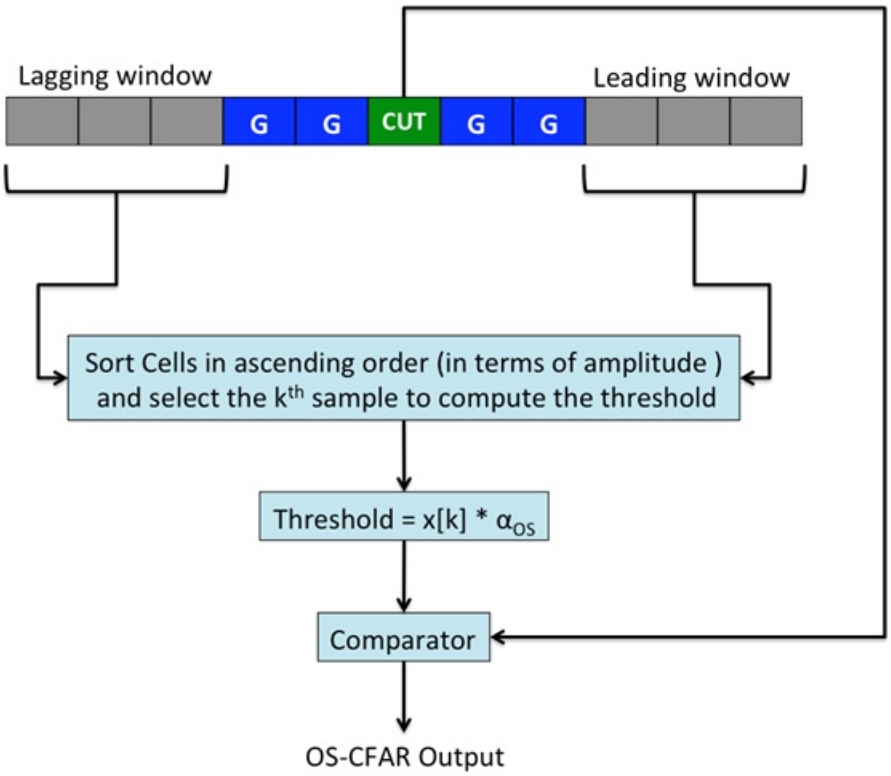

Figure 6.3 Order statistic CFAR Algorithm [27].

statistic OS-CFAR [27] and [123], for its robustness against interfering peaks on the cell under test (CUT). Fig. 6.3 shows the algorithm used for implementing the OS-CFAR. Cells before and after a CUT are utilised to estimate the noise floor level around the CUT, by arranging them in ascending order in terms of their amplitude value and taking only the kth sample to compute the threshold for a specific probability of false alarm (P_{FA}). Guard cells before and after the CUT are needed in case the energy of the CUT is dispersed onto adjacent cells. The threshold for determining whether a target exist in the CUT is computed for a

specific P_{FA} using the following equation [123]:

$$P_{FA} = \frac{N!(\alpha_{OS} + N - k)!}{(N-k)!(\alpha_{OS} + N)!}. \tag{6.20}$$

where α_{OS} is the OS scaling factor, k is the representative sample rank and N is the total number of background samples.

6.5 Numerical Results

In this section, the performance of the GTDA technique on simulated data is demonstrated. The tracking and association of the target state estimates of four targets are considered. These targets enter and exit the tracking scene at various times. Fig. 6.4 shows the x and y components of each track against time. A triangular and circular dot denote the start and the end of a track respectively.

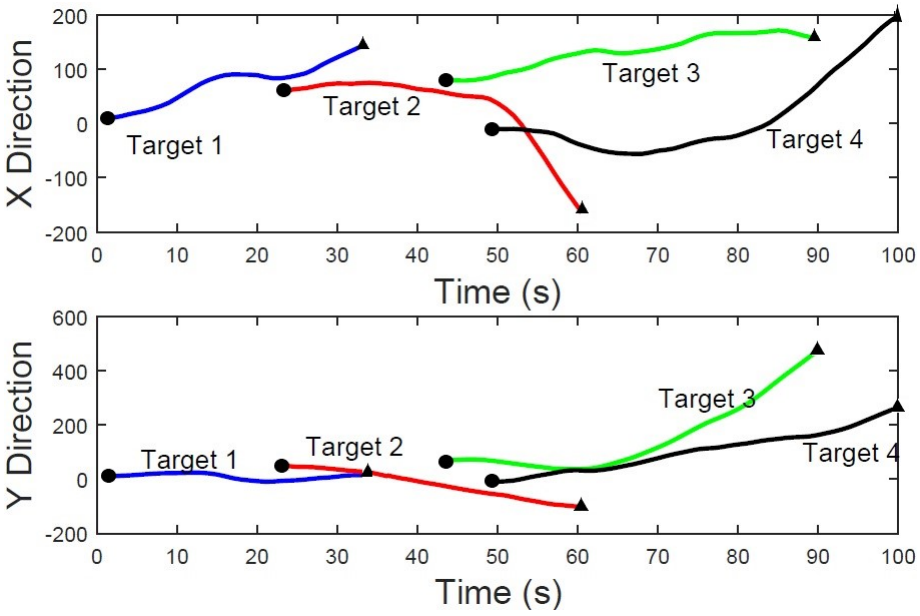

Figure 6.4 Ground truth showing the plot of the true x and y components against time for the four tracks over 100 time steps

Fig. 6.5 shows the average of 100 MC simulations of the KG-SMC-PHD filter estimates of the target trajectories in both x and y directions superimposed on the true target trajectories of Fig. 6.4.

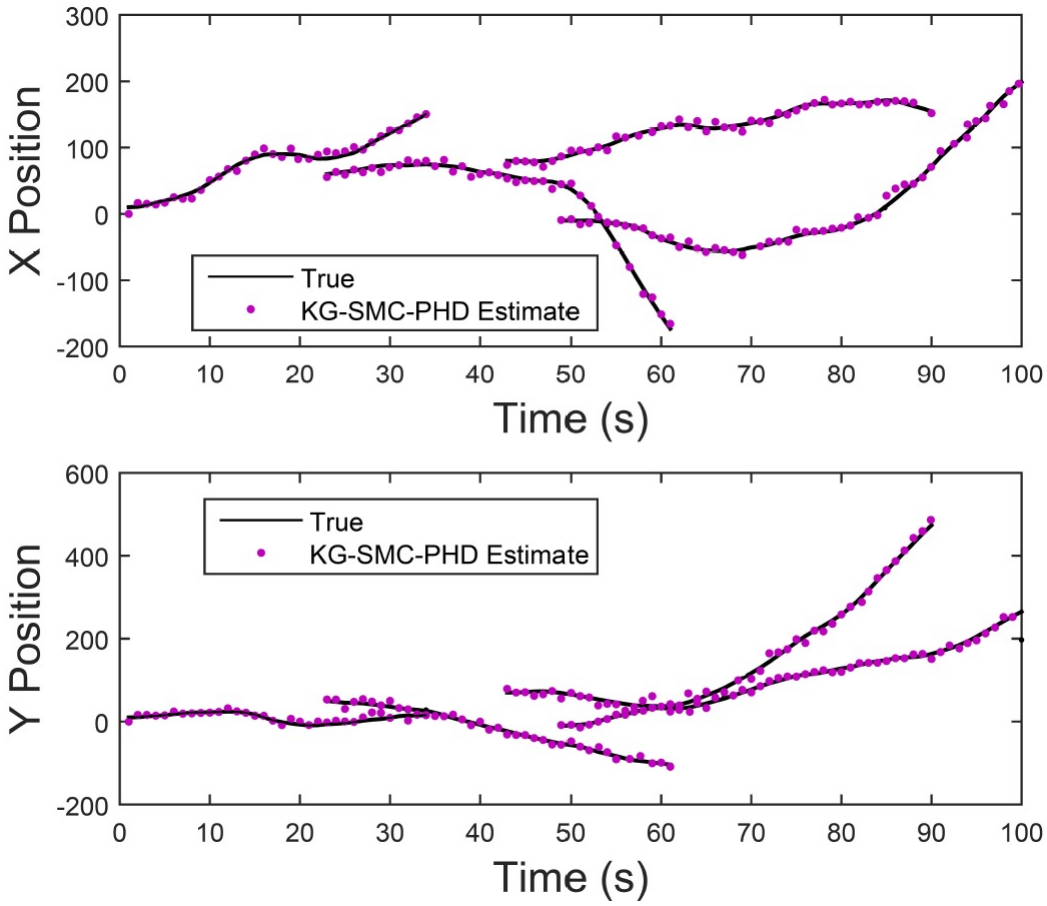

Figure 6.5 KG-SMC-PHD filter estimates superimposed on true target positions in both x and y direction averaged over 100 MC runs.

To evaluate performance, the root mean squared error (RMSE), track continuity [40] and computational time (CT) are used. The RMSE is computed individually for each target as

$$\mathrm{RMSE}_t = \sqrt{\frac{1}{K}\sum_{i=1}^{K}(\boldsymbol{x}_t^i - \tilde{\boldsymbol{x}}_t^i)^2} \tag{6.21}$$

where t denotes the tth target, K is the number of KG-SMC-(C)PHD filter iterations which is same as the time up to now; $\{\boldsymbol{x}_t^i\}_{i=1}^K$ denotes the set of ground truth of the tth target and $\left\{\tilde{\boldsymbol{x}}_t^i\right\}_{i=1}^K$ denotes the set of the tth target state estimates after game theoretic data association.

Table 6.1 show results averaged over 100 Monte Carlo simulations for different data association algorithms with 1000 number of particles used for the KG-SMC-

Table 6.1 The performance of the proposed algorithm in terms of RMSE, track continuity and computation time (CT).

Algorithm	Track continuity (%) / RMSE				CT (s)
	Target 1	Target 2	Target 3	Target 4	
PDA	94.3 / 3.2	93.9 / 2.9	96.1 / 2.2	96.5 / 2.7	25.0
JPDA	95.3 / 1.1	94.4 / 1.1	96.7 / 0.9	96.0 / 1.0	22.4
GTDA	97.1 / 0.7	98.0 / 0.9	98.2 / 1.0	98.8 / 0.8	19.6

(C)PHD filter. PDA is the probabilistic data association technique [13], JPDA denote joint-PDA [59] and GTDA is the proposed method. Comparing the three algorithms, the GTDA gave the best performance both in terms of accuracy and CT. The JPDA gave a similar level of performance in accuracy when compared with the GTDA but has higher computational time. This is because in JPDA many hypotheses are considered and the hypotheses are merged to form a single one after considering all targets and measurements. The GTDA gave a lower CT and only half of the regrets of the players were kept ($\lambda_f = 0.5$).

6.6 Experimental Results

This section presents filter and parameter settings, results and discussions from the PBR experiment.

6.6.1 State and Measurement Models

Let the constant velocity state evolution model of a target be:

$$\hat{\boldsymbol{x}}_k = \boldsymbol{F}\hat{\boldsymbol{x}}_{k-1} + \boldsymbol{w}_k \tag{6.22}$$

with

$$\boldsymbol{F} = \begin{bmatrix} 1 & \delta t \\ 0 & 1 \end{bmatrix},$$

where $\boldsymbol{F}$ is the system transition function, $\hat{\boldsymbol{x}}_k = [\hat{r}_k, \hat{v}_k]^{\bar{T}}$, $\hat{r}_k$ and $\hat{v}_k$ denotes the bi-static range and bi-static radial velocity respectively, and $\boldsymbol{w}_k$ is an independent

and identically distributed (i.i.d.) process noise vector. Then the multi-target state at time k can be written as $\boldsymbol{X}_k = \{\hat{\boldsymbol{x}}_{1,k}, ..., \hat{\boldsymbol{x}}_{M,k}\} \in E_s$ where M is the number of targets present at time k, and E_s denotes the state space.

Let the target-originated measurement model be:

$$\hat{\boldsymbol{z}}_k = \mathbf{H} \begin{bmatrix} \hat{r}_k \\ \hat{v}_k \end{bmatrix} + \hat{\boldsymbol{n}}_k \tag{6.23}$$

where $\mathbf{H}$ is the transformation matrix, and $\hat{\boldsymbol{n}}_k$ is an i.i.d. process noise vector. Measurements consist of both target-originated measurements and false alarms. The multi-target measurement set at time k in the measurement space is: $\boldsymbol{Z}_k = \{\hat{\boldsymbol{z}}_{1,k}, ..., \hat{\boldsymbol{z}}_{a,k}\} \bigcup \{\mathbf{c}_{1,k}, ...\mathbf{c}_{b,k}\} \in E_o$ where $\{\mathbf{z}_{1,k}, ..., \mathbf{z}_{\alpha,k}\}$ denotes the target-originated measurement set with number of measurements, α; $\{\mathbf{c}_{1,k}, ...\mathbf{c}_{\beta,k}\}$ denotes the false measurement set with the number of measurements, β and E_o denotes the measurement space. Then the multi-target cumulative measurement set at time K is $\boldsymbol{Z}_{1:K} = \{\mathbf{Z}_1, \mathbf{Z}_2, ..., \mathbf{Z}_K\} \in E_o$.

6.6.2 Experimental Set-up

The goal of the PBR experiment was to track aeroplanes that are either passing through Loughborough town, taking off from or landing at a nearby airport, the East Midlands Airport (which is 10km away from Loughborough University). In this experiment, the aim was to use bi-static range and radial velocity measurements of the aeroplanes obtained from a passive radar set-up to track the aeroplanes and then associate the target-state-estimates to the various aeroplane tracks using the GTDA technique. The experiment was carried out on the 7th of July, 2016 on top the roof of Sir David Davies Building, Loughborough University, UK.

In this experiment, the transmitter of opportunity is an FM transmitter with a center frequency of 106MHz and located some 6.5km away from the receiver. Fig. 6.6 shows the coverage area of the FM transmitter, the receiver location and the location of the East Midlands Airport. The passive receive end consists of a National Instruments SDR platform (the NI-USRP-2950R) and two omni-directional FM

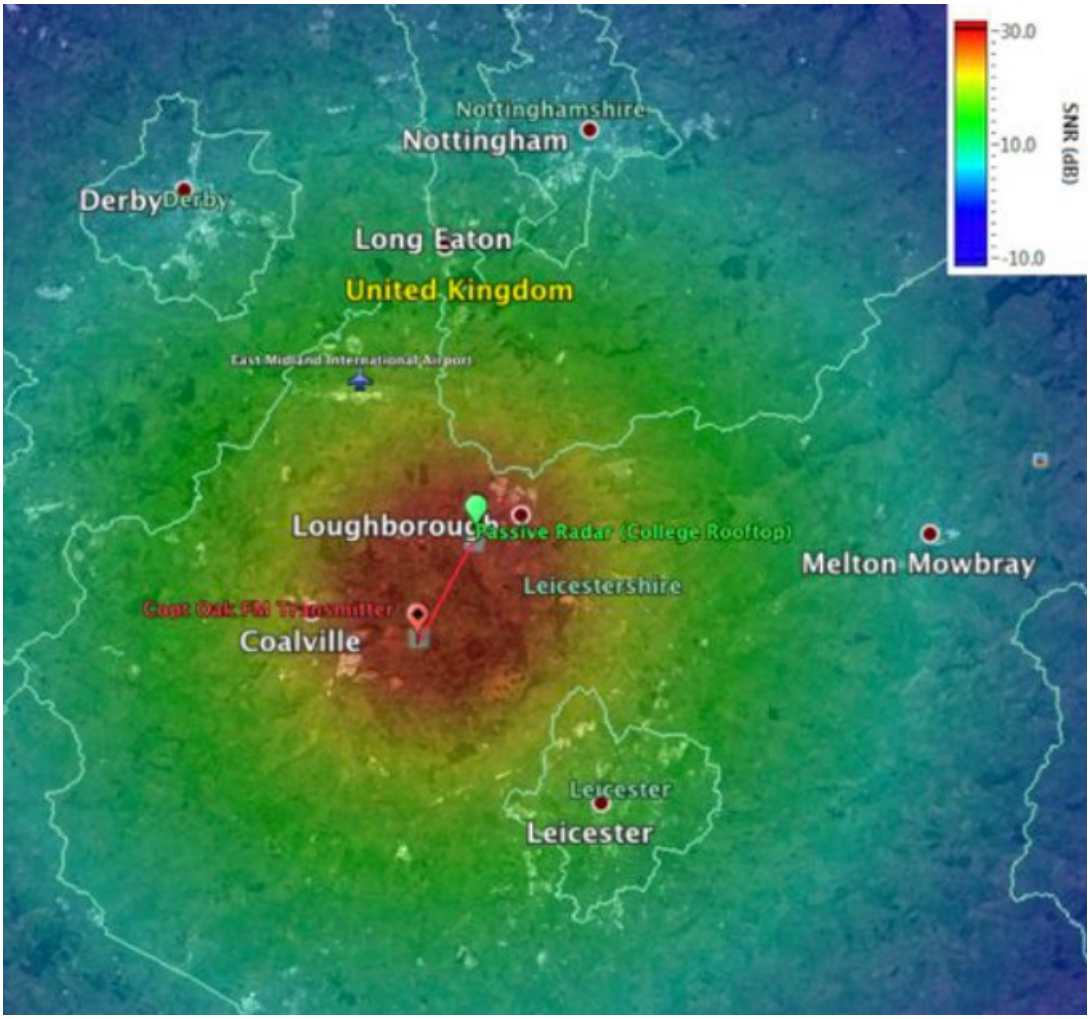

Figure 6.6 The coverage area of the FM transmitter.

antennas; one is used for the surveillance channel and the other is used for the reference channel. Figure 6.7 shows the passive receiver setup on the roof top for Sir David Davis Building, Loughborough University. The SDR platform was interfaced with LabVIEW to record the raw in-phase and quadrature (I-Q) data for a duration of 12mins 12secs and processed to obtain the bi-static range and radial velocity measurements of planes within the surveillance scene. The receiver had a bi-static range resolution of 937.5m and bi-static radial velocity resolution of 1.4m/s. The system was set to have a maximum detection range of approximately 48km and only detections above an altitude of 100m were considered. During the duration of the recording, a total of six aeroplanes entered and exited the detectable region of the receiver. The processed passive radar data were recorded

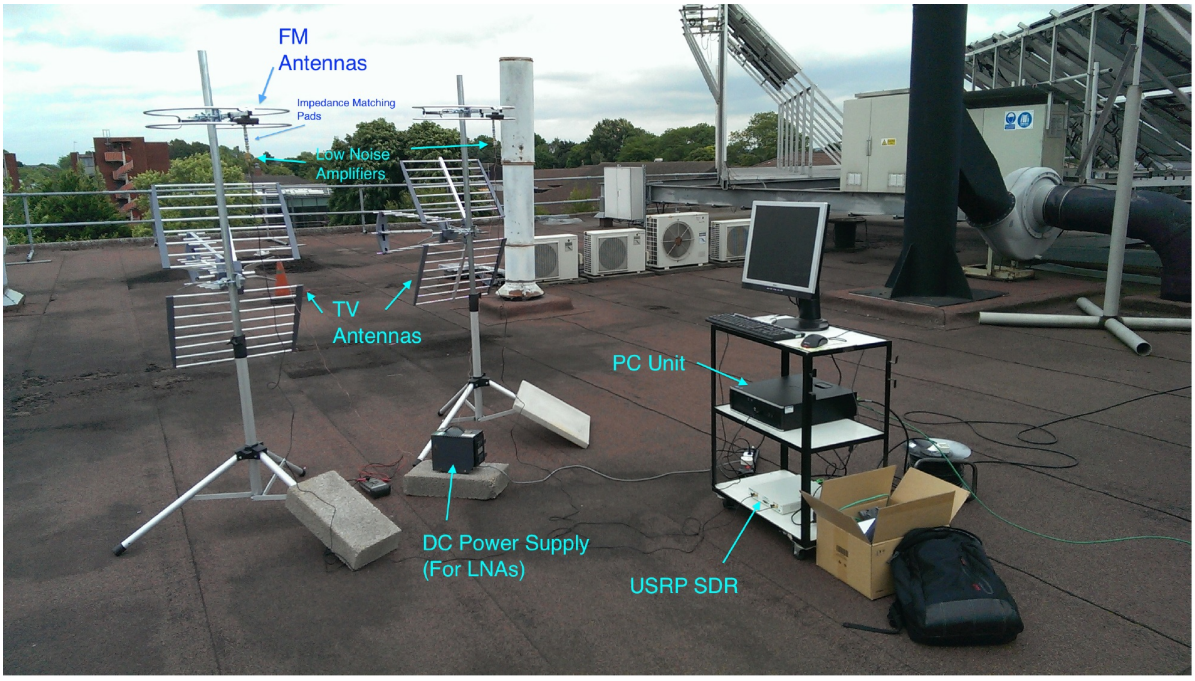

Figure 6.7 Passive receiver setup.

as an intensity map with the bi-static radial velocity (in m/s) on the y-axis and the bi-static range (in km) on the x-axis. CFAR detection was then applied to the raw intensity map measurements to obtain a binary intensity map to facilitate tracking. The probability of false alarm used for the CFAR was 1×10^{-4}. The intensity maps of the bi-static range and radial velocity measurements recorded at time = $109s$ before and after applying CFAR are shown in Fig. 6.8a and Fig. 6.8b respectively. In Fig. 6.8b, the colour white indicates detections and black indicates no detection. It is observed from Fig. 6.8b that the detections are smeared therefore, centroiding was performed to obtain single point detection before being passed to the tracking filter.

The tracking filter (the KG-SMC-(C)PHD filter) takes in the centroided CFAR detections as measurements to perform MTT and output target-state-estimates. the process noise in (6.22) $\boldsymbol{w}_k$ was modelled to be distributed according to $\mathcal{N}(0, \sigma^2\boldsymbol{Q})$, where $\sigma = 0.02$km/s^2, the sampling period $\delta t = 1s$ and

$$\boldsymbol{Q} = \begin{bmatrix} \frac{\delta t^4}{4} & \frac{\delta t^3}{2} \\ \frac{\delta t^3}{2} & \delta t^2 \end{bmatrix}.$$

The measurement noise in (6.23) was modelled as $\hat{\boldsymbol{n}}_k = \mathcal{N}(0, \hat{\boldsymbol{R}})$ where $\hat{\boldsymbol{R}} = \text{diag}([\sigma_{\hat{r}}^2, \sigma_{\hat{v}}^2])$ with $\sigma_{\hat{r}} = 30$m and $\sigma_{\hat{v}} = 4.5$m/s; where $\mathbf{H} = \text{diag}([1, 1]^{\bar{T}})$.

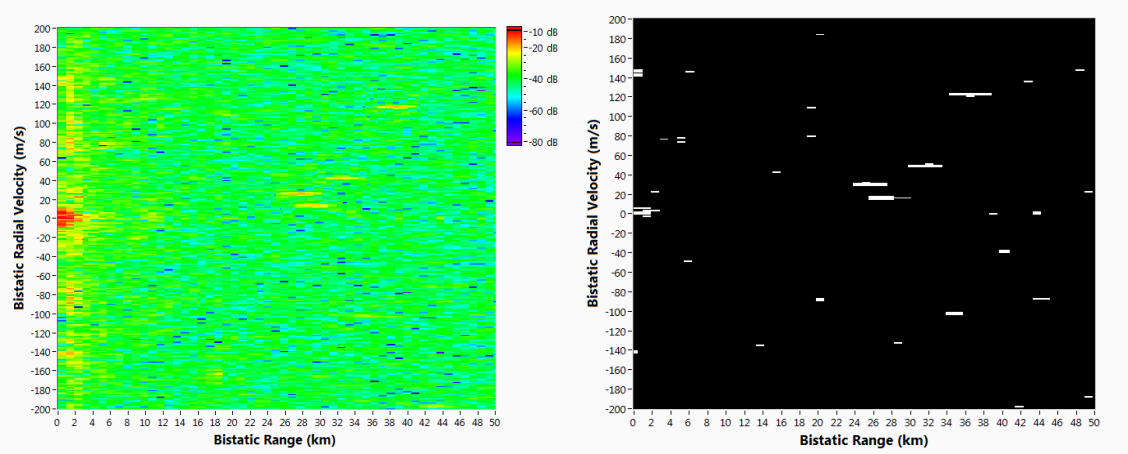

(a) Bi-static radial velocity vs bi-static range intensity map before CFAR.

(b) Bi-static radial velocity vs bi-static range map after CFAR.

Figure 6.8 Bi-static radial velocity vs bi-static range map obtained from the passive radar set-up at time = 109s.

6.6.3 Results

Fig. 6.9a and Fig. 6.9b show results obtained from one sample run of the KG-SMC-(C)PHD filter on the passive radar detections for the whole duration of the experiment. The number of particles per existing target was set to $\rho = 4000$ and the number of particles for new born tracks was set to $\frac{\rho}{5}$. In Fig. 6.9a, solid black lines represent the true flight paths on the bi-static range and radial velocity map, while the dots represent the filter estimates. The circle and triangle denote the start and end measurements of the flights. The true flight bi-static range and radial velocity data were obtained from [58]. Notice from Fig. 6.9a that there are a total of six targets throughout the duration of the experiment. Three of the targets having a "C" like trajectory correspond to targets passing over the transmit/receive set-up of the passive radar. Hence, the upper part of the "C" shape corresponds to approaching targets and thus have positive bi-static radial velocity and the lower part of the "C" shape corresponds to receding targets having a negative bi-static radial velocity. A zero bi-static radial velocity corresponds to when targets are

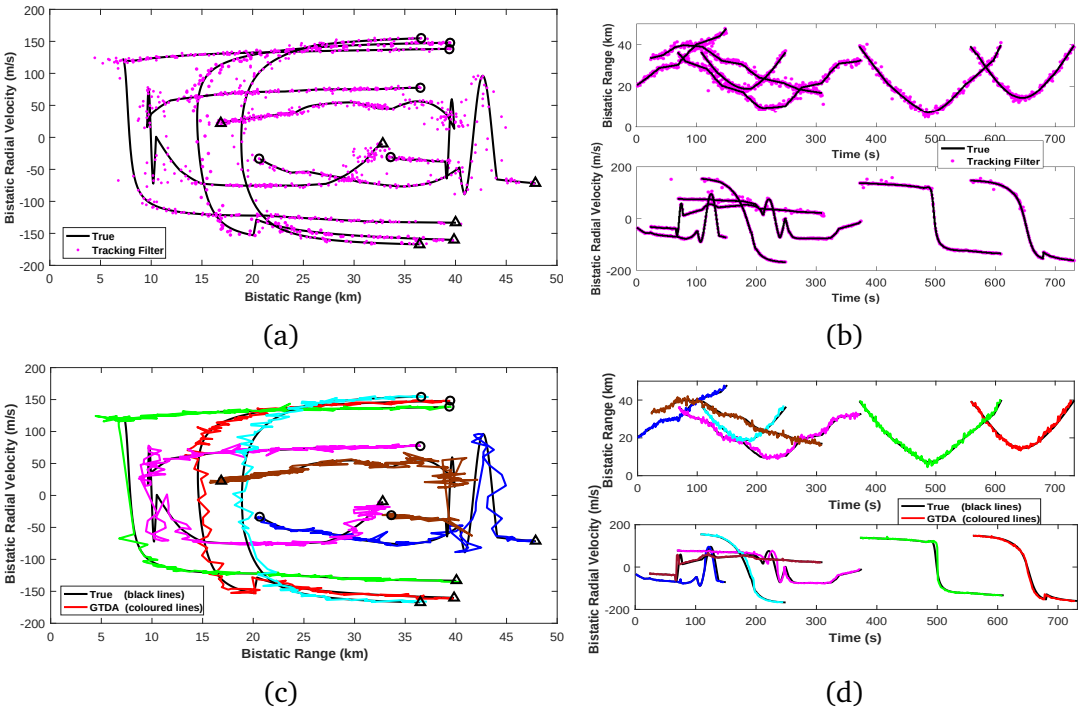

Figure 6.9 Tracking filter and GTDA plots: (a) Bi-static radial velocity vs bi-static range plot showing various true flight paths and tracking filter estimates for the whole duration of the experiment. Start/End for each target are shown with ◯/△; (b) Tracking filter estimates superimposed on true flight positions in both bi-static range and bi-static radial velocity axis (versus time); (c) Bi-static radial velocity vs bi-static range plot showing various true flight paths and GTDA data association for the whole duration of the experiment. Start/End for each target are shown with ◯/△; (d) True flight positions in both bi-static range and bi-static radial velocity axis and GTDA data association (versus time) showing target entry and exit.

closest in bi-static range to the transmit/receive set-up. The other three targets having irregular trajectories correspond to targets taking position after having taken off or taking position to land at an airport within the detection range of the receiver. In Fig. 6.9b, the bi-static range and radial velocity of the true flight path (solid lines) and the tracking filter estimates (dots) versus time are shown. From this figure the time each target enters and exits the tracking scene can be observed.

In Fig. 6.9c, the bi-static range and radial velocity of the true flight path (black) and the target-state-estimate after GTDA (coloured) are shown. In Fig. 6.9d, the bi-static range and radial velocity of the true flight path (black) versus time and the target-state-estimate after GTDA (coloured) are shown. These results suggest

that the proposed GTDA technique is able to properly associate the target-state-estimates of different targets to their corresponding tracks.

6.7 Summary

In this chapter, a data association technique for MTT with varying number of targets using game theory namely, the GTDA has been proposed. The strategies and the utility functions of the players were defined, and a regret matching with forgetting factor was used to find the equilibrium of the game. The proposed technique was evaluated using both simulated and real data. As for the the simulated data, the performance of the proposed technique is compared to other data association algorithms such as the PDA and JPDA. The proposed method showed better performance in terms of accuracy and computation complexity when compared to PDA. However, the proposed approach showed similar performance in terms of accuracy when compared with JPDA but takes less computational time. Secondly, the effectiveness of the GTDA was further demonstrated on real field measurements collected by an NI-USRP based PBR system. In the experiment, the KG-SMC-(C)PHD filter was used to track aeroplanes and the GTDA was used for track association. Results showed that the GTDA technique was able to successfully associate the target-state-estimates to various target tracks.

Thus far, new and improved techniques for MTT have been proposed specifically for tracking *point targets*, that is, targets that generate at most one detection per time step and whose detection can be approximated as a *point*, for example, on the x and y coordinate. These techniques were able to estimate multiple target states, number of targets and perform data association of target state estimates. However, this *point target* assumption cannot hold for all targets. Some targets can generate more than one measurement per time step and thus a *point* representation of such targets isn't sufficient. These targets are termed *extended targets* and are characterised with some extension parameters. A framework to effectively estimate the target states, number of targets and association of such targets is the subject of the next chapter.

Chapter 7

Bayesian Multiple Extended Target Tracking Using Labelled Random Finite Sets and Splines

7.1 Introduction

In this chapter, a multiple ET tracking technique using the framework of labelled random finite set is proposed. This technique is namely, the ET generalised labelled multi-Bernoulli spline (ET-GLMB-S) filter. In this approach, the measurement rate of the ETs is modelled as a Poisson mixture and a Poisson mixture variational Bayesian (PMVB) is used to simultaneously estimate the measurement rate of all ETs present. Based on [61], the target extent is modelled as a diffuse model of the measurement generating process such that the target extent is represented by a spatial probability distribution instead of modelling explicit measurement sources. B-splines were used to model this spatial probability distribution. The PMVB and spline approaches are employed in the modified GLMB filter of [138] to achieve joint recursive estimate of ET state estimate, number of target and targets label tracking.

The main contributions of these chapter are as follows. Firstly, a variational Bayesian based method is used to simultaneously estimate the measurement rate

of targets present. Use of VB avoids explicitly pre-setting a window size and converges to the true rate parameter given the number of detections. This has the advantage of maximising an explicit objective, and fast convergence in most cases. Secondly, the lower bound for our variational Bayesian method is derived to aid in monitoring convergence. Third, B-splines are used to model the target extent which will allow for more accurate modelling of targets with arbitrary extensions rather than the restrictive elliptical model of [20, 21]. Lastly, the prediction and likelihood update equations for target extension under the B-spline model are derived.

The remainder of this chapter is organised as follows. Section 7.2 presents additional notations that would be helpful in this chapter. Section 7.3 presents some background information on B-Splines. The proposed ET-GLMB-S filter along with related derivations are introduced in Section 7.4. The simultaneous measurement rate estimator, the PMVB is described and derived in Section 7.5. Section 7.6 contains simulation results highlighting the performance of our proposed technique followed by concluding remarks in Section 7.7.

7.2 Preliminaries

In addition to the notations and definitions of Section 3.7, the following notation is added. These notations and definitions are useful in understanding some key concepts in this chapter.

Notation 3

A bold upper-case letter ($\boldsymbol{X}$) and bold lower-case letter ($\boldsymbol{x}$) are used to denote labelled sets and labelled vectors respectively. Regular upper -case letter (X) and regular lower-case letter (x) are adopted for unlabelled sets and unlabelled vectors respectively.

7.3 B-Splines

This section gives a brief background on B-spline [29, 48, 122]. A B-spline is a piecewise polynomial function which can be used to represent a curve. Any arbitrary geometrical, numerical or statistical function can be described by the B-spline transformation [74]. One can control the shape of any curve by adjusting the locations of the control points. This movement can be on the entire curve in which case there is a global effect or on certain part of the curve (i.e. which will have a local effect) [130]. A key benefit of using B-spline is its local controllability. That is to say, by applying appropriate control point movements, a curve can be controlled locally. This feature is useful when approximating/modelling target extension from the multiple (and stochastic) measurements generated by the target. This feature is also useful in spline filter implementation [74].

Mathematically, a one-dimensional p-th order B-spline curve $\mathbb{S}(s)$ of degree $p-1$ of a certain variable s can be defined as:

$$\mathbb{S}(s) = \sum_{i=1}^{n_p} \mathbb{P}_i \mathcal{B}_{i,p,\mathbf{t}}(s) \;\; 2 \leq p \leq n_p, \tag{7.1}$$

where $\mathbb{P}_i$ is the i-th control point, n_p denotes the total number of control points and $\mathbf{t}$ denotes a knot vector consisting of non-decreasing sequence of real valued numbers, where $\mathbf{t} = \{t_1, \cdots, t_r\}$, that is, $t_i \leq t_{i+1}, i = 1, \cdots, \tau$. The knot vector $\mathbf{t}$ relates the variable x to the control points [29, 48, 122]. The total number of knots is always greater than the total number of control points [29]. Adding or removing knots using appropriate control point movement can exactly replicate the function/curve, which is suitable for implementing filtering algorithms using splines [116, 129]. Also, a higher-order (three or more) B-spline curve tends to be smooth and maintains the continuity of the curve. The continuity of the B-spline curve enables continuous state estimation [116, 129]. The i-th B-spline basis

functions of a variable s are denoted by $\mathcal{B}_{i,p,\mathbf{t}}(s)$ and defined as [29, 48, 122]:

$$\mathcal{B}_{i,1}(s) = \begin{cases} 1 & \text{if } t_i \leq s < t_{i+1}, \\ 0 & \text{otherwise.} \end{cases} \tag{7.2}$$

$$\mathcal{B}_{i,p}(s) = \frac{s - t_i}{t_{i+p-1} - t_i}\mathcal{B}_{i,p-1}(s) + \frac{t_{i+p} - s}{t_{i+p} - t_{i+1}}\mathcal{B}_{i+1,p-1}(s) \tag{7.3}$$

where variables t_i denote knot elements; $\mathcal{B}_{i,p}(s)$ is non-zero in the interval $[t_i, t_{i+p}]$. The basis function $\mathcal{B}_{i,p}(s)$ can have the form $0/0$, in which case it assumes $0/0 = 0$ [48]. Furthermore,

$$\sum_{i=1}^{n_p} \mathcal{B}_{i,p}(s) = 1 \tag{7.4}$$

for any value of the parameter s. The basis functions are polynomials of degree $p - 1$ [29, 48]. Moreover, a B-spline curve can be open, clamped or closed. An open B-spline curve is formed if the knot vector does not have any particular structure, hence the generated curve will not touch the first and last legs of the control polyline (see Fig. 7.1a). A B-spline is clamped when the curve is tangent to the first and the last legs of the control polyline (see Fig. 7.1b). This is achieved by repeating the first knot and the last knot $p + 1$ times (i.e., of multiplicity $p + 1$). A closed B-spline can be formed by repeating some knots and control points. In this case, the start and the end of the generated curve join together forming a closed loop (see Fig. 7.1c). This can be obtained by first designing a uniform knot sequence and then wrapping the first p and the last p control points. More specifically let $\mathbb{P}_1 = \mathbb{P}_{n_p-p+1}, \mathbb{P}_1 = \mathbb{P}_{n_p-p+2}, ..., \mathbb{P}_{p-2} = \mathbb{P}_{n-1}$and $\mathbb{P}_{p-1} = \mathbb{P}_{n_p}$. Furthermore, unidimensional splines can be extended to multidimensional splines by using tensor product spline construction, see [29]. A spline subspace $\mathcal{B}_{i_j,p_j,\mathbf{t}_j}(s_j)$ is defined for each dimension where s_j denotes the variable in the j-th dimension. Thus, the spline representation of a multidimensional function $\mathbb{S}(x_1, \ldots, s_m)$ is

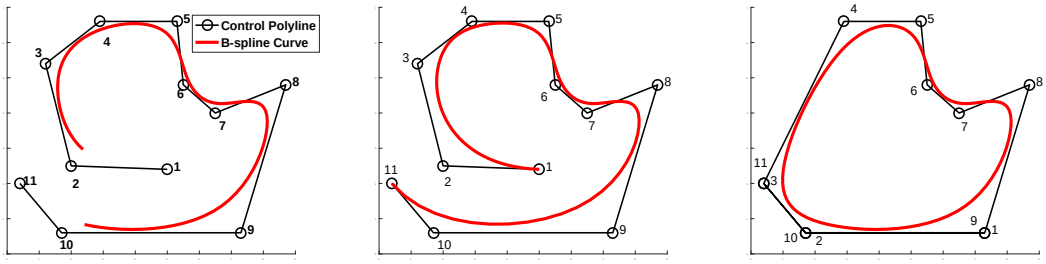

(a) Open spline. (b) Clamped spline. (c) Closed spline.

Figure 7.1 Plots showing different constructions of B-splines. The control points are indicated by circles and numbered on the plots.

given as

$$\begin{aligned}&\mathbb{S}(s_1,\ldots,s_m)\\&\quad=\sum_{i_1}^{n_p}\cdots\sum_{i_m}^{n_p}\mathbb{P}_{i_1,\ldots,i_m}\mathcal{B}_{i_1,p_1,\mathbf{t}_1}(s_1)\ldots\mathcal{B}_{i_m,p_m,\mathbf{t}_m}(s_m).\end{aligned}\tag{7.5}$$

The construction of the multidimensional spline polynomials above can be done by solving a corresponding set of linear equations [129, 130]. Moreover, the B-spline approach has been used in target tracking applications [74, 116, 129, 130] in a continuous state space primarily because no special assumption on the noises is required, and it is able to accurately approximate arbitrary probability density or probability hypothesis density surfaces [130]. In most tracking algorithms, during the update stage, the states are updated, but in B-spline-based target tracking only the knots are updated [74, 116, 129].

7.4 Multiple Extended Target Tracking with Labelled RFS and B-Splines

7.4.1 Problem Formulation

Consider an ET with scattering points along its boundary and within its body such that it generates measurements along its boundary and within its body. Let the

labelled set of extended targets at time k be denoted by:

$$\boldsymbol{X}_k = \{(\mathfrak{x}, \ell)_{i,k}\}_{i=1}^{|\boldsymbol{X}|} \triangleq \left\{\mathfrak{x}_{i,k}\right\}_{i=1}^{|\boldsymbol{X}|} \tag{7.6}$$

where $\ell \in \mathcal{L}(\boldsymbol{X})$ and $\mathcal{L}(\boldsymbol{X})$ is a set of unique labels in $\boldsymbol{X}$. $\mathfrak{x}_i$ is the labelled augmented state of the i-th target composed of the kinematic state, extension state and measurement rate parameter; henceforth $(\mathfrak{x}, \ell)$ and $\mathfrak{x}$ are used interchangeably.

The set of measurements received at time k is denoted

$$Z_k = \{z_{j,k}\}_{j=1}^{M_k}, \tag{7.7}$$

where M_k is the total number of measurements obtained at time k. The cumulative measurement sequence up to and including time k is $Z_{1:k} : Z_1, Z_2, \cdots, Z_k$. Note that the set Z includes both target originated measurements and measurements due to clutter. Each target, when present can generate one or more measurements. The measurements due to clutter are assumed to be Poisson distributed in number with rate parameter γ and having spatial distribution $\mathfrak{c}(\cdot)$. These clutter measurements are modelled as being uniformly distributed over the tracking scene. The goal at each time k is to estimate the labelled set of extended targets $\boldsymbol{X}_k$ given a set of corrupted measurements Z_k.

7.4.2 Extended Target Measurement Model

Here, the extended target measurement model similar to [20] and [21] is presented. At a given measurement time, let the labelled RFS of multiple extended targets be $\boldsymbol{X} = \{\mathfrak{x}_1, ..., \mathfrak{x}_n\}$. Hence it is assumed that a particular target $\mathfrak{x} \in \boldsymbol{X}$ has probability of $p_D(\mathfrak{x})$ of being detected or misdetected with the probability $1 - p_D(\mathfrak{x})$. Furthermore, it is assumed that if the extended target $\mathfrak{x}$ is detected, it generates a set of measurements D with likelihood $g'(D|\mathfrak{x})$. Let $\mathfrak{D} = \{D_1, ..., D_d\}$ be the set of target detections. Then the set $\mathfrak{D}$ is distributed according to (see [105]):

$$g_{\mathfrak{D}}(\mathfrak{D}|\boldsymbol{X}) = \sum_{D_1 \uplus \cdots \uplus D_d = |\boldsymbol{X}|} \tilde{g}(D_1|\mathfrak{x}_1) \cdots \tilde{g}(D_{|\boldsymbol{X}|}|\mathfrak{x}_{|\boldsymbol{X}|}), \tag{7.8}$$

where $\tilde{g}(D|\mathfrak{x}_i)$ is an RFS distribution defined by

$$\tilde{g}(D|\mathfrak{x}_i) \propto \begin{cases} 1 - p_D(\mathfrak{x}) & \text{if } D = \emptyset, \\ p_D(\mathfrak{x}) g'(D|\mathfrak{x}_i) & \text{otherwise.} \end{cases} \tag{7.9}$$

The symbol $\uplus$ denotes that the summation is taken over all mutually disjoint subsets of $\mathfrak{D}$, such that $D_1 \cup \cdots \cup D_{|\boldsymbol{X}|} = \mathfrak{D}$. Let the set $\mathfrak{K}$, which is independent of the target detections be a set of clutter measurements and modelled as a Poisson RFS with rate γ and spatial distribution $\mathfrak{c}(\cdot)$, hence $\mathfrak{K}$ is distributed according to:

$$g_{\mathfrak{K}}(\mathfrak{K}) = e^{-\gamma}[\gamma \mathfrak{c}(\cdot)]^{\mathfrak{K}}. \tag{7.10}$$

Given the above, the set of multi-target measurements, Z, is the union of the set of target detections and clutter measurements, that is, $Z = \mathfrak{D} \cup \mathfrak{K}$. Moreover, since $\mathfrak{D}$ and $\mathfrak{K}$ are independent, the multi-target likelihood is given by the convolution

$$g(Z|\boldsymbol{X}) = \sum_{\mathfrak{D} \subset Z} g_{\mathfrak{D}}(\mathfrak{D}|\boldsymbol{X}) g_{\mathfrak{K}}(Z - \mathfrak{D}) \tag{7.11a}$$

$$= \sum_{\mathfrak{D} \subset Z} g_{\mathfrak{D}}(\mathfrak{D}|\boldsymbol{X}) g_{\mathfrak{K}}(\mathfrak{K}). \tag{7.11b}$$

Furthermore, the multi-target likelihood can be expressed as a double summation over partitions of Z up to $|\boldsymbol{X}| + 1$, and mappings of measurement groups to targets as [21, 20]

$$g(Z|\boldsymbol{X}) = g_{\mathfrak{K}}(\mathfrak{K}) \sum_{i=1}^{|\boldsymbol{X}|+1} \sum_{\substack{\mathcal{W}(Z) \in \mathcal{P}_i(Z) \\ \theta \in \Theta(\mathcal{W}(Z))}} \left[\psi_{\mathcal{W}(Z)}(\cdot;\theta)\right]^{\boldsymbol{X}}, \tag{7.12a}$$

$$= e^{-\gamma}[\gamma \mathfrak{c}(\cdot)]^{Z} \sum_{i=1}^{|\boldsymbol{X}|+1} \sum_{\substack{\mathcal{W}(Z) \in \mathcal{P}_i(Z) \\ \theta \in \Theta(\mathcal{W}(Z))}} \left[\psi_{\mathcal{W}(Z)}(\cdot;\theta)\right]^{\boldsymbol{X}}, \tag{7.12b}$$

where $\mathcal{P}_i(Z)$ partitions Z into exactly i groups, and $\Theta(\mathcal{W}(Z))$ is the set of all one-to-one mappings $\theta : \mathcal{L}(\boldsymbol{X}) \to \{0, 1, \cdots, |\mathcal{W}(Z)|\}$ taking the labels in $\boldsymbol{X}$ to either a group of measurements in $\mathcal{W}(Z)$, or a misdetection. The term $\psi_{\mathcal{W}(Z)}(\mathfrak{x};\theta)$ is

denoted as

$$\psi_{\mathcal{W}(Z)}(\mathfrak{x};\theta) = \begin{cases} 1 - p_D(\mathfrak{x}) & \theta(\ell) = 0, \\ \frac{p_D(\mathfrak{x}) g'(\mathcal{W}_{\theta(\ell)}(Z)|\mathfrak{x})}{[\gamma_{\mathfrak{c}}(\cdot)]^{\mathcal{W}_{\theta(\ell)}(Z)}} & \theta(\ell) > 0, \end{cases} \tag{7.13}$$

where $\mathcal{W}_{\theta(\ell)}(Z)$ is the group of measurements in partition $\mathcal{P}_i(Z)$ that was assigned to label ℓ under the mapping θ, and $g'(D|\mathfrak{x})$ is the likelihood that a single extended target with labelled state $\mathfrak{x}$ generates measurement D. From (7.12b), it is quickly observed that computing $g(Z|\boldsymbol{X})$ requires summation over all partitions of the measurements, Z. This in general, will be numerically intractable because the sets of measurement partitions and group-to-target mappings can potentially become extremely large [20]. The idea of partitioning the measurement set Z is discussed next.

7.4.2.1 Measurement Set Partition

At time k, consider a set of measurements $Z_k = \{z_{1,k}, z_{2,k}, z_{3,k}\}$ as in Fig. 7.2. The Figure shows five possible partitions $\mathcal{P}_i(Z)$ of the set Z, with each partition containing non-empty cells $\mathcal{W}(Z)$. The index i represents the i-th partition, that is, $\mathcal{P}_i(Z)$. In each partition, say $i = 2$ (where there are two sub-groups/cells), the sub-groupings assume that measurements in the same sub-group/cell belong to the same target or a clutter source.

Furthermore, the number of possible partitions grows as the size of the measurement set increases [64, 66]. Therefore, for a target tracking method to be computationally tractable, only a subset of the possible partitions needs to be considered [64, 66]. In addition, these subset of possible measurement partitions must represent the most likely of all partitions in order to achieve good tracking performance [64]. To this end, a number of techniques can be used such as a technique called distance partition was suggested by [64] and another technique namely subpartition algorithm was also proposed in [64] to better handle the case of spatially close targets. Two other methods for achieving feasible measurement set partitioning known as the predictive partition and the expectation maximisation (EM) partition were also proposed in [66]. Moreover, the authors

in [66] suggests that the distance partitioning, subpartition, prediction partition and EM (for Gaussian mixtures) partition can all be used together to achieve a feasible set of partition $\mathcal{P}_i(Z)$. Instead of using all four techniques as suggested by

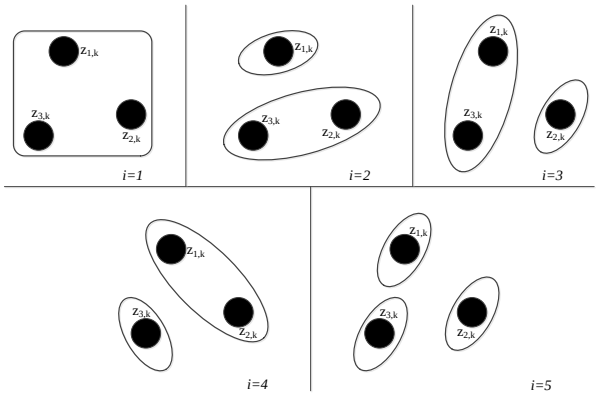

Figure 7.2 Possible partitions of a set of three extended targets. Each black dot represents measurements. The index i represents the i-th partition. In each partition, say $i = 2$, the sub-groupings assume that measurements in the same sub-group belong to the same target.

[66], it is suggested that using the prediction partition of [66] with a variational Bayesian (VB) technique (for Gaussian mixtures) (see [24] chap. 10) suffices and offers improved performance in terms of computation. Furthermore, using VB has the advantage of not knowing the number of clusters and does not suffer from singularity issues when compared to EM as highlighted in Chapter 10 of [24].

7.4.3 Extended Target State Model

The extended target state of the i-th target at time k with label ℓ is modelled as the tuple

$$\mathfrak{x}_{i,k} \triangleq (\lambda_{i,k}, x_{i,k}, \mathcal{X}_{i,k}) \tag{7.14}$$

where $\lambda_{i,k}$ is the Poisson measurement rate parameter, $x_{i,k}$ is the target kinematic state (such as position, velocity, acceleration) and $\mathcal{X}_{i,k}$ denotes the target extension/shape state. The rate parameter is modelled as a gamma distribution, the kinematic state as a Gaussian distribution and the extent as spatial probability

distribution characterised by control points of a B-spline function. Since only the i-th target is considered, the subscript i and the label ℓ are suppressed from here on. The distribution of the extended target state is given by the density in (7.15). For simplicity, henceforth the notations for indices is adopted so that $(\cdot)_{k-1}$, $(\cdot)_k$ and $(\cdot)_k^+$ represent $(\cdot)_{k-1|k-1}$, $(\cdot)_{k|k-1}$ and $(\cdot)_{k|k}$ respectively.

$$\begin{aligned} p(\mathfrak{x}_{k-1}|Z_{1:k-1}) = p(\lambda_{k-1}|Z_{1:k-1})p(x_{k-1}|\mathcal{X}_{k-1}, Z_{1:k-1}) \\ \times p(\mathcal{X}_{k-1}|Z_{1:k-1}). \end{aligned} \tag{7.15}$$

The prediction and update stages of the extended target density of (7.15) are discussed next.

7.4.3.1 Prediction

The predicted density $p(\mathfrak{x}_k|Z_{1:k-1})$ of an extended target is now computed. To this end, we solve the Champan-Kolmogorov equation below:

$$p(\mathfrak{x}_k|Z_{1:k-1}) = \int f(\mathfrak{x}_k|\mathfrak{x}_{k-1})p(\mathfrak{x}_{k-1}|Z_{1:k-1})d\mathfrak{x}_{k-1} \tag{7.16}$$

where $f(\cdot|\cdot)$ denotes the transition density from time $k-1$ to k and $p(\mathfrak{x}_{k-1}|Z_{1:k-1})$ is the extended target density at time $k-1$. Next, let us assume the transition density can be written as

$$f(\mathfrak{x}_k|\mathfrak{x}_{k-1}) = \int f(\lambda_k|\lambda_{k-1})f(x_k|x_{k-1}, \mathcal{X}_{k-1})f(\mathcal{X}_k|\mathcal{X}_{k-1}). \tag{7.17}$$

This equation assumes independence between the kinematic state $\mathfrak{x}_{k-1}$ and the extent state $\mathcal{X}_k$. This approximation is inherited from [84], where it was noted that this implies restrictions that can be justified in many practical applications. Relaxing this assumption will mean that χ_k is dependent on x_{k-1} which is a

consideration for future work. Hence, the density of (7.16) yields

$$\begin{aligned} p(\mathfrak{x}_k|Z_{1:k-1}) = &\int p(\lambda_{k-1}|Z_{1:k-1}) f(\lambda_k|\lambda_{k-1}) d\lambda_{k-1} \\ &\times \int p(x_{k-1}|\mathcal{X}_{k-1}, Z_{1:k-1}) f(x_k|x_{k-1}, \mathcal{X}_{k-1}) dx_{k-1} \\ &\times \int p(\mathcal{X}_{k-1}|Z_{1:k-1}) f(\mathcal{X}_k|\mathcal{X}_{k-1}) d\mathcal{X}_{k-1}. \end{aligned} \tag{7.18}$$

To solve for (7.18), firstly, it is assumed that the density of the measurement rate can be approximated as

$$\begin{aligned} \int p(\lambda_{k-1}|Z_{1:k-1}) f(\lambda_k|\lambda_{k-1}) d\lambda_{k-1} \approx \mathcal{GAM}(\lambda_k; \alpha_k, \beta_k), \\ \alpha_k = \frac{\alpha_{k-1}}{u}, \quad \beta_k = \frac{\beta_{k-1}}{u}, \end{aligned} \tag{7.19}$$

where $\mathcal{GAM}(\lambda_k; \alpha_k, \beta_k)$ means λ_k is gamma distributed and governed by parameters α_k and β_k. The term $u > 0$ is a scaling term that ensures prediction such that the expected value of the rate parameter is retained, and its variance is scaled (increased) by u. In our approach, choosing u such that it is positive suffices because the rate parameter converges to the true value when the PMVB is used.

The second line of (7.18) captures the kinematic component of the density. The kinematic density $p(x_{k-1}|\mathcal{X}_{k-1}, Z_{1:k-1}) = \mathcal{N}(x_{k-1}; m_{k-1}, P_{k-1} + \Sigma_{k-1})$ and under a linear Gaussian dynamic model, $f(x_k|x_{k-1}, \mathcal{X}_{k-1}) = \mathcal{N}(x_k; Fx_{k-1}, Q + \Sigma_{k-1})$. This has a closed form solution given by:

$$\begin{aligned} \int \mathcal{N}(x_{k-1}; m_{k-1}, P_{k-1} + \Sigma_{k-1}) f(x_k|x_{k-1}, \mathcal{X}_{k-1}) dx_{k-1} \\ = \mathcal{N}(x_k; m_k, P_k + \Sigma_k), \\ m_k = Fm_{k-1}, \quad P_k = FP_{k-1}F^{\bar{T}} + Q. \end{aligned} \tag{7.20}$$

where Σ_{k-1} denotes the covariance of control points. The last component on the RHS of (7.18) (i.e., the last line) represents the extended target extension component which is assumed to be a spatial probability distribution. This is

approximated as

$$\int p(\mathcal{X}_{k-1}|Z_{1:k-1}) f(\mathcal{X}_k|\mathcal{X}_{k-1}) d\mathcal{X}_{k-1} \approx \mathbb{S}_k(\mathcal{X}_k; \mathbb{P}_k) \triangleq \mathbb{S}_k, \tag{7.21a}$$

where $\mathbb{S}_k$ is a d dimensional B-spline curve of order p, degree $p-1$, having knots $\mathbf{t}$ and characterised by control points $\mathbb{P}_k$.
The B-spline curve $\mathbb{S}_k$ is given as:

$$\mathbb{S}_k = \sum_{j_1}^{N_k} \mathbb{P}_{k,j_1} \mathcal{B}_{i_1,p,\mathbf{t}}(s^{j_1}) \cdots \sum_{j_d}^{N_k} \mathbb{P}_{k,j_d} \mathcal{B}_{i_d,p,\mathbf{t}}(s^d), \tag{7.21b}$$

$$\mathbb{P}_k = F\mathbb{P}_{k-1} + w_{k-1}, \tag{7.21c}$$

where the subscript d in (7.21b) denotes the dimension of the control points, $\mathbb{P}_{k,j_d}$ denotes the vector of control points in the d-th dimension and N_k is the number of control points; w_{k-1} is an independent and identically distributed (i.i.d.) Gaussian noise vector with zero mean and covariance Σ_{k-1}. The B-spline used here is a closed spline which can be obtained as described in Section III. The spline has order $p = 4$ (degree 3). The knot elements are determined between intervals $[a, b]$ as [48]:

$$\mathbf{t} = \begin{cases} t_1, \cdots, t_p & = a \\ t_{i+p} & = a + \frac{i(b-a)}{N_k+p-1} \quad \text{for } i = 1, \cdots, (N_k - p) \\ t_{l-p}, \cdots, t_l & = b, \end{cases} \tag{7.21d}$$

where $l = N_k + p$.

The above gives the extended target predicted density $p(\mathfrak{x}_k|Z_{1:k-1}) \approx \mathcal{ETS}(\mathfrak{x}_k; \xi_k)$ where $\xi_k = (\alpha_k, \beta_k, m_k, P_k, \mathbb{S}_k, \mathbb{P}_k)$ is an array containing the predicted parameters which are defined by (7.19), (7.20) and (7.21a).

7.4.3.2 Update

When the set of measurements Z_k is available, each extended target needs to undergo measurement update using feasible subsets D of Z_k. The update procedure

of a single extended target having a predicted density $\mathcal{ETS}(\cdot)$ given D is now described. It is assumed that an extended target, when present and detected, generates measurements D and each element of D is generated according to the measurement model

$$\bar{z}_k = Hx_k + v_k \tag{7.22}$$

where matrix H is a transformation matrix and v_k is an independent and identically distributed (i.i.d.) Gaussian noise vector with mean zero and a covariance Σ_k; where Σ_k denotes the covariance of the control points.

Given the predicted density, the aim is to use Bayes rule to compute the posterior density

$$p(\mathfrak{x}_k^+|Z_{1:k}) = \frac{p(\mathfrak{x}_k|Z_{1:k-1})g'(D|\mathfrak{x}_k)}{\int p(\mathfrak{x}_k|Z_{1:k-1})g'(D|\mathfrak{x}_k)d\mathfrak{x}_k} \tag{7.23}$$

The single target likelihood term $g'(D|\mathfrak{x}_k)$ of (7.23) is defined in a similar manner to [84, 21] as

$$g'(D|\mathfrak{x}_k) = \mathcal{POIS}(|D|;\lambda_k)\prod_{j=1}^{|D|}\mathcal{N}(z_j;Hx_k,\Sigma_k) \tag{7.24}$$

so that the numerator of (7.23) is

$$\begin{aligned} p(\mathfrak{x}_k|Z_{1:k-1})g'(D|\mathfrak{x}_k) &= \mathcal{GAM}(\lambda_k;\alpha_k,\beta_k)\mathcal{N}(x_k;m_k,P_k+\Sigma_k) \\ &\quad\times \mathbb{S}_k\mathcal{POIS}(|D|;\lambda_k)\prod_{j=1}^{|D|}\mathcal{N}(z_j;Hx_k,\Sigma_k). \end{aligned} \tag{7.25}$$

Rearranging (7.25) yields

$$\begin{aligned} &= \mathcal{GAM}(\lambda_k;\alpha_k,\beta_k)\mathcal{POIS}(|D|;\lambda_k) \\ &\times \mathcal{N}(x_k;m_k,P_k+\Sigma_k)\prod_{j=1}^{|D|}\mathcal{N}(z_j;Hx_k,\Sigma_k) \\ &\times \mathbb{S}_k(\mathcal{X}_k;\mathbb{P}_k). \end{aligned} \tag{7.26}$$

where the first line captures the measurement rate component, the second line is the kinematic component and the last line is the extension component. From

(7.26), given that the measurement rate component is independent of the extension and kinematic components, and can be treated separately.

As for the measurement rate component, the updated parameters α_k^+, β_k^+ and λ_k^+ are obtained using the Poisson mixture variational Bayesian (PMVB) technique which is described in detail in Section 7.5. The PMVB is initialised using the predicted α_k, and β_k as in (7.19), the mixture components C and the number of measurements from the ETs as obtained from the measurement partitioning technique of Section (7.4.2.1). The number of mixture components C can be set to the maximum expected number of components. Setting such a value for C, the VB model will not over fit the measurements to this number but rather converge to the true number of components present given the measurements. This is one of the advantages of the VB method over techniques such EM.

For the kinematic components, the update parameters are given by the following:

$$\hat{z}_k = \frac{1}{|D|} \sum_{z_k \in D} z_k \tag{7.27a}$$

$$m_k^+ = m_k + K_k(\hat{z}_k - H m_k) \tag{7.27b}$$

$$K_k = P_k H^T S_k^{-1} \tag{7.27c}$$

$$S_k = H P_k H^T + \frac{1}{|D|} \tag{7.27d}$$

$$P_k^+ = P_k - K_k H P_k \tag{7.27e}$$

$$\Sigma_k^+ = \sum_{z \in D} (z - \hat{z})(z - \hat{z})^T \tag{7.27f}$$

As for the extension component, the number of control points are given as

$$N_k^+ = \begin{cases} |D|, & \text{if } |D| < \tau \\ \text{convx}(D), & \text{if } |D| > \tau, \end{cases} \tag{7.28}$$

where convx(D) denotes those elements of D that form the convex polyline of the set of measurements D and τ is a suitable threshold. A threshold τ is introduced to avoid using all the elements of D as control points particularly when $|D|$ and hence

λ_k is large. This heuristic is based on the assumption that the ET has scattering points along its boundary (and within the body of the ET for an ET with large rate parameter λ_k). Applying this heuristic especially for a large λ_k would give the boundary outline of the ET. The control points are updated as

$$\mathbb{P}_k^+ = \begin{cases} \mathbb{P}_k + K_k(D - H\mathbb{P}_k), & \text{if } |\mathbb{P}_k| = |D| \\ (\mathbb{P}_k + K_k(D^a - H\mathbb{P}_k)) \cup D^b, & \text{if } |\mathbb{P}_k| < |D| \end{cases} \tag{7.29}$$

where D^a and D^b are such that $D = D^a \cup D^b$. This means the detections D are split into two subsets D^a and D^b. The elements of D^a are elements in D with high association probabilities to $\mathbb{P}_k$ such that $|D^a| = |\mathbb{P}_k|$. This is achieved using the computationally attractive association method proposed in [44]. The control points update in (7.29) is akin to removal or addition of control points (and knots) in a B-spline. This translates to controlling the shape of the closed B-spline curve.

7.4.4 ET-GLMB filter with B-splines

Based on the proposed state space and measurement likelihood models presented above, the ET-GLMB filter with B-splines (ET-GLMB-S) is presented. The proposed ET-GLMB-S has two main stages (as is common to approximations of the Bayes multi-object filters), the prediction stage and the update stage. This is akin to respectively computing (3.8) and (3.10) of the Bayes multi-object filter. Using Notation 3, (3.8) and (3.10) are rewritten as:

$$\zeta_k(\boldsymbol{X}_k|Z_{1:k-1}) = \int f_k(\boldsymbol{X}_k|\boldsymbol{X})\zeta_{k-1}(\boldsymbol{X}|Z_{1:k-1})\delta\boldsymbol{X}, \tag{7.30a}$$

$$\zeta_k^+(\boldsymbol{X}_k|Z_{1:k}) = \frac{g_k(Z_k|\boldsymbol{X}_k)\zeta_k(\boldsymbol{X}_k|Z_{1:k-1})}{\int g_k(Z_k|\boldsymbol{X})\zeta_k(\boldsymbol{X}|Z_{1:k-1})\delta\boldsymbol{X}}. \tag{7.30b}$$

For the purpose of our derivation, the standard birth/death model similar to the one in [21] and [138] are used for the multi-target dynamics.

$$\pi(\boldsymbol{X} \mid Z) = \frac{\pi(\boldsymbol{X}) g(Z \mid \boldsymbol{X})}{\int \pi(\boldsymbol{X}) g(Z \mid \boldsymbol{X}) \delta \boldsymbol{X}} \tag{7.32a}$$

$$= \frac{\Delta(\boldsymbol{X}) g_C(Z) \sum\limits_{c \in \mathbb{C}} \sum_{i=1}^{|\mathcal{L}(\boldsymbol{X})|+1} \sum\limits_{\substack{\mathcal{W}(Z) \in \mathcal{P}_i(Z) \\ \theta \in \Theta(\mathcal{W}(Z))}} w^{(c)}(\mathcal{L}(\boldsymbol{X})) \left[\eta^{(c,\theta)}_{\mathcal{W}(Z)}(\,\cdot\,)\right]^{\mathcal{L}(\boldsymbol{X})} \left[p^{(c,\theta)}(\cdot \mid \mathcal{W}(Z))\right]^{\boldsymbol{X}}}{g_C(Z) \sum\limits_{c \in \mathbb{C}} \sum_{L \subseteq \mathbb{L}} \sum_{i=1}^{|L|+1} \sum\limits_{\substack{\mathcal{W}(Z) \in \mathcal{P}_i(Z) \\ \theta \in \Theta(\mathcal{W}(Z))}} w^{(c)}(L) \left[\eta^{(c,\theta)}_{\mathcal{W}(Z)}\right]^{L}} \tag{7.32b}$$

$$\pi(\boldsymbol{X} \mid Z) = \Delta(\boldsymbol{X}) \sum_{c \in \mathbb{C}} \sum_{i=1}^{|\boldsymbol{X}|+1} \sum_{\substack{\mathcal{W}(Z) \in \mathcal{P}_i(Z) \\ \theta \in \Theta(\mathcal{W}(Z))}} w^{(c,\theta)}_{\mathcal{W}(Z)}(\mathcal{L}(\mathbf{X})) \times \left[p^{(c,\theta)}(\cdot \mid \mathcal{W}(Z))\right]^{\boldsymbol{X}}. \tag{7.32c}$$

7.4.4.1 Prediction

For the prediction step, denote the probability of target survival and target death from present to next time as $p_S(\mathfrak{x}, \ell)$ and $q_S(\mathfrak{x}, \ell) = 1 - p_S(\mathfrak{x}, \ell)$ respectively. The birth density is an LMB having weight $w_B(\cdot)$, single target densities $p_B(\cdot, \ell)$ and a label space denoted by $\mathbb{B}_k$. Given that the multi-target posterior is a GLMB of the form (3.59) with label space $\mathbb{L}_{k-1}$, the predicted multi-target density at the next time step is the GLMB with label space $\mathbb{L}_k = \mathbb{L}_{k-1} \cup \mathbb{B}_k$ given by (see for example, [21, 138])

$$\zeta_k(\boldsymbol{X}) = \Delta(\boldsymbol{X}) \sum_{c \in \mathbb{C}} w_k^{(c)}(\mathcal{L}(\boldsymbol{X})) \left[p_k^{(c)}(\,\cdot\,)\right]^{\boldsymbol{X}} \tag{7.31a}$$

$$w_k^{(c)}(L) = w_B(L - \mathbb{L}) w_S^{(c)}(L \cap \mathbb{L}), \tag{7.31b}$$

$$p_k^{(c)}(\mathfrak{x}_k, \ell) = 1_{\mathbb{L}}(\ell) p_S^{(c)}(\mathfrak{x}, \ell) + (1 - 1_{\mathbb{L}}(\ell)) p_B(\mathfrak{x}_k, \ell), \tag{7.31c}$$

$$p_S^{(c)}(\mathfrak{x}_k, \ell) = \frac{\int p_S(\mathfrak{x}_k, \ell) f(\mathfrak{x}_k | \mathfrak{x}_{k-1}, \ell) p^{(c)}(\mathfrak{x}_{k-1}, \ell) d\mathfrak{x}_{k-1}}{\eta_S^{(c)}(\ell)}, \tag{7.31d}$$

$$\eta_S^{(c)}(\ell) = \int \int p_S(\mathfrak{x}_k, \ell) f(\mathfrak{x}_k \mid \mathfrak{x}_{k-1}, \ell) \times p^{(c)}(\mathfrak{x}_{k-1}, \ell) d\mathfrak{x}_{k-1} d\mathfrak{x}_k, \tag{7.31e}$$

$$w_S^{(c)}(J) = \left[\eta_S^{(c)}\right]^J \sum_{I \subseteq \mathbb{L}} 1_I(J) [q_S]^{I-J} w^{(c)}(I), \tag{7.31f}$$

$$q_S^{(c)}(\ell) = \int q_S(\mathfrak{x}_k, \ell) p^{(c)}(\mathfrak{x}_k, \ell) d\mathfrak{x}_k. \tag{7.31g}$$

7.4.4.2 Update

The update equations for the ET-GLMB-S filter is given in (7.32a) - (7.32c) where

$$w^{(c,\theta)}_{\mathcal{W}(Z)}(L) = \frac{w^{(c)}(L)\left[\eta^{(c,\theta)}_{\mathcal{W}(Z)}\right]^{L}}{\sum_{c\in\mathbb{C}}\sum_{J\subseteq\mathbb{L}}\sum_{i=1}^{|J|+1}\sum_{\substack{\mathcal{W}(Z)\in\mathcal{P}_i(Z)\\ \theta\in\Theta(\mathcal{W}(Z))}} w^{(c)}(J)\left[\eta^{(c,\theta)}_{\mathcal{W}(Z)}\right]^{J}},$$

$$p^{(c,\theta)}(x,\ell\,|\,\mathcal{W}(Z)) = \frac{p^{(c)}(\mathfrak{x},\ell)\psi_{\mathcal{W}(Z)}(\mathfrak{x};\theta)}{\eta^{(c,\theta)}_{\mathcal{W}(Z)}(\ell)},$$

$$\eta^{(c,\theta)}_{\mathcal{W}(Z)}(\ell) = \int p^{(c)}(\mathfrak{x},\ell)\psi_{\mathcal{W}(Z)}(\mathfrak{x};\theta)d\mathfrak{x}, \tag{7.33}$$

with the term $\psi_{\mathcal{W}(Z)}(\mathfrak{x};\theta)$ given in (7.13).

The above prediction and update stages provide the ET-GLMB-S filter. Notice in both the prediction and update equations that the sum over $c \in \mathbb{C}$ is to facilitate the propagation of multiple hypotheses. These hypotheses involve different set of track labels which arise due to uncertainty in data association seen in the update stage of the Bayes multi-target filter [117]. Performing this can allow for a more accurate filtering process albeit at an increased computational effort. An efficient way will be to use just a single component (as in the Definition 4 above) to propagate the uncertainty of a single set of track labels. This can save on computational time but may sacrifice filtering accuracy. This method is called the ET-GLMB-Sr filter.

7.5 The MCMC-VB Model for Poisson Distributed Multiple Extended Target Measurements

In this section, a technique for jointly estimating the measurement rate per target for all targets using variational inference is presented.

7.5.1 Context

Multiple extended targets under the measurement model of [61] and [62] are considered. It is assumed that the target's proximity to the sensor is such that

the detections are geometrically structured. Furthermore, recall that the set of measurements at time k is a union of all target originated measurements and measurements due to clutter is given by (7.7). At time k, the number of measurements generated by the i-th target is a Poisson distributed random variable with rate parameter $\lambda_{k,i}$. The number of measurements due to clutter is assumed to be Poisson distributed with rate parameter γ_k. The set of measurements used to update the i-th target at time k is denoted as $Z_k^{(i)}$[1]. Let $\mathfrak{N}_k = \{N_1, N_2, \cdots, N_T\}$ be set of the number of measurements generated per extended target and $N_i = \left|Z_k^{(i)}\right|$. Using the measurement model of [62], each element of $\mathfrak{N}_k$ is Poisson distributed with rate parameter $\lambda_k^{(i)}$. Denote $\Lambda_k = \{\lambda_1, \lambda_2, \cdots, \lambda_T\}$ to be the set of rate parameters. Our goal is to jointly estimate at each time k, the measurement rates parameters which constitute of the elements of set Λ_k given $Z_{1:k}$ for each extended target. To this end, a recursive estimator of Λ_k using a PMVB technique is presented in Section 7.5.2.

7.5.2 Poisson Mixture

In order to develop the PMVB model for our multiple extended target parameter estimation technique, the mixture model equations for the Poisson distributed random variable is derived. Figure 7.3 shows the graphical representation of the PMVB model.

Suppose that the number of extended target measurements, Z_k, of Section 7.5.1 are independent and identically distributed (i.i.d.) and the measurements are from a Poisson distribution with rate parameter $\lambda_{k,i}$. From here on,the time index subscript k is omitted for ease of presentation. For each observable variable n_j, there is a corresponding latent variable $y_j \in Y$ (where $Y = \{y_1, y_2, \cdots, y_J\}$) is comprised of 1-of-$C$ binary vector with elements y_{jc} for $c = 1, \cdots, C$. The

[1]where $Z_k^{(i)} \equiv \mathcal{W}(Z)$ and $\mathcal{W}(Z) \in \mathcal{P}(Z); \mathcal{P}(Z) \angle Z_k$. The notation $\mathcal{P}(Z) \angle Z_k$ denotes the chosen partition of Z_k from all most likely feasible partitions $\mathcal{P}_i(Z)\ \forall i$ (note that $\mathcal{P}_i(Z)\ \forall i$ includes other data associations with significant probabilities)

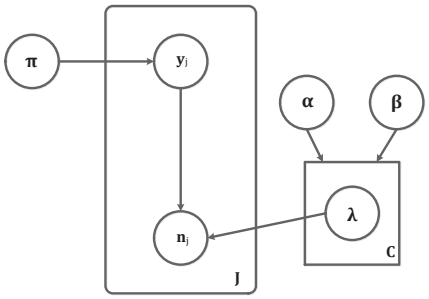

Figure 7.3 Graphical model representation of the Poisson mixture model. n_j are observables which are governed by the Poisson distribution parameter λ. The latent variable y_j is a vector with a single component equal to 1 and the rest equal to 0, indicating cluster assignment of n_j. α, β are hyper-parameters of the Gamma distribution. π indicates the proportional of the components. J and C denote the number of measurements and number of components respectively.

likelihood function of the Poisson distributed n is defined by

$$p(n|\lambda) = \frac{\lambda^n}{n!} e^{-\lambda} \tag{7.34}$$

Then the Poisson finite mixture is defined as:

$$p(n|\lambda, \pi) = \sum_{c=1}^{C} \pi_c p(n|\lambda_c) \tag{7.35}$$

where each Poisson density $p(n|\lambda_c)$ is a component of the mixture and has its own rate parameter λ_c; C denote total number of mixture components. π_c are the mixing coefficients with $0 \leq \pi_c \leq 1$ and $\sum_{c=1}^{C} \pi_c = 1$. The conditional distribution of the latent variables, Y, given the mixing coefficients, π, is defined as:

$$p(y|\pi) = \prod_{j=1}^{J} \prod_{c=1}^{C} \pi_c^{y_{jc}}. \tag{7.36}$$

The conditional distribution of the measurement vectors given the component parameters and latent variables is

$$p(\mathfrak{N}|Y, \Lambda) = \prod_{j=1}^{J} \prod_{c=1}^{C} p(n_j|\lambda_c)^{y_{jc}}, \tag{7.37}$$

To simplify analysis, conjugate priors are used in Bayesian learning and therefore the Dirichlet distribution is chosen for the mixing coefficients (see Chapter 10 of [24]) as

$$p(\pi) = \mathrm{Dir}(\pi|\mathfrak{a}_0) = \mathcal{C}(\mathfrak{a}_0)\prod_{c=1}^{C}\pi_c^{a_0-1}, \tag{7.38}$$

and a Gamma distribution for the rate parameters [60] as

$$p(\Lambda) = \mathrm{Gam}(\Lambda|\alpha,\beta) = \prod_{c=1}^{C}\frac{\beta^{\alpha}\lambda_c^{\alpha-1}e^{-\lambda_c\beta}}{\Gamma(\alpha)}, \tag{7.39}$$

where $\mathcal{C}(\mathfrak{a}_0)$ is the normalisation constant for the Dirichlet distribution.

7.5.3 Variational Distribution

Given that the joint distribution of the observed data, latent variables and hidden parameters from Sec. 7.5.2 is

$$p(\mathfrak{N}, Y, \pi, \Lambda) = p(\mathfrak{N}|Y,\Lambda)p(Y|\pi)p(\pi)p(\Lambda); \tag{7.40}$$

the aim in variational learning is to find a variational distribution, $q(Y,\pi,\Lambda)$, on the latent variables and hidden parameters such that the variational lower bound $\mathcal{L}(q)$ given by

$$\mathfrak{L}(q) = \int\int q(Y,\pi,\Lambda)\ln\left\{\frac{p(\mathfrak{N},Y,\pi,\Lambda)}{q(Y,\pi,\Lambda)}\right\}d\pi d\Lambda, \tag{7.41}$$

is maximised or the Kullback-Leibler (KL) divergence given by

$$\mathrm{KL}(q||p) = -\int\int q(Y,\pi,\Lambda)\ln\left\{\frac{p(Y,\pi,\Lambda|\mathfrak{N})}{q(Y,\pi,\Lambda)}\right\}d\pi d\Lambda, \tag{7.42}$$

is minimised. Note that maximising the lower bound is equivalent to minimising the KL divergence and the maximum of the lower bound occurs when the KL divergence vanishes and this occurs when $q(Y,\pi,\Lambda)$ equals the posterior distribution $p(Y|\mathfrak{N})$. $q(Y,\pi,\Lambda)$ is optimised in the set of probability distributions where the parameters are independent of each other. The variational distribution $q(Y,\pi,\Lambda)$ is factorised

as

$$q(Y, \pi, \Lambda) = q_1(Y)q_2(\pi, \Lambda) \tag{7.43a}$$

The log of the optimised factors are:

$$\log q_1(Y) = \mathrm{E}_{q_1}[\log p(\mathfrak{N}, Y, \pi, \Lambda)] + \mathrm{const}_1 \tag{7.43b}$$

$$\log q_2(\pi, \Lambda) = \mathrm{E}_{q_2}[\log p(\mathfrak{N}, Y, \pi, \Lambda)] + \mathrm{const}_2 \tag{7.43c}$$

where const_1 and const_2 are normalisation constants.

7.5.4 The Variational Learning

Equations (7.43b) and (7.43c) are recursively calculated to perform the VB learning. We further factorise $q_2(\pi, \Lambda)$ from (7.43a) as

$$q_2(\pi, \Lambda) = q_\pi(\pi)q_\Lambda(\Lambda), \tag{7.44a}$$

where the optimal distributions for $q_\pi(\cdot)$ and $q_\Lambda(\cdot)$ are given by

$$q_\pi(\pi) = \mathrm{Dir}(\pi|\mathfrak{a}), \tag{7.44b}$$

$$q_\Lambda(\Lambda) = \prod_{c=1}^{C} \mathrm{Gam}(\lambda_c|\alpha, \beta) \tag{7.44c}$$

The expectation step of the VB model is computed using:

$$\begin{aligned}\log \rho_{jc} = {} & \psi_0(a_c) - \psi_0\left(\sum_c^C a_c\right) \\ & + (\psi_0(\alpha_c) - \log \beta_c) \sum_{j=1}^{J} n_j - J(\frac{\alpha_c}{\beta_c}) - \sum_{j=1}^{J} \log(n_j!),\end{aligned} \tag{7.45a}$$

with

$$r_{jc} = \frac{\rho_{jc}}{\sum_{c=1}^{C} \rho_{jc}} \tag{7.45b}$$

where $\psi_0(\cdot)$ is the digamma function (also known as the polygamma function of order 0) given by $\psi_0(a) = \frac{d}{da}\log\Gamma(a)$. The VB maximisation step is computed using:

$$N_c = \sum_{c=1}^{C} r_{jc}, \qquad a_c = a_0 + N_c \tag{7.46a}$$

$$\alpha_c = \alpha_0 + \sum_{j=1}^{J} n_j, \quad \beta_c = \beta_0 + J \tag{7.46b}$$

$$\mathbb{E}[\lambda_c] = \frac{\alpha_c}{\beta_c} \qquad \mathrm{Var}(\lambda_c) = \frac{\alpha_c}{\beta_c^2} \tag{7.46c}$$

where N_c denotes the number of measurements generated up to now by a target with measurement rate λ_c. After PMVB step, the updated set of α_k^+ and β_k^+ are available as well as the set of the measurement rate, $\Lambda_k^+ = \{\lambda_1, \cdots, \lambda_C\}$ with $|\mathfrak{N}_k^+| = |\Lambda_k^+|$.

7.6 Simulation Example

In this section, the performance of the proposed ET-GLMB-S and ET-GLMB-Sr filters are compared to the GLMB and random matrix based multiple extended target tracker of [21] which are referred to here as the ET-GLMB-E filter. Additionally, the proposed approach is also compared with a filter referred to here as the ET-GLMB-Em filter where the random matrix in [21] is replaced with the multiple sub-object method in [70].

7.6.1 Tracking Setup

Two different tracking scenarios are considered. One scenario has four targets with different measurement rates and the other scenario has three targets also with different measurement rates. The dynamics of the target centroid is described using

$$x_k = Fx_{k-1} + w_k, \tag{7.47}$$

where x_k encapsulates the kinematic components, that is, position and velocity, $w_k \sim \mathcal{N}(0, Q_k)^{\bar{T}}$ is a vector representing the process noise. The transition matrix F and the process noise covariance matrix Q_k are given as

$$F = \begin{bmatrix} 1 & \delta t \\ 0 & 1 \end{bmatrix} \otimes I_d, \quad Q_k = \sigma^2 \begin{bmatrix} \frac{\delta t^4}{4} & \frac{\delta t^3}{2} \\ \frac{\delta t^3}{2} & \delta t^2 \end{bmatrix} \otimes \Sigma_k \tag{7.48}$$

with the sample period $\delta t = 1$ and the process noise standard deviation is $\sigma = 2\text{m/s}^2$. Furthermore, the probability of target survival is set to be $p_S = 0.99$. The initial gamma parameters used in the PMVB were set as $\alpha = 0.5$ and $\beta = 0.5$. The measurement rate threshold was set as $\tau = 20$.

7.6.2 Performance Metrics

The performance of the proposed filter is evaluated using filter run computation time (CT) and a metric based on the optimal sub-pattern assignment (OSPA) [125]. The OSPA metric used is similar to the modified (mOSPA) metric proposed in [95]. The mOSPA penalises not only the cardinality and state estimations errors but also the measurement rate and extension errors. The main difference between the method here and that in [95] is that (45c) in [95] which was given as

$$d_{j,i}^{(c_X)} = \min(c_X, ||X_k^{(j)} - \hat{X}_{k|k}^{(i)}||_F) \tag{7.49a}$$

was modified to read

$$d_{j,i}^{(c_\mathcal{X})} = \min(c_\mathcal{X}, \frac{1}{M}\sum^{M} |r(\mathcal{X}_k^{(j)}) - r(\hat{\mathcal{X}}_{k|k}^{(i)})|^2). \tag{7.49b}$$

From (7.49a), X denotes the true positive semi-definite matrix capturing the target extension and $\hat{X}$ is its estimate; $||\cdot||_F$ denotes the Frobenius norm and the constant c_X is chosen so that it corresponds to the maximum expected error for the target extension state. From (7.49b), $\mathcal{X}$ denotes the true shape of the target and $\hat{\mathcal{X}}$ denotes its B-spline estimate; $r(\cdot)$ denotes a radial function that maps an angle to the radius of an arbitrary shape from its centroid (from 0 to 2π, M is the number

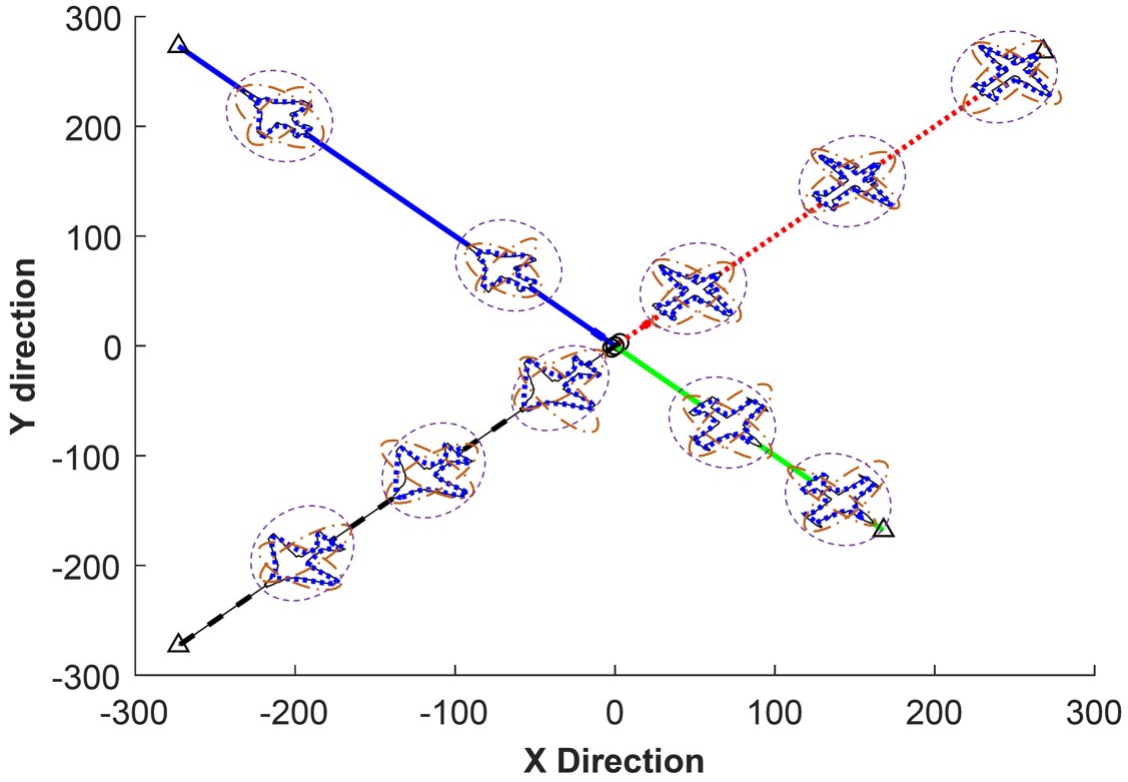

Figure 7.4 Scenario I. True target trajectories (the straight lines) in the *x*-*y* plane with start/end (◯/△). The true target shape is shown in black line, the B-spline method in blue dotted line, the multi-sub-object method in red-dash-dotted line and the random matrix method in purple dash line. All four targets start from the origin. The target plots shown are at intervals of 20 time steps.

of points $r(\cdot)$ was evaluated at) and it is convenient for representing and learning abstract shapes; $|\cdot|^2$ denotes the instantaneous error and $c_{\mathcal{X}}$ is chosen so that it corresponds to the maximum expected error for the target extension state. For brevity, only the section of the mOSPA metric for extended targets that differs from the one in [95] is presented. Aside from this modification, all other aspects of the mOSPA are as in [95].

7.6.3 Scenario I (where $\lambda_k < \tau$)

In this scenario, four targets with measurement rates less than the measurement threshold are tracked in a $[-300, 300] \times [-300, 300]$ 2D surveillance area. The measurement rates and the time the targets enter and exit the tracking scene are

given below:

$$\lambda_k^{(1)} = 5, \quad t_b^{(1)} = 1, \quad t_d^{(1)} = 70, \tag{7.50a}$$

$$\lambda_k^{(2)} = 10, \quad t_b^{(2)} = 26, \quad t_d^{(2)} = 80, \tag{7.50b}$$

$$\lambda_k^{(3)} = 15, \quad t_b^{(3)} = 51, \quad t_d^{(3)} = 90, \tag{7.50c}$$

$$\lambda_k^{(4)} = 20, \quad t_b^{(4)} = 76, \quad t_d^{(4)} = 100. \tag{7.50d}$$

This scenario lasts 100 time steps. The ground truth of the kinematic state of the targets are shown in Fig. 7.4. In this scenario, two sub-objects were considered for the ET-GLMB-Em filter.

In this scenario,the performance of the proposed filter was evaluated against the ET-GLMB-E and ET-GLMB-Em filters in terms of CT and mOSPA measure. Furthermore, since the targets enter and exit the scene at different times, the cardinality estimates of both filters were also evaluated. It is assumed that the clutter distribution is Poisson with uniform intensity. When evaluating the mOSPA measure and the cardinality, a moderate clutter case was considered where the average number of Poisson clutter points per scan is $\gamma_k = 50$. As for the CT performance evaluation, three clutter cases were considered. The first clutter has an average number of $\gamma_k = 30$ clutter points per scan with $pD = 0.8$, the second had $\gamma_k = 50$ with $pD = 0.9$ and the third case had $\gamma_k = 100$ clutter points per scan with $pD = 0.95$. The cardinality estimation is more challenging in the high clutter case.

The target extent estimate of the ET-GLMB-S filter (blue dotted line), the ET-GLMB-E (purple dash line) and ET-GLMB-Em (red dashed-dotted line) filters are shown in Fig. 7.4. The true target extent is shown in black line. As observed from the figure, the ET-GLMB-S filter is able to give a better estimate of the target extent, shape and orientation when compared to the other two methods. This improvement in the target extent estimation is due to our B-spline approach.

Figure 7.5a depicts the averaged mOSPA measures for the filters over 100 Monte Carlo (MC) runs for the case where $\gamma_k = 50$. From the figure, it is observed that the ET-GLMB-S filter out performs the other three filters with the ET-GLMB-

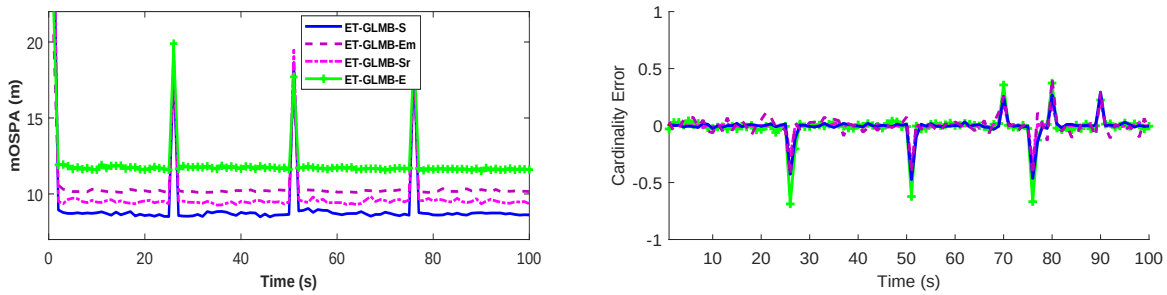

(a) (b)

Figure 7.5 Scenario I:(a) mOSPA measure against time (b) Number of target estimation error against time. Results shown are for an average clutter rate of 20 Poisson clutter points per scan over 100 MC runs.

Em filter offering a similar level of performance to the ET-GLMB-Sr filter. The improved accuracy of the ET-GLMB-S filter when compared to the ET-GLMB-E filter is due to the proposed B-spline target extent model approach. The ET-GLMB-Em outperformed the ET-GLMB-E filter because it uses more the one ellipse to estimate the target extent and is therefore able to estimate the target extension better. The ET-GLMB-S filter offers a better tracking accuracy when compared to the ET-GLMB-Sr filter. This is because the implementation of the ET-GLMB-S filter includes multiple hypotheses propagation during the update stage of the filter. In Fig. 7.5b, the cardinality errors of all four filters are shown. This error measures the difference between the estimated and true number of multiple extended targets present to three decimal places. It can be seen that all four filters are able to estimate the cardinality of the targets with minimal error.

The results obtained for the CT of the filters for the three clutter rates and the different probability of detections for scenario I are presented in Table 7.1. These are averaged over 100 MC runs. From the table, it is observed that the ET-GLMB-S filter and the ET-GLMB-Em filter have almost comparable CT. These two filters however take more time to compute when compared to the ET-GLMB-E filter for the scenario considered under the different p_D and γ_k settings. This is due mainly to the PMVB step required by the ET-GLMB-S filter to estimate the measurement rates for the targets as the lower bound computation in the PMVB step needs to converge in each iteration of the ET-GLMB-S filter. The ET-GLMB-Sr filter on the

other hand gave the least CT when compared to the other two techniques despite the computation of the PMVB step. This is because the uncertainty of only a single set of track labels was propagated each time.

Table 7.1 Filter performance comparison in terms of computation time (CT) for different probability of detection p_D and average number of clutter points γ_k.

Filter	p_D, γ_k		
	0.8, 30	0.9, 50	0.95, 100
ET-GLMB-E	6.65s	8.02s	9.83s
ET-GLMB-Em	6.90s	9.27s	10.15s
ET-GLMB-Sr	2.62s	3.11s	5.72s
ET-GLMB-S	6.93s	9.25s	10.11s

7.6.4 Scenario II (where $\lambda_k > \tau$)

For the second scenario, the case where if $\lambda_k > \tau$, only the measurements that constitute of the convex hull of the targets are used in updating the control points of the spline was considered . Therefore, in this scenario, three closely spaced targets that enter and exit the tracking area at the same time but have different measurement rates were of interest. The measurement rates and the time instants the targets enter and exit the tracking scene are given below:

$$\lambda_k^{(1)} = 21, \quad t_b^{(1)} = 1, \quad t_d^{(1)} = 100, \tag{7.51a}$$

$$\lambda_k^{(2)} = 30, \quad t_b^{(2)} = 1, \quad t_d^{(2)} = 100, \tag{7.51b}$$

$$\lambda_k^{(3)} = 40, \quad t_b^{(3)} = 1, \quad t_d^{(3)} = 100. \tag{7.51c}$$

This scenario also lasts 100 time steps. The ground truth of the kinematic state of the targets are shown in the bottom plot of Figure 7.6. The surveillance area is $[-1000, 1000] \times [-1000, 1000]$. In this scenario, three sub-objects were considered for the ET-GLMB-Em filter.

In this scenario, the performance of the filters under high clutter ($\gamma_k = 100$) conditions is highlighted. The focus here is on evaluating only the mOSPA measure and not the cardinality given that the number of targets is fixed during the entire time. Particularly, in this scenario, the performance of the filters in terms of their

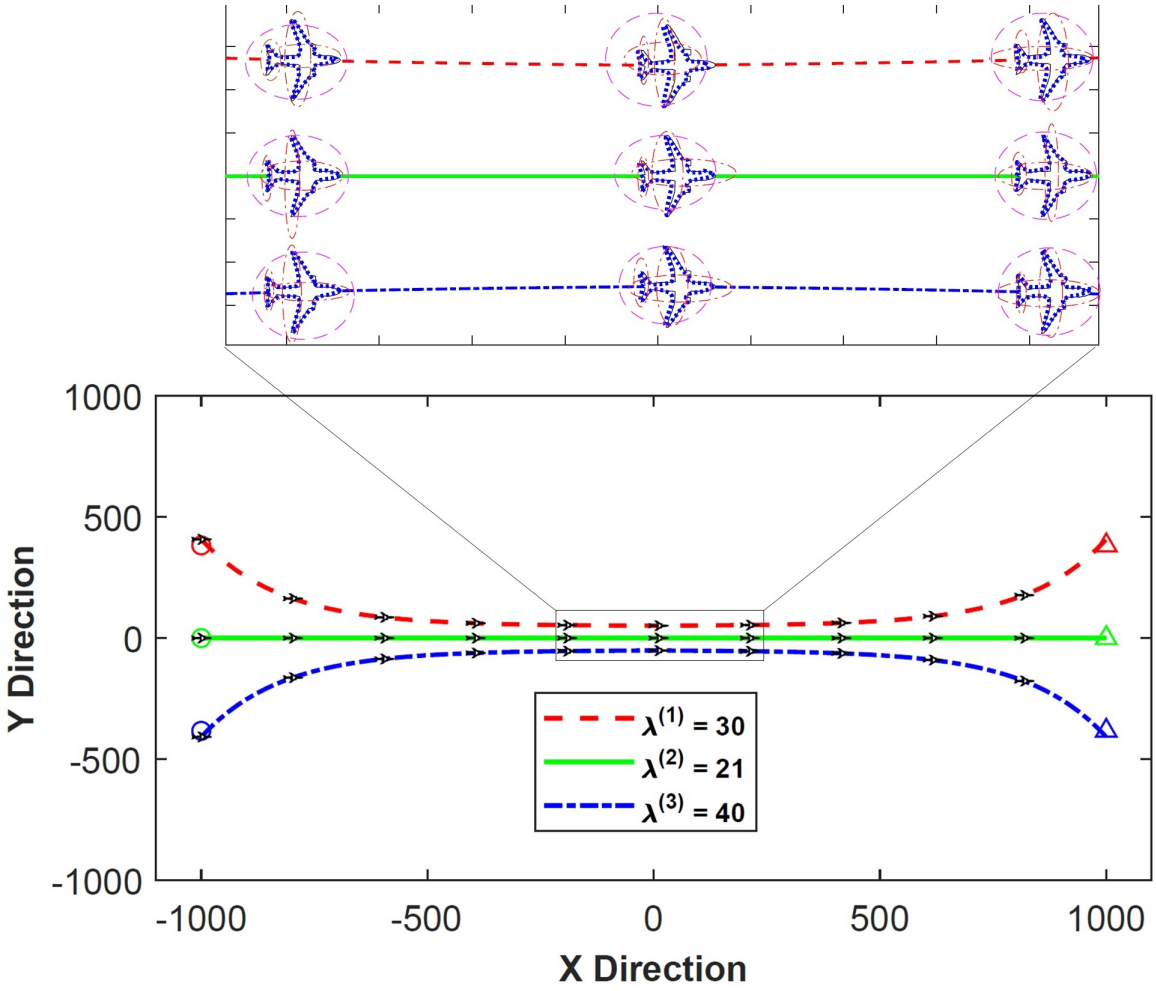

Figure 7.6 Scenario II. In the top figure, the true target shape is shown in black line, the B-spline method in blue dotted line, the multi-sub-object method in red-dash-dotted line and the random matrix method in purple dash line. All targets are simulated. The target plots shown are at intervals of 10 time steps.

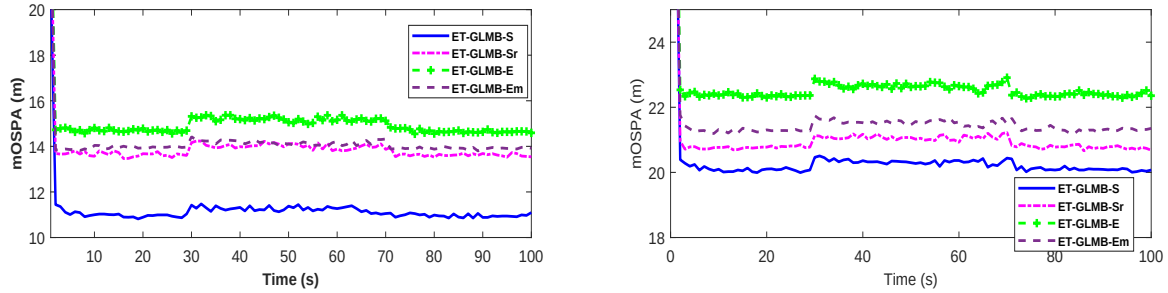

(a) (b)

Figure 7.7 Scenario II: (a) mOSPA measure against tracking time for $\gamma_k = 50$. (b) mOSPA measure against tracking time for $\gamma_k = 100$. Results shown are averaged over 100 MC trials.

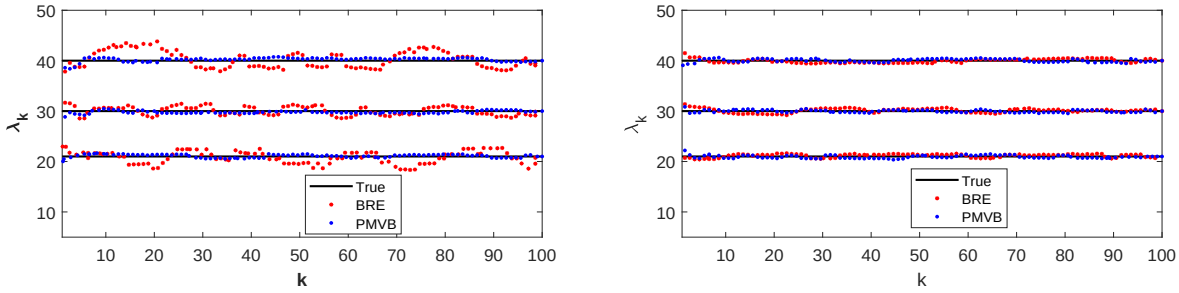

(a) Window size = 10 (b) Window size = 105.

Figure 7.8 Plot showing Poisson rate parameter estimation results for the three measurement rates of Scenario II.

ability to track closely spaced targets is highlighted. In this scenario, the three targets are in the closest proximity between time $k = 32$ and $k = 68$.

The target extent estimate of the ET-GLMB-S filter (blue dotted line), the ET-GLMB-E (purple dash line) and ET-GLMB-Em (red dashed-dotted line) filters are shown in 7.6. The true target extent is shown in black line. As observed from the figure, the ET-GLMB-S filter is able to give a better estimate of the target extent, shape and orientation when compared to the other two methods. This improvement in the target extent estimation is due to our B-spline approach.

Figure 7.7 depicts the averaged mOSPA measures for the filters over 100 Monte Carlo MC runs for the case of low (Fig. 7.7a) and high (Fig. 7.7b) clutter rates respectively. In both figures, notice the increase in the estimation error in the ET-GLMB-Sr, ET-GLMB-Em and the ET-GLMB-E filters particularly during the times when all three targets are closest. This further highlight the drawback of the

ET-GLMB-Sr filter where only the uncertainty of a single set of track labels is propagated during update of the filter.

Table 7.2 RMSE result comparison between the BRE and the PMVB methods.

Method	RMSE	
	Window size = 10	Window size = 105
BRE	2.11	0.27
PMVB	0.29	0.26

Figure 7.8 shows measurement rate estimation results obtained from applying the Bayesian rate estimation (BRE) used in [21] and our PMVB method to scenario II. In Fig. 7.8a, a window size of 10 was used while a window size of 105 was used in 7.8b (for both methods). The estimated measurement rates appear to be noisy when a smaller window size is used for the BRE method (as observed from 7.8a). However, when a larger window size was used for the BRE method for the same problem, the estimation error reduces (see 7.8b). The proposed PMVB method however is less sensitive to the pre-set window size. Table II shows the root mean squared error (RMSE) computed for the two window size cases for both methods. It is observed that the RMSE for the PMVB relatively small for both cases. However, the RMSE for the BRE varied greatly for the BRE when different window sizes are used for the same application.

Overall, our proposed ET-GLMB-S filter has been shown to give improvement in terms of measurement rate and target extent estimation by giving a lower mOSPA measure when compared to the ET-GLMB-E and the ET-GLMB-Em filters. In addition, the ET-GLMB-Sr filter allows for an efficient implementation of the proposed technique as seen by the CT comparison.

7.7 Summary

This chapter featured the development of a new MTT algorithm for the tracking of multiple extended targets in clutter. The new algorithm namely the ET-GLMB-S filter is capable of providing state estimates, number of targets and target labels (data association) for multiple extended targets in clutter. The algorithm was based

on the labelled random finite sets framework which estimates multiple targets states and the number of targets while allowing continuous target tracks (labelling). The proposed algorithm in addition to estimating extended target kinematics also jointly estimates target measurement rate and extension. The main advantage of the proposed algorithms is the use of variational Bayesian approach to estimate measurement rates and the B-spline to model target extension. Simulation study was carried out to demonstrate the performance improvement offered by this method.

7.8 Appendix

7.8.1 Expectation of a Logarithm

Given a random variable x, if there exists a $u > 0$ such that

$$M_x(t) \triangleq \mathbb{E}_y[e^{xt}], \tag{7.52}$$

for $|t| < u$, then $M_x(t)$ is called the moment generating function (mgf). In terms of the mgf, the expected value of x is

$$\mathbb{E}[x] = \left.\frac{\mathrm{d}M_x(t)}{\mathrm{d}t}\right|_{t=0}. \tag{7.53}$$

Consider the rate parameter λ of a Poisson distribution and let $x = \log \lambda$; where λ is gamma distributed with shape parameter $\alpha > 0$ and rate parameter $\beta > 0$. The pdf of λ is given as

$$p(\lambda|\alpha, \beta) = \frac{\beta^\alpha}{\Gamma(\alpha)}\lambda^{\alpha-1}e^{-\beta\lambda}, \quad \lambda \geq 0. \tag{7.54}$$

The mgf of x is

$$\begin{aligned} M_x(t) = \mathbb{E}[\lambda^t] &= \int \lambda^t \frac{\beta^\alpha}{\Gamma(\alpha)} \lambda^{\alpha-1} e^{-\beta\lambda} \mathrm{d}\lambda \\ &= \frac{\beta^\alpha}{\Gamma(\alpha)} \int \overbrace{\lambda^{t+\alpha-1} e^{-\beta\lambda}}^{\mathcal{GAM}(\lambda; t+\alpha, \beta)} \mathrm{d}\lambda \\ &= \frac{\beta^\alpha}{\Gamma(\alpha)} \frac{\Gamma(t+\alpha)}{\beta^{t+\alpha}} \int \overbrace{\frac{\beta^{t+\alpha}}{\Gamma(t+\alpha)} \lambda^{t+\alpha-1} e^{-\beta\lambda}}^{\text{integral over gamma density which = 1}} \mathrm{d}\lambda \\ &= \frac{\beta^\alpha}{\Gamma(\alpha)} \frac{\Gamma(t+\alpha)}{\beta^{t+\alpha}} = \frac{\Gamma(t+\alpha)}{\Gamma(\alpha)\beta^t}. \end{aligned} \tag{7.55}$$

The expected value of x is

$$\begin{aligned} \mathbb{E}[x] = \mathbb{E}[\log \lambda] &= \frac{\mathrm{d}}{\mathrm{d}t} \left(\frac{\Gamma(t+\alpha)}{\Gamma(\alpha)\beta^t} \right) \Bigg|_{t=0} \\ &= \left(\frac{\frac{\mathrm{d}}{\mathrm{d}t}\Gamma(t+\alpha)}{\Gamma(\alpha)\beta^t} \right) \Bigg|_{t=0} + \left(\frac{\Gamma(t+\alpha)}{\Gamma(\alpha)} \frac{\mathrm{d}}{\mathrm{d}t} \beta^{-t} \right) \Bigg|_{t=0} \\ &= \psi_0(\alpha) - \log \beta, \end{aligned} \tag{7.56}$$

where $\psi_0(\cdot)$ is the digamma function.

7.8.2 Variational Lower Bound Derivation

For the variational mixture of Poissons, the lower bound of (7.41) is given by

$$\mathfrak{L} = \sum_Y \int \int q(Y, \pi, \Lambda) \frac{p(\mathfrak{N}, Y, \pi, \Lambda)}{q(Y, \pi, \Lambda)} d\pi\Lambda \tag{7.57a}$$

$$= \mathbb{E}[\log p(\mathfrak{N}, Y, \pi, \Lambda)] - \mathbb{E}[\log q(Y, \pi, \Lambda)] \tag{7.57b}$$

where from (7.57b) above, we have:

$$\begin{aligned} \mathbb{E}[\log p(\mathfrak{N}, Y, \pi, \Lambda)] = \mathbb{E}[\log p(\mathfrak{N}|Y, \Lambda)] + \mathbb{E}[\log p(Y|\pi)] \\ + \mathbb{E}[\log p(\pi)] + \mathbb{E}[\log p(\Lambda)] \end{aligned} \tag{7.57c}$$

and

$$-\mathbb{E}[\log q(Y,\pi,\Lambda)] = -\mathbb{E}[\log q(Y)] - \mathbb{E}[\log q(\pi)] - \mathbb{E}[\log q(\Lambda)] \tag{7.57d}$$

The various terms on the RHS of (7.57c) are:

$$\mathbb{E}[\log p(\mathfrak{N}|Y,\Lambda)] = \sum_{c=1}^{C} M_c \left(\mathbb{E}[\log \lambda_c] \sum_{j=1}^{J} n_j - J\mathbb{E}[\lambda_c] - \sum_{j=1}^{J} n_j! \right) \tag{7.58a}$$

$$\mathbb{E}[\log p(Y|\pi)] = \sum_{c=1}^{C}\sum_{j=1}^{J} r_{jc} \log \tilde{\pi}_c \tag{7.58b}$$

$$\mathbb{E}[\log p(\pi)] = \log \mathcal{C}(\mathfrak{a}_0) + (a_0 - 1)\sum_{c=1}^{C} \log \tilde{\pi}_c \tag{7.58c}$$

$$\mathbb{E}[\log p(\Lambda)] = \alpha_0 \log \beta_0 - \log \Gamma(\alpha_0) + \sum_{c=1}^{C} (\alpha_0 - 1)\mathbb{E}[\log \lambda_c] - \beta_0 \mathbb{E}[\lambda_c] \tag{7.58d}$$

where $\mathbb{E}[\log \lambda_c] = (\psi_0(\alpha_c) - \log \beta_c)$, $\mathbb{E}[\lambda_c] = \frac{\alpha_c}{\beta_c}$ and $\log \tilde{\pi}_c = \psi_0(a_c) - \psi_0(\sum_{c=1}^{C} a_c)$. Similarly, the terms on the RHS of (7.57d) are:

$$\mathbb{E}[\log q(Y)] = \sum_{c=1}^{C}\sum_{j=1}^{M} r_{jc} \log r_{jc} \tag{7.59a}$$

$$\mathbb{E}[\log q(\pi)] = \log \mathcal{C}(\mathfrak{a}) + \sum_{c=1}^{C} (a_c - 1) \log \tilde{\pi}_c \tag{7.59b}$$

$$\mathbb{E}[\log q(\Lambda)] = \sum_{c=1}^{C} (\alpha_c - 1)\psi_0(\alpha_c) + \log \beta_c - \alpha_c - \log \Gamma(\alpha_c). \tag{7.59c}$$

This completes the variational lower bound derivation. ■

Chapter 8

Conclusion and Future Work

The contributions of this thesis along with concluding remarks are summarised in Section 8.1 followed by suggestions for future work in Section 8.2.

8.1 Conclusions

In this thesis, advanced signal processing methods were employed within the RFS based filtering adaptation of Bayesian filtering to successfully develop new and improved multi-target tracking algorithms for cluttered environments. Results presented herein from both simulation and practice show that the developed methods are not only valid but feasible and effective approaches to multiple target tracking. In particular, the proposed algorithms for point and extended multiple target tracking respectively, offer reliable and computationally efficient solutions for the joint estimation of target state, target number and target track association of an unknown and time-varying number of targets observed with imperfect sensors in the presence of clutter. Furthermore, the proposed techniques were shown to outperform standard approaches in both simulated and practical scenarios. A critique of the key contributions of this thesis is given as follows.

In Chapter 4, a new and efficient multi-target SMC filter, namely the KG-SMC-PHD filter for MTT which seeks to minimise the MSE between received and estimated measurements at any given time has been proposed. This was achieved by first partitioning the measurement set into target-originated measurements

and clutter for weight computation and applying the Kalman-gain to selected particles for state correction. Besides the improved tracking accuracy achieved by this method, fewer particles are required to attain high tracking performance, hence making the proposed filter more efficient. Furthermore, the improved resampling method was proposed in this chapter addressed a conceptual issue with the standard systematic resampling method. This meant that the SR method had a tendency of resampling very low weight particles especially when a large number of resampled particles are required which in turn lead to poor state estimates in SMC methods post the resampling process. The proposed ISR method addressed this issue by implementing a weight re-lowering technique to the weights of selected particles. The overall tracking performance of the KG-SMC-PHD filter was improved because, i) only target-originated measurements were used for weight computation and ii) the MSE at each time step was reduced resulting in fewer number of particles for state estimation. Simulation studies with dense clutter demonstrate that the KG-SMC-PHD filter algorithm outperformed the standard SMC-PHD filter as well as other alternative implementations of the PHD filter. Additionally, simulation results showed that the proposed ISR resampling method outperformed the standard SR method particularly when a large number of resampled particles is required.

The PHD filter and the KG-SMC-PHD filter of Chatper 4 have a pronounced bias in target number estimation especially when large number of targets are being tracked. To address this, Chapter 5 introduced the cardinalised version (KG-SMC-CPHD) of the KG-SMC-PHD filter of chapter 4. The new approach not only propagate the PHD at each time dwell but also propagates the probability distribution of target number. The KG-SMC-CPHD filter was applied to simulated data and results show that the KG-SMC-CPHD filter had improved cardinality estimate (both in mean and standard deviation) when compared to the KG-SMC-PHD filter. Furthermore, results showed that the KG-SMC-CPHD filter to be more efficient when compared to the standard SMC-CPHD filter in terms of the number of particles needed for tracking, execution time for higher number of particles and accuracy as indicated by the OSPA distance.

In principle, both the KG-SMC-PHD filter of Chapter 4 and the KG-SMC-CPHD filter of Chapter 5 perform target "filtering" and not "tracking". In other words, they provide only "point" estimates of target states but do not provide "connected" estimates of target trajectories from one time step to the next. Chapter 6 investigated a post processing step using game theory as a solution to this "filtering" - "tracking" problem. This approach was named the GTDA method. The players in the game were the trajectories or tracks of the targets. The strategies were the output of the filter, that is, the target-state-estimates. Each player aims to assign a new target-state-estimate to its existing track. The utility functions of the players were defined, and a regret matching with forgetting factor was used to find the equilibrium of the game. The GTDA method was employed in the KG-SMC-(C)PHD filter as a post processing technique and was evaluated using both simulated and real data. As for the simulated data, the performance of the proposed technique was compared to other data association algorithms such as the PDA and JPDA. The proposed method showed a better performance in terms of accuracy and computational complexity when compared to PDA. However, the proposed approach showed similar performance in terms of accuracy when compared with JPDA but takes less computational time. Secondly, the effectiveness of the GTDA was further demonstrated on real field measurements collected by an NI-USRP based PBR system. In the experiment, the KG-SMC-(C)PHD filter was used to track aeroplanes and the GTDA was used for track association. Results showed that the GTDA technique was able to successfully associate the target-state-estimates to various target tracks.

Chapter 7 featured the development of a new MTT algorithm for the tracking of multiple extended targets in clutter. The new algorithm namely the ET-GLMB-S filter is capable of providing state estimates, number of targets and target labels (data association) for multiple extended targets in clutter. The algorithm was based on the labelled random finite sets framework which estimates multiple targets states and the number of targets while allowing continuous target tracks (labelling). The proposed algorithm in addition to estimating extended target kinematics also jointly estimates target measurement rate and extension. The main advantages of

the proposed algorithms were the use of a VB approach to estimate measurement rates and the use B-spline to model target extension. The VB approach allows for the simultaneous estimation of the measurement rate of multiple targets. B-spline method offers the flexibility of modelling standard-shaped and arbitrary target extensions. Simulation study was carried out to demonstrate the performance improvement offered by this method.

8.2 Future Work

In what follows, interesting directions for future works are explored both in terms of contributions to theoretical and algorithmic developments. In particular, the following may be of interest:

- ⋆ Works in the literature exist characterising the performance limits of the (C)PHD filter. A characterisation of the developed KG-SMC-(C)PHD filter would be an addition to the field as it will establish the filter performance limits as well as indicate filter stability parameters.

- ⋆ In the utility function of the GTDA method of Chapter 6, it is worth exploring the characterisation of the feasibility of the equilibrium obtained using the RMFF particularly in the case when the commonly observed distribution $\beta_{p,n}(k)$ converges to a pure equilibrium.

- ⋆ The miss-distance metric applied in Chapter 7 serves as a basis for further theoretical investigations. An entropy-based information theoretic approach may be of particular significance in terms of developing a consistent metric for ET tracker since it is a well-established theoretical framework which readily facilitates a principled and impartial investigation.

- ⋆ In both the RFS and the labelled RFS adaptation of the Bayesian filter for MTT in this thesis, they have the prediction step in common. This step includes an RFS of predicted target states which is a union of the RFS of surviving targets and new born targets. The target birth model used in this

thesis was context specific. A more general and robust birth model will be a useful addition to the field.

References

[1] S. Ahlberg, P. Hörling, K. Johansson, K. Jöred, H. Kjellström, C. Mårtenson, G. Neider, J. Schubert, P. Svenson, P. Svensson *et al.*, "An Information Fusion Demonstrator for Tactical Intelligence Processing in Network-Based Defense," *Information Fusion*, vol. 8, no. 1, pp. 84–107, 2007.

[2] D. Angelova, L. Mihaylova, N. Petrov, and A. Gning, "A Convolution Particle Filtering Approach for Tracking Elliptical Extended Objects," in *Proceedings of the 16th International Conference on Information Fusion*, July 2013, pp. 1542–1549.

[3] M. Arulampalam, S. Maskell, N. Gordon, and T. Clapp, "A Tutorial on Particle Filters for Online Nonlinear/Non-Gaussian Bayesian Tracking," *IEEE Transactions on Signal Processing*, vol. 50, no. 2, pp. 174–188, 2002.

[4] R. J. Aumann, "Subjectivity and Correlation in Randomized Strategies," *Journal of mathematical Economics*, vol. 1, no. 1, pp. 67–96, 1974.

[5] B.-N. Vo, M. Mallick, Y. Bar-Shalom, S. Coraluppi, R. Osborne III, R. Mahler, and B.-T. Vo, "Multitarget Tracking," *Wiley Encyclopedia of Electrical and Electronics Engineering*, Sept 2015.

[6] Ba-Tuong Vo and Ba-Ngu Vo and Cantoni, Antonio, "The Cardinalized Probability Hypothesis Density Filter for Linear Gaussian Multi-Target Models," in *2006 40th Annual Conference on Information Sciences and Systems*, 2006, pp. 681–686.

[7] B. Balakumar, A. Sinha, T. Kirubarajan, and J. Reilly, "PHD Filtering for Tracking an Unknown Number of Sources Using an Array of Sensors," in *2005 IEEE/SP 13th Workshop onStatistical Signal Processing*. IEEE, 2005, pp. 43–48.

[8] Y. Bar-Shalom and T. Fortmann, *Tracking and Data Association*, ser. Mathematics in Science and Engineering Series. Academic Press, 1988.

[9] Y. Bar-Shalom, P. Willett, and X. Tian, *Tracking and Data Fusion: A Handbook of Algorithms*. YBS Publishing, 2011.

[10] Y. Bar-Shalom, "Multitarget-Multisensor Tracking: Advanced Applications," *Norwood, MA, Artech House, 1990, 391 p.*, vol. 1, 1990.

[11] Y. Bar-Shalom, X. R. Li, and T. Kirubarajan, *Estimation with Applications to Tracking and Navigation: Theory Algorithms and Software*. John Wiley & Sons, 2004.

[12] Y. Bar-Shalom and X.-R. Li, "Multitarget-Multisensor Tracking: Principles and Techniques," *Storrs, CT: University of Connecticut, 1995.*, 1995.

[13] Y. Bar-Shalom and E. Tse, "Tracking in a Cluttered Environment with Probabilistic Data Association," *Automatica*, vol. 11, no. 5, pp. 451–460, 1975.

[14] E. Baser and M. Efe, "A Novel Auxiliary Particle PHD Filter," in *2012 15th International Conference on Information Fusion (FUSION)*, 2012, pp. 165–172.

[15] M. Baum and U. D. Hanebeck, "Extended Object Tracking with Random Hypersurface Models," *IEEE Transactions on Aerospace and Electronic Systems*, vol. 50, no. 1, pp. 149–159, January 2014.

[16] M. Baum, B. Noack, and U. D. Hanebeck, "Extended Object and Group Tracking with Elliptic Random Hypersurface Models," in *2010 13th International Conference on Information Fusion*, July 2010, pp. 1–8.

[17] M. Baum and U. D. Hanebeck, "Random Hypersurface Models for Extended Object Tracking," in *2009 IEEE International Symposium on Signal Processing and Information Technology (ISSPIT)*. IEEE, 2009, pp. 178–183.

[18] M. Baum and U. D. Hanebeck, "Shape Tracking of Extended Objects and Group Targets with Star-Convex RHMs," in *2011 Proceedings of the 14th International Conference on Information Fusion (FUSION)*. IEEE, 2011, pp. 1–8.

[19] E. R. Beadle and P. M. Djuric, "A Fast-Weighted Bayesian Bootstrap Filter for Nonlinear Model State Estimation," *IEEE Transactions on Aerospace and Electronic Systems*, vol. 33, no. 1, pp. 338–343, 1997.

[20] M. Beard, S. Reuter, K. Granström, B. T. Vo, B. N. Vo, and A. Scheel, "A Generalised Labelled Multi-Bernoulli Filter for Extended Multi-Target Tracking," in *2015 18th International Conference on Information Fusion (Fusion)*, July 2015, pp. 991–998.

[21] M. Beard, S. Reuter, K. Granström, B. T. Vo, B. N. Vo, and A. Scheel, "Multiple Extended Target Tracking With Labeled Random Finite Sets," *IEEE Transactions on Signal Processing*, vol. 64, no. 7, pp. 1638–1653, April 2016.

[22] M. Beard, B. T. Vo, and B. N. Vo, "Bayesian Multi-Target Tracking With Merged Measurements Using Labelled Random Finite Sets," *IEEE Transactions on Signal Processing*, vol. 63, no. 6, pp. 1433–1447, March 2015.

[23] N. Bergman, "*Recursive Bayesian Estimation: Navigation and Tracking Applications*," Ph.D. dissertation, Linköping University, Linköping, Sweden, 1999.

[24] C. Bishop, *Pattern Recognition and Machine Learning*, ser. Information Science and Statistics. Springer, 2006.

[25] S. S. Blackman, "Multiple Hypothesis Tracking for Multiple Target Tracking," *IEEE Aerospace and Electronic Systems Magazine*, vol. 19, no. 1, pp. 5–18, Jan 2004.

[26] S. Blackman and R. Popoli, *Design and Analysis of Modern Tracking Systems*, ser. Artech House radar library. Artech House, 1999.

[27] S. Blake, "OS-CFAR Theory for Multiple Targets and Nonuniform Clutter," *IEEE Transactions on Aerospace and Electronic Systems*, vol. 24, no. 6, pp. 785–790, Nov 1988.

[28] M. Bolić, P. M. Djurić, and S. Hong, "Resampling Algorithms for Particle Filters: A Computational Complexity Perspective," *EURASIP Journal on Applied Signal Processing*, vol. 2004, pp. 2267–2277, 2004.

[29] S. R. Buss, *3-D Computer Graphics: A Mathematical Introduction with OpenGL*. Cambridge University Press, 2003.

[30] X. Cao, J. Lan, and X. R. Li, "Extension-deformation approach to extended object tracking," in *2016 19th International Conference on Information Fusion (FUSION)*, July 2016, pp. 1185–1192.

[31] O. Cappé, S. J. Godsill, and E. Moulines, "An Overview of Existing Methods and Recent Advances in Sequential Monte Carlo," *Proceedings of the IEEE*, vol. 95, no. 5, pp. 899–924, 2007.

[32] J. Carpenter, P. Clifford, and P. Fearnhead, "Improved Particle Filter for Nonlinear Problems," *IEE Proceedings-Radar, Sonar and Navigation*, vol. 146, no. 1, pp. 2–7, 1999.

[33] S. Challa, *Fundamentals of Object Tracking*. Cambridge University Press, 2011.

[34] P. Chavali and A. Nehorai, "Concurrent Particle Filtering and Data Association Using Game Theory for Tracking Multiple Maneuvering Targets," *IEEE Transactions on Signal Processing*, vol. 61, no. 20, pp. 4934–4948, 2013.

[35] P. Chavali and A. Nehorai, "Distributed Data Association for Multiple-Target Tracking Using Game Theory," in *2013 IEEE Radar Conference (RADAR)*, April 2013, pp. 1–6.

[36] D. Clark, B.-T. Vo, and B.-N. Vo, "Gaussian Particle Implementations of Probability Hypothesis Density Filters," in *2007 IEEE Aerospace Conference*, 2007, pp. 1–11.

[37] D. Clark, A.-T. Cemgil, P. Peeling, and S. Godsill, "Multi-Object Tracking of Sinusoidal Components in Audio with the Gaussian Mixture Probability Hypothesis Density Filter," in *2007 IEEE Workshop on Applications of Signal Processing to Audio and Acoustics*. IEEE, 2007, pp. 339–342.

[38] D. Clark, B. Ristic, and B.-N. Vo, "PHD Filtering with Target Amplitude Feature," in *2008 11th International Conference onInformation Fusion*. IEEE, 2008, pp. 1–7.

[39] D. E. Clark, "*Multiple Target Tracking with the Probability Hypothesis Density Filter*," Ph.D. dissertation, Heriot-Watt University, 2006.

[40] C. Coman and T. Kreitmair, "Evaluation of the Tracking Process in Ground Surveillance Applications," in *EuRAD 2009. European Radar Conference*, 2009, pp. 553–556.

[41] D. Crisan, P. D. Moral, and T. J. Lyons, "Non-Linear Filtering Using Branching and Interacting Particle Systems," *Markov Processes Related Fields*, 1999.

[42] D. Crisan, P. Del Moral, and T. Lyons, *Discrete Filtering Using Branching and Interacting Particle Systems*. Université de Toulouse. Laboratoire de Statistique et Probabilités [LSP], 1998.

[43] A. Daniyan, A. Aldowesh, Y. Gong, and S. Lambotharan, "Data Association using Game Theory for Multi-Target Tracking in Passive Bistatic Radar," in *2017 IEEE Radar Conference (RadarConf)*, May 2017, pp. 0042–0046.

[44] A. Daniyan, Y. Gong, and S. Lambotharan, "Game Theoretic Data Association for Multi-Target Tracking with Varying Number of Targets," in *2016 IEEE Radar Conference (RadarConf)*, May 2016.

[45] A. Daniyan, Y. Gong, and S. Lambotharan, "An Improved Resampling Approach for Particle Filters in Tracking," in *2017 22nd International Conference on Digital Signal Processing (DSP)*, Aug 2017, pp. 1–5.

[46] A. Daniyan, Y. Gong, S. Lambotharan, P. Feng, and J. Chambers, "Kalman-Gain Aided Particle PHD Filter for Multitarget Tracking," *IEEE Transactions on Aerospace and Electronic Systems*, vol. 53, no. 5, pp. 2251–2265, Oct 2017.

[47] A. Daniyan, "Performance analysis of sequential monte carlo mcmc and phd filters on multi-target tracking in video," in *Modelling Symposium (EMS), 2014 European*, Oct 2014, pp. 195–202.

[48] C. De Boor and E.-U. Mathématicien, *A Practical Guide to Splines*. Springer-Verlag New York, 1978, vol. 27.

[49] J. Degerman, J. Wintenby, and D. Svensson, "Extended Target Tracking Using Principal Components," in *2011 Proceedings of the 14th International Conference on Information Fusion (FUSION)*. IEEE, 2011, pp. 1–8.

[50] P. Del Moral, "Non-Linear Filtering: Interacting Particle Resolution," *Markov Processes and Related Fields*, vol. 2, no. 4, pp. 555–581, 1996.

[51] P. M. Djuric, J. H. Kotecha, J. Zhang, Y. Huang, T. Ghirmai, M. F. Bugallo, and J. Miguez, "Particle Filtering," *IEEE Signal Processing Magazine*, vol. 20, no. 5, pp. 19–38, Sep 2003.

[52] R. Douc and O. Cappé, "Comparison of Resampling Schemes for Particle Filtering," in *Proceedings of the 4th International Symposium on Image and Signal Processing and Analysis, ISPA*. IEEE, 2005, pp. 64–69.

[53] A. Doucet, A. Smith, N. de Freitas, and N. Gordon, *Sequential Monte Carlo Methods in Practice*, ser. Information Science and Statistics. Springer New York, 2001.

[54] A. Doucet, N. De Freitas, and N. Gordon, *Sequential Monte Carlo Methods in Practice*. Springer, 2001.

[55] A. Doucet, S. Godsill, and C. Andrieu, "On Sequential Monte Carlo Sampling Methods for Bayesian Filtering," *Statistics and computing*, vol. 10, no. 3, pp. 197–208, 2000.

[56] A. Doucet and A. M. Johansen, "A Tutorial on Particle Filtering and Smoothing: Fifteen Years Later," *Handbook of nonlinear filtering*, vol. 12, no. 656-704, p. 3, 2009.

[57] O. Erdinc, P. Willett, and Y. Bar-Shalom, "A Physical-Space Approach for the Probability Hypothesis Density and Cardinalized Probability Hypothesis Density Filters," in *Signal and Data Processing of Small Targets 2006*, vol. 6236. International Society for Optics and Photonics, 2006, p. 623619.

[58] Flightradar24. (2016) Flightradar24.com - Live Flight Tracker! [Online]. Available: https://www.flightradar24.com

[59] T. E. Fortmann, Y. Bar-Shalom, and M. Scheffe, "Sonar Tracking of Multiple Targets Using Joint Probabilistic Data Association," *IEEE Journal of Oceanic Engineering*, vol. 8, no. 3, pp. 173–184, Jul 1983.

[60] A. Gelman, J. B. Carlin, H. S. Stern, and D. B. Rubin, *Bayesian Data Analysis*. Chapman & Hall/CRC Boca Raton, FL, USA, 2014, vol. 2.

[61] K. Gilholm and D. Salmond, "Spatial Distribution Model for Tracking Extended Objects," *IEE Proceedings - Radar, Sonar and Navigation*, vol. 152, no. 5, pp. 364–371, October 2005.

[62] K. Gilholm, S. Godsill, S. Maskell, and D. Salmond, "Poisson Models for Extended Target and Group Tracking," in *Proceedings of Signal and Data Processing of Small Targets*, vol. 5913, 2005, pp. 230–241.

[63] N. J. Gordon, D. J. Salmond, and A. F. M. Smith, "Novel Approach to Nonlinear/Non-Gaussian Bayesian State Estimation," *IEE Proceedings F - Radar and Signal Processing*, vol. 140, no. 2, pp. 107–113, April 1993.

[64] K. Granström, C. Lundquist, and O. Orguner, "Extended target tracking using a gaussian-mixture phd filter," *IEEE Transactions on Aerospace and Electronic Systems*, vol. 48, no. 4, pp. 3268–3286, October 2012.

[65] K. Granström, A. Natale, P. Braca, G. Ludeno, and F. Serafino, "Gamma Gaussian Inverse Wishart Probability Hypothesis Density for Extended Target Tracking Using X-Band Marine Radar Data," *IEEE Transactions on Geoscience and Remote Sensing*, vol. 53, no. 12, pp. 6617–6631, Dec 2015.

[66] K. Granström and U. Orguner, "A PHD Filter for Tracking Multiple Extended Targets Using Random Matrices," *IEEE Transactions on Signal Processing*, vol. 60, no. 11, pp. 5657–5671, Nov 2012.

[67] K. Granström and U. Orguner, "Estimation and Maintenance of Measurement Rates for Multiple Extended Target Tracking," in *2012 15th International Conference on Information Fusion (FUSION)*, July 2012, pp. 2170–2176.

[68] K. Granström, S. Reuter, D. Meissner, and A. Scheel, "A Multiple Model PHD Approach to Tracking of Cars Under an Assumed Rectangular Shape," in *17th International Conference on Information Fusion (FUSION)*, July 2014, pp. 1–8.

[69] K. Granström, C. Lundquist, and U. Orguner, "Tracking Rectangular and Elliptical Extended Targets Using Laser Measurements," in *2011 Proceedings of the 14th International Conference on Information Fusion (FUSION)*. IEEE, 2011, pp. 1–8.

[70] K. Granström, P. Willett, and Y. Bar-Shalom, "An Extended Target Tracking Model with Multiple Random Matrices and Unified Kinematics," in *2015 18th International Conference on Information Fusion (Fusion)*. IEEE, 2015, pp. 1007–1014.

[71] B. K. Habtemariam, R. Tharmarasa, and T. Kirubarajan, "PHD Filter Based Track-Before-Detect for MIMO Radars," *Signal Processing*, vol. 92, no. 3, pp. 667–678, 2012.

[72] S. Hart and A. Mas-Colell, "A Simple Adaptive Procedure Leading to Correlated Equilibrium," *Econometrica*, vol. 68, no. 5, pp. 1127–1150, 2000.

[73] C. D. Haworth, Y. De Saint-Pern, D. Clark, E. Trucco, and Y. R. Petillot, "Detection and Tracking of Multiple Metallic Objects in Millimetre-Wave Images," *International Journal of Computer Vision*, vol. 71, no. 2, pp. 183–196, 2007.

[74] X. He, R. Sithiravel, R. Tharmarasa, B. Balaji, and T. Kirubarajan, "A Spline Filter for Multidimensional Nonlinear State Estimation," *Signal Processing*, vol. 102, pp. 282–295, 2014.

[75] T. Hirscher, A. Scheel, S. Reuter, and K. Dietmayer, "Multiple Extended Object Tracking Using Gaussian Processes," in *2016 19th International Conference on Information Fusion (FUSION)*, July 2016, pp. 868–875.

[76] J. D. Hol, T. B. Schon, and F. Gustafsson, "On Resampling Algorithms for Particle Filters," in *Nonlinear Statistical Signal Processing Workshop, 2006 IEEE*. IEEE, 2006, pp. 79–82.

[77] N. Ikoma, R. Yamaguchi, H. Kawano, and H. Maeda, "Tracking of Multiple Moving Objects in Dynamic Image of Omni-Directional Camera Using PHD Filter." *JACIII*, vol. 12, no. 1, pp. 16–25, 2008.

[78] B. Jia, M. Xin, and Y. Cheng, "Sparse-Grid Quadrature Nonlinear Filtering," *Automatica*, vol. 48, no. 2, pp. 327–341, 2012.

[79] B. Kalyan, A. Balasuriya, and S. Wijesoma, "Multiple Target Tracking in Underwater Sonar Images using Particle-PHD Filter," in *OCEANS 2006-Asia Pacific*. IEEE, 2007, pp. 1–5.

[80] K. Kanazawa, D. Koller, and S. Russell, "Stochastic simulation algorithms for dynamic probabilistic networks," in *Proceedings of the Eleventh Conference on Uncertainty in Artificial Intelligence*. Morgan Kaufmann Publishers Inc., 1995, pp. 346–351.

[81] S. Kay, *Fundamentals of Statistical Signal Processing: Estimation Theory*. Prentice-Hall PTR, 1993, vol. 1, no. 1.

[82] Z. Khan, T. Balch, and F. Dellaert, "MCMC-Based Particle Filtering for Tracking a Variable Number of Interacting Targets," *IEEE Transactions on Pattern Analysis and Machine Intelligence*, vol. 27, no. 11, pp. 1805–1819, 2005.

[83] G. Kitagawa, "Monte Carlo Filter and Smoother for Non-Gaussian Nonlinear State Space Models," *Journal of Computational and Graphical Statistics*, vol. 5, no. 1, pp. 1–25, 1996.

[84] J. W. Koch, "Bayesian Approach to Extended Object and Cluster Tracking Using Random Matrices," *IEEE Transactions on Aerospace and Electronic Systems*, vol. 44, no. 3, 2008.

[85] W. Koch, "Tracking and Sensor Data Fusion," *English, Mathematical Engineering. Springer Berlin Heidelberg*, pp. 157–185, 2014.

[86] J. Lan and X. R. Li, "Tracking of Extended Object or Target Group Using Random Matrix Part II: Irregular Object," in *2012 15th International Conference on Information Fusion*, July 2012, pp. 2185–2192.

[87] J. Lan and X. R. Li, "Tracking of Maneuvering Non-Ellipsoidal Extended Object or Target Group Using Random Matrix," *IEEE Transactions on Signal Processing*, vol. 62, no. 9, pp. 2450–2463, May 2014.

[88] J. Lan and X. R. Li, "Tracking of Extended Object or Target Group Using Random Matrix: New Model and Approach," *IEEE Transactions on Aerospace and Electronic Systems*, vol. 52, no. 6, pp. 2973–2989, December 2016.

[89] T. Li, M. Bolic, and P. M. Djuric, "Resampling Methods for Particle Filtering: Classification, Implementation, and Strategies," *IEEE Signal Processing Magazine*, vol. 32, no. 3, pp. 70–86, May 2015.

[90] F. Lian, C. Han, W. Liu, J. Liu, and J. Sun, "Unified Cardinalized Probability Hypothesis Density Filters for Extended Targets and Unresolved Targets," *Signal Processing*, vol. 92, no. 7, pp. 1729 – 1744, 2012.

[91] J. S. Liu and R. Chen, "Sequential Monte Carlo Methods for Dynamic Systems," *Journal of the American Statistical Association*, vol. 93, no. 443, pp. 1032–1044, 1998.

[92] J. S. Liu, R. Chen, and W. H. Wong, "Rejection Control and Sequential Importance Sampling," *Journal of the American Statistical Association*, vol. 93, no. 443, pp. 1022–1031, 1998.

[93] M. Liu, T. Jiang, and S. Zhang, "The Sequential Monte Carlo Multi-Bernoulli Filter for Extended Targets," in *2015 18th International Conference on Information Fusion (Fusion)*. IEEE, 2015, pp. 984–990.

[94] C. Lundquist, K. Granström, and U. Orguner, "Estimating the Shape of Targets with a PHD Filter," in *14th International Conference on Information Fusion*, July 2011, pp. 1–8.

[95] C. Lundquist, K. Granström, and U. Orguner, "An Extended Target CPHD Filter and a Gamma Gaussian Inverse Wishart Implementation," *IEEE Journal of Selected Topics in Signal Processing*, vol. 7, no. 3, pp. 472–483, June 2013.

[96] W. Ma, B. Ma, and X. Zhan, "Kalman Particle PHD Filter for Multi-Target Visual Tracking," in *Intelligent Science and Intelligent Data Engineering*. Springer, 2012, pp. 341–348.

[97] J. MacCormick and A. Blake, "A Probabilistic Exclusion Principle for Tracking Multiple Objects," *International Journal of Computer Vision*, vol. 39, no. 1, pp. 57–71, 2000.

[98] M. Maehlisch, W. Ritter, and K. Dietmayer, "ACC Vehicle Tracking with Joint Multisensor Multitarget Filtering of State and Existence," in *PReVENT Fusion Forum e-Journal*, vol. 1, 2006, pp. 37–43.

[99] E. Maggio, E. Piccardo, C. Regazzoni, and A. Cavallaro, "Particle PHD Filtering for Multi-Target Visual Tracking," in *ICASSP 2007 IEEE International Conference onAcoustics, Speech and Signal Processing*, vol. 1. IEEE, 2007, pp. I–1101.

[100] R. Mahler, "PHD Filters of Higher Order in Target Number," *IEEE Transactions on Aerospace and Electronic Systems*, vol. 43, no. 4, pp. 1523–1543, October 2007.

[101] R. Mahler, "PHD Filters for Nonstandard Targets, I: Extended Targets," in *2009 12th International Conference on Information Fusion*, July 2009, pp. 915–921.

[102] R. P. S. Mahler, "Multitarget Bayes Filtering via First-Order Multitarget Moments," *IEEE Transactions on Aerospace and Electronic Systems*, vol. 39, no. 4, pp. 1152–1178, Oct 2003.

[103] R. Mahler, ""Statistics 102" for Multisource-Multitarget Detection and Tracking," *IEEE Journal of Selected Topics in Signal Processing*, vol. 7, no. 3, pp. 376–389, 2013.

[104] R. P. Mahler, ""Statistics 101" for Multisensor, Multitarget Data Fusion," *IEEE Aerospace and Electronic Systems Magazine*, vol. 19, no. 1, pp. 53–64, 2004.

[105] R. P. Mahler, *Statistical Multisource-Multitarget Information Fusion*. Artech House, Inc., 2007.

[106] R. P. Mahler, *Advances in Statistical Multisource-multitarget Information Fusion*. Artech House, 2014.

[107] M. Mallick, V. Krishnamurthy, and B.-N. Vo, *Integrated Tracking, Classification, and Sensor Management: Theory and Applications*. John Wiley & Sons, 2012.

[108] S. Maskell and S. Julier, "Optimised Proposals for Improved Propagation of Multi-Modal Distributions in Particle Filters," in *2013 16th International Conference on Information Fusion (FUSION)*, 2013, pp. 296–303.

[109] M. Melzi and A. Ouldali, "Joint Multiple Target Tracking and Classification Using the Unscented Kalman Particle PHD Filter," in *2011 IEEE 9th International New Circuits and Systems Conference (NEWCAS)*, 2011, pp. 534–537.

[110] J. Mullane, B. Vo, M. D. Adams, and W. S. Wijesoma, "A PHD Filtering Approach to Robotic Mapping," in *IEEE Conf. on Control, Automation, Robotics and Vision*, 2008.

[111] J. Mullane, B.-N. Vo, M. D. Adams, and W. S. Wijesoma, "A Random Set Formulation for Bayesian SLAM," in *IROS 2008 IEEE/RSJ International Conference on Intelligent Robots and Systems, 2008*. IEEE, 2008, pp. 1043–1049.

[112] U. Orguner, C. Lundquist, and K. Granström, "Extended Target Tracking with a Cardinalized Probability Hypothesis Density filter," in *14th International Conference on Information Fusion*, July 2011, pp. 1–8.

[113] F. Papi, B. N. Vo, B. T. Vo, C. Fantacci, and M. Beard, "Generalized Labeled Multi-Bernoulli Approximation of Multi-Object Densities," *IEEE Transactions on Signal Processing*, vol. 63, no. 20, pp. 5487–5497, Oct 2015.

[114] Y. Petetin and F. Desbouvries, "A mixed GM/SMC Implementation of the Probability Hypothesis Density Filter," in *2012 11th International Conference on Information Science, Signal Processing and their Applications (ISSPA)*, 2012, pp. 425–430.

[115] N. T. Pham, W. Huang, and S. H. Ong, "Multiple Sensor Multiple Object Tracking with GMPHD Filter," in *2007 10th International Conference on Information Fusion*. IEEE, 2007, pp. 1–7.

[116] K. Punithakumar, M. McDonald, and T. Kirubarajan, "Spline Filter for Multidimensional Nonlinear/Non-Gaussian Bayesian Tracking," in *SPIE Defense and Security Symposium*. International Society for Optics and Photonics, 2008, pp. 69 690K–69 690K.

[117] S. Reuter, B. T. Vo, B. N. Vo, and K. Dietmayer, "The Labeled Multi-Bernoulli Filter," *IEEE Transactions on Signal Processing*, vol. 62, no. 12, pp. 3246–3260, June 2014.

[118] S. Reuter, B. Wilking, and K. Dietmayer, "Methods to Model the Motion of Extended Objects in Multi-Object Bayes Filters," in *2012 15th International Conference on Information Fusion*, July 2012, pp. 527–534.

[119] S. Reuter and K. Dietmayer, "Pedestrian Tracking Using Random Finite Sets," in *2011 Proceedings of the 14th International Conference on Information Fusion (FUSION)*. IEEE, 2011, pp. 1–8.

[120] B. Ristic, D. Clark, B. N. Vo, and B. T. Vo, "Adaptive Target Birth Intensity for PHD and CPHD Filters," *IEEE Transactions on Aerospace and Electronic Systems*, vol. 48, no. 2, pp. 1656–1668, April 2012.

[121] B. Ristic, S. Arulampalam, and N. Gordon, *Beyond the Kalman Filter: Particle Filters for Tracking Applications*. Artech House, 2004.

[122] D. F. Rogers, *An Introduction to NURBS: With Historical Perspective*. Elsevier, 2000.

[123] H. Rohling, "Radar CFAR Thresholding in Clutter and Multiple Target Situations," *IEEE Transactions on Aerospace and Electronic Systems*, vol. AES-19, no. 4, pp. 608–621, July 1983.

[124] D. B. Rubin, "The Calculation of Posterior Distributions by Data Augmentation: Comment: A noniterative sampling/importance resampling alternative to the data augmentation algorithm for creating a few imputations when fractions of missing information are modest: The SIR Algorithm," *Journal of the American Statistical Association*, vol. 82, no. 398, pp. 543–546, 1987.

[125] D. Schuhmacher, B. T. Vo, and B. N. Vo, "A Consistent Metric for Performance Evaluation of Multi-Object Filters," *IEEE Transactions on Signal Processing*, vol. 56, no. 8, pp. 3447–3457, Aug 2008.

[126] M. Schuster, J. Reuter, and G. Wanielik, "Probabilistic Data Association for Tracking Extended Targets Under Clutter Using Random Matrices," in *2015 18th International Conference on Information Fusion (Fusion)*. IEEE, 2015, pp. 961–968.

[127] H. Sidenbladh and S.-L. Wirkander, "Tracking Random Sets of Vehicles inTerrain," in *CVPRW'03. Conference onComputer Vision and Pattern Recognition Workshop, 2003*, vol. 9. IEEE, 2003, pp. 98–98.

[128] R. Sithiravel, X. Chen, M. McDonald, and T. Kirubarajan, "Spline Probability Hypothesis Density Filter for Nonlinear Maneuvering Target Tracking," in *2013 Asilomar Conference on Signals, Systems and Computers*, 2013, pp. 1743–1450.

[129] R. Sithiravel, X. Chen, R. Tharmarasa, B. Balaji, and T. Kirubarajan, "The Spline Probability Hypothesis Density Filter," *IEEE Transactions on Signal Processing*, vol. 61, no. 24, pp. 6188–6203, 2013.

[130] R. Sithiravel, M. McDonald, B. Balaji, and T. Kirubarajan, "Multiple Model Spline Probability Hypothesis Density Filter," *IEEE Transactions on Aerospace and Electronic Systems*, vol. 52, no. 3, pp. 1210–1226, June 2016.

[131] A. Smith, A. Doucet, N. de Freitas, and N. Gordon, *Sequential Monte Carlo Methods in Practice*. Springer Science & Business Media, 2013.

[132] L. D. Stone, R. L. Streit, T. L. Corwin, and K. L. Bell, *Bayesian Multiple Target Tracking*. Artech House, 2013.

[133] X. Tang, J. Zhou, J. Huang, and P. Wei, "Improved Particle Implementation of the Probability Hypothesis Density Filter in Resampling," in *2012 IEEE 12th International Conference on Computer and Information Technology (CIT)*, 2012, pp. 56–61.

[134] S. Tian, Y. He, and X. Sun, "Distributed Multi-Sensor Multi-Target Tracking with Random Sets I," in *Proc. Int'l. Conf. Natural Computation*. IEEE, 2007, pp. 128–131.

[135] S. Tian, Y. He, and G. Wang, "PHD Filter of Multi-Target Tracking with Passive Radar Observations," in *2006 8th International Conference on Signal Processing*, vol. 4. IEEE, 2006.

[136] P. N. Trung, "*Tracking of Multiple Objects Using the PHD Filter*," Ph.D. dissertation, National University of Singapore, 2007.

[137] B. N. Vo, B. T. Vo, and D. Phung, "Labeled Random Finite Sets and the Bayes Multi-Target Tracking Filter," *IEEE Transactions on Signal Processing*, vol. 62, no. 24, pp. 6554–6567, Dec 2014.

[138] B. T. Vo and B. N. Vo, "Labeled Random Finite Sets and Multi-Object Conjugate Priors," *IEEE Transactions on Signal Processing*, vol. 61, no. 13, pp. 3460–3475, July 2013.

[139] B. T. Vo, B. N. Vo, and A. Cantoni, "Analytic Implementations of the Cardinalized Probability Hypothesis Density Filter," *IEEE Transactions on Signal Processing*, vol. 55, no. 7, pp. 3553–3567, July 2007.

[140] B.-N. Vo and W.-K. Ma, "The Gaussian Mixture Probability Hypothesis Density Filter," *IEEE Transactions on Signal Processing*, vol. 54, no. 11, pp. 4091–4104, 2006.

[141] B.-N. Vo, S. Singh, and A. Doucet, "Random Finite Sets and Sequential Monte Carlo Methods in Multi-Target Tracking," in *Radar Conference, 2003. Proceedings of the International*, 2003, pp. 486–491.

[142] B.-N. Vo, S. Singh, and A. Doucet, "Sequential Monte Carlo Methods for Multitarget Filtering with Random Finite Sets," *IEEE Transactions on Aerospace and Electronic Systems*, vol. 41, no. 4, pp. 1224–1245, 2005.

[143] B. T. Vo, "*Random Finite Sets in Multi-Object Filtering*," Ph.D. dissertation, University of Western Australia, 2008.

[144] B.-T. Vo, B.-N. Vo, and A. Cantoni, "The Cardinality Balanced Multi-Target Multi-Bernoulli Filter and Its Implementations," *IEEE Transactions on Signal Processing*, vol. 57, no. 2, pp. 409–423, Feb 2009.

[145] N. Wahlström and E. Özkan, "Extended Target Tracking using Gaussian Processes," *IEEE Transactions on Signal Processing*, vol. 63, no. 16, pp. 4165–4178, 2015.

[146] N. Whiteley, S. Singh, and S. Godsill, "Auxiliary Particle Implementation of Probability Hypothesis Density Filter," *IEEE Transactions on Aerospace and Electronic Systems*, vol. 46, no. 3, pp. 1437–1454, 2010.

[147] J. Yin, J. Zhang, and J. Zhao, "The Gaussian Particle Multi-Target Multi-Bernoulli Filter," in *2010 2nd International Conference on Advanced Computer Control (ICACC)*, vol. 4, 2010, pp. 556–560.

[148] J. H. Yoon, D. Y. Kim, and K.-J. Yoon, "Gaussian Mixture Importance Sampling Function for Unscented SMC-PHD Filter," *Signal Processing*, vol. 93, no. 9, pp. 2664–2670, 2013.

[149] T. Zajic, R. B. Ravichandran, R. P. Mahler, R. K. Mehra, and M. J. Noviskey, "Joint Tracking and Identification with Robustness against Unmodeled Targets," in *Signal Processing, Sensor Fusion, and Target Recognition XII*, vol. 5096. International Society for Optics and Photonics, 2003, pp. 279–291.

[150] G. Zhang, F. Lian, and C. Han, "CB-MeMBer Filters for Nonstandard Targets, I: Extended Targets," in *17th International Conference on Information Fusion (FUSION)*, July 2014, pp. 1–6.

[151] H. Zhang, H. Xu, X. Y. Wang, and W. An, "A PHD Filter for Tracking Closely Spaced Objects with Elliptic Random Hypersurface Models," in *Proceedings of the 16th International Conference on Information Fusion*, July 2013, pp. 1558–1565.

[152] J. Zhang, H. Ji, and C. Ouyang, "A New Gaussian Mixture Particle CPHD Filter for Multitarget Tracking," in *2010 International Symposium on Intelligent Signal Processing and Communication Systems (ISPACS)*, 2010, pp. 1–4.

[153] Y. Zheng, Z. Shi, R. Lu, S. Hong, and X. Shen, "An Efficient Data-Driven Particle PHD Filter for Multitarget Tracking," *IEEE Transactions on Industrial Informatics*, vol. 9, no. 4, pp. 2318–2326, 2013.

[154] H. Zhu, C. Han, and C. Li, "An Extended Target Tracking Method with Random Finite Set Observations," in *2011 Proceedings of the 14th International Conference on Information Fusion (FUSION)*. IEEE, 2011, pp. 1–6.